Dynamics and Synchronization of Weak Chimera States for a Coupled Oscillator System

Submitted by

Mary Ghadbaan Thoubaan

to the University of Exeter as a thesis for the degree of Doctor of Philosophy in Mathematics.

July 2018

I certify that all material in this thesis which is not my own work has been identified and that no material has previously been submitted and approved for the award of a degree by this or any other University.

Signature: .....

UNIVERSITY OF EXETER

ABSTRACT

This thesis is an investigation of chimera states in a network of identical coupled phase oscillators. Chimera states are intriguing phenomena that can occur in systems of coupled identical phase oscillators, when synchronized and desynchronized oscillators coexist. We use the Kuramoto model and coupling function of Hansel for a specific system of six oscillators to prove existence of chimera states.

More precisely, we prove analytically there are chimera states in a small network of six phase oscillators previously investigated numerically by Ashwin and Burylko [8]. We can reduce to a two-dimensional system within an invariant subspace, in terms of phase differences. This system is found to have an integral of motion for a specific choice of parameters. Using this we prove there is a set of periodic orbits that is a weak chimera. Moreover, we are able to confirm that there is an infinite number of chimera states at the special case of parameters, using the weak chimera definition of [8].

We approximate the Poincaré return map for these weak chimera solutions and demonstrate several results about their stability and bifurcation for nearby parameters. These agree with numerical path following of the solutions.

We also consider another invariant subspace to reduce the Kuramoto model of six coupled phase oscillators to a first order differential equation. We analyse this equation numerically and find regions of attracting chimera states exist within this invariant subspace. By computing eigenvalues at a nonhyperbolic point for the system of phase differences, we numerically find there are chimera states in the invariant subspace that are attracting within full system.

ACKNOWLEDGEMENT

In the name of Allah, first, I would like to thank God Almighty for giving me the strength, knowledge, ability and opportunity to do this work.

Firstly, I would like to express my deep gratitude to my supervisor Prof. Peter Ashwin for his excellent scientific advice on my work. This PhD thesis would not be possible without his expertise, understanding, guidance and constructive criticism, which were really essential to develop and achieve this work. I really appreciated his encouragement for me to attend conferences and workshops, also for his time, patience and constant help, even in the days of his vacation or travel. He taught me fundamental steps to enter an interesting scientific field, Dynamical systems of coupled oscillators. It was a real honour for me to study under his supervision.

I am also grateful for the contributions and advices of my second supervisor Dr Ana Rodrigues. Special thanks for Dr Christian Bick for his understanding and invaluable advice.

Secondly, I extend my thanks to my colleagues at Dynamics Reading Group and mathematics department especially to Damian Smug, Daniel Miller, Lauric Ferrat, Rungployphan Kieokaew and Paul Ritchie for interesting discussions, feedback and tips on computer use.

My special personal thanks to my husband, Haider Ahmed. And, my lovely and friendly thanks to my children Fatima and Mustafa who always pray for me and miss me when I was studying late in the college or going to a conference. May Allah bless you forever.

I would like to give special thanks and appreciation to my mum for her unstoppable prayer for me, wishing me luck. I would like to express my deepest gratitude to every member of my family for their lasting support and encouragement. With my broken heart I give special and great thanks to my father, he died when I was in the first year of my studying PhD. Wherever you are, I'm sure you will be very proud of your the little daughter.

DEDICATION

Dedicated to the memory of my father who always supported me, whatever path I took.

CONTENTS

Page

List of Tables **11**

List of Figures **13**

1 Dynamical systems and coupled oscillators **15**

1.1 Qualitative behaviour of ODEs 15

1.2 Weakly coupled oscillators 17

1.3 Kuramoto's model and coupled phase oscillators 18

1.4 Other examples of chimera states for phase oscillator systems 23

1.4.1 Definitions of a chimera state 23

1.5 Motivation of this work 24

1.6 Essential concepts from dynamics 24

1.6.1 Hyperbolic invariant sets and structural stability 26

1.6.2 Bifurcation theory 27

1.6.3 Types of bifurcation 28

1.6.4 Global bifurcation theory 29

1.6.5 Chain recurrent and invariant sets 29

1.6.6 Poincaré section 30

1.6.7 Numerical simulation continuation and bifurcation analysis 31

1.7 Outline 32

2 Symmetries and the dynamics of coupled systems **34**

2.1 Group and representation theory 35
2.2 Symmetries of dynamical systems 37
2.3 Oscillators and reduction normal form 39
2.3.1 Spatio-temporal symmetries oscillators network 41
2.3.2 The isotropy subgroups $S_n \times \mathbb{T}^1$ 41
2.3.3 The isotropy subgroups of $\Gamma \times \mathbb{T}^1$ 44
2.4 Synchrony and symmetry in networks 46
2.4.1 Tools for symmetric networks 46
2.4.2 Balanced equivalence relations and symmetric networks 47
2.4.3 Symmetry group of networks 50

3 Weak chimera and bifurcations of a six-oscillator system 53
3.1 Definition and existence of a weak chimera state 53
3.2 Weak chimera in six- oscillators networks 55
3.3 Simulation and bifurcation of weak chimera in a six oscillator system 61
3.4 Using parameter symmetries to relate $r > 0$ and $r < 0$ 68

4 Weak chimera solutions and integrability for a system of six oscillators 71
4.1 Integrability and reversibility of the system in A_1 for $\beta = r = 0$ 71
4.1.1 Partition of the set M 74
4.2 Dynamics for the integrable case 76
4.3 Extending the trajectories on H_r to trajectories on M 79
4.4 Dynamics on A_1 and weak chimeras 81

5 Stability of weak chimera chimera solutions for $\beta, r \neq 0$ 85
5.1 Calculating the period for the chimera solutions with $\beta, r = 0$ 86
5.2 Approximation of chimera solutions for $\beta, r \neq 0$ 89
5.3 Bifurcation of the chimera solutions 94

6 Weak chimeras and bifurcations within A_6 99
6.1 Bifurcation of chimera solution within A_6 99

6.2 Stability of chimera states near the saddle-node bifurcation 104
6.3 Stability of chimera states in the full system 107

7 Conclusion **114**
7.1 Summary and main results 114
7.2 Future work 117

A Appendices **119**
A.1 Reversing symmetries of the six oscillator system for $r = 0,\ \alpha = \pi/2$ 119
A.2 Maple code for the chapter 5 121
A.2.1 Code for Figures 5.2, 5.3 and 5.5 121
A.2.2 Code for Figures 5.6 124
A.2.3 Code for Figures 6.2(a),(b) 127

Bibliography **131**

LIST OF TABLES

TABLE **Page**

2.1 Table for isotropy subgroups of eight oscillators 43

3.1 Isotropy subgroup and their fixed-point subspaces for a network of six oscillators 58

5.1 Table for compares the bifurcations of chimeras for (5.22) and (5.1). 97

6.1 Comparing between a discrite and continuous system 106

LIST OF FIGURES

FIGURE **Page**

1.1 Order parameter 20
1.2 Homoclinic bifurcation 27

2.1 Isotropy of eight oscillators 43
2.2 Partial order of fixed-point subspace for $Z_4 \times \mathbb{T}^1$. 45
2.3 Trivial symmetry for a network has four oscillators 49
2.4 Exotic balanced polydiagonal on a symmetric network (A_4) 52

3.1 Example of modular networks 55
3.2 Networks of coupled six oscillators. 57
3.3 Quotient networks 58
3.4 Phase portriats are for sysytem (3.10) [8] and system (3.13). 60
3.5 Time series and phase portraits for system 3.2, 3.13 with $\alpha = 0.5, 1.12, 1.3016, 1.5$. 63
3.6 Time series and phase portraits for system 3.2, 3.13 with $r = 0$ and $\alpha = \pi/2$, $1.64, 1.84, 2.0216$. 64
3.7 Time series and phase portraits for system 3.2, 3.13 with $r = -0.01$ and $\alpha = 1.561, 1.558, 1.5517, 1.97794$. 65
3.8 Bifurcation diagram for the system 3.2, 3.13 with varying α and $r = 0$. 66
3.9 Bifurcation diagram for the system 3.2, 3.13 with varying α and $r = -0.001$. . . . 67
3.10 Parameters symmetry for the system (3.1, 3.12) 69

4.1 The level curves of (4.2). 73
4.2 Description of the flow (4.1) on the invariant set $\overline{M} \subset \mathbb{T}^2$ 74

5.1 Two areas left H_ℓ and right H_r that are subsets of M 86
5.2 The values of y_{max} and y_{min} for (5.5) 88
5.3 The periodic time $T(\tilde{E})$ for (5.1) 89
5.4 Approximation solutions for $\Lambda_1(E)$ and $\Lambda_2(E)$ 94
5.5 Approximation solutions for equation (5.22) 96
5.6 Bifurcation digrams for systems (5.22) and (5.1) 97
5.7 Figure to compare between bifurcation digram for system (5.22) and (5.1). 98

6.1 Bifurcation diagram region of chimera states in the parametr space r, α for sytem(6.3) and time series for system (6.2). 103
6.2 Curve of eigenvalues at bifurcation point ξ^* for the system (6.5) 107
6.3 Time series, snapshots and time frequency for the system (3.6) for an unperturbed initial condition at parameters u^*, v^* and w^* 111
6.4 Time series, snapshots and time frequency for the system (3.6) for a perturbed initial condition at parameters u^*, v^* and w^* 112
6.5 Time series, snapshots and time frequency for the system (3.6) for a perturbed initial condition at parameters u, v and w 113

CHAPTER 1

DYNAMICAL SYSTEMS AND COUPLED OSCILLATORS

Neural systems can be thought of as networks of coupled cells, each of which has comparatively simple dynamics. This chapter gives some background on dynamical systems and synchrony in the qualitative dynamics of networks and introduces to the concept of a chimera state. Section 1.1 introduces types of dynamical system and essential objects in the study of dynamics. In section 1.2, we introduce briefly literature review about weakly coupled oscillators. Section 1.3 highlights the first steps for the Kuramoto model, a coupling function and order parameter. Motivational examples in the study of chimera states and different definitions for chimeras are presented in Section 1.4. Section 1.5 gives the main motivation for this work which is to prove existence of such states. Section 1.6 discusses relevant information from two references [28, 86] and mentions numerical methods that are used to analyse and simulate solutions. Other background references include [30, 33, 51, 95, 96].

1.1 Qualitative behaviour of ODEs

Differential equations play an important role in the sciences to model dynamic behaviours. Any phenomenon can be written as a simple model of ODEs that have one or more variables. These variables vary continuously depending on time [28]. Analytical solutions for some

nonlinear ordinary differential equations are often difficult or impossible to determine. Therefore, since the 1880s, scientists such as Poincaré developed methods to characterize the qualitative aspects of long term behaviour for a solution of a system rather than the quantitative analysis. The technique to study the qualitative behaviour of solutions of these ODEs is called **dynamical systems**. Two main types of dynamical system are encountered in applications. In the first type, the time variable is **discrete** ($t \in \mathbb{Z}$ or $\mathbb{N}$) and there is a **map** that represents function $g : \mathbb{R}^n \to \mathbb{R}^n$, this map defines a discrete dynamical system by $x_{n+1} = g(x_n)$. The set of points $\{x, g(x), g(g(x)), ..., g^n(x)\}$ is the **orbit** of x under g. A point x is a **fixed point** of the discrete system g if $g(x) = x$. The second type is where time is **continuous** ($t \in \mathbb{R}$) [28]. In this thesis our focus will be on continuous dynamical systems described as an ordinary differential equation

$$\dot{x} = \frac{dx}{dt} = f(x,t), \qquad x \in \mathbb{R}^n, \quad t \in \mathbb{R}. \tag{1.1}$$

Such equations are called **autonomous differential equations** if time does not be written explicitly on the right hand side of the equation, whereas it is **non-autonomous** if time does appear explicitly. Let $x(0) = x_0$ be an initial condition for an autonomous differential equation. Then a solution with given x_0 can be thought as a continuous curve in $\mathbb{R}^n$ over time and it is called **integral curve, orbit or trajectory**. This solution can be represented in the space $\mathbb{R}^n$ called the **phase space** of the differential equation. Arrows on the curve (**vector field**) represent the direction of increasing time.

The solution curves of (1.1) with the initial condition x_0 defined on a phase space give a **flow** $\varphi(x,t)$ which is a continuous function of x and t, $\varphi : \mathbb{R}^n \times \mathbb{R} \to \mathbb{R}^n$ such

$$\frac{d}{dt}\varphi(x_0,t) = f(\varphi(x_0,t)) \qquad \text{for all} \quad t \in \mathbb{R},$$

such that the solution through x_0 exists, and $\varphi(x_0,t) = x_0$, at $t = 0$. This solution x is called an **equilibrium point** of the flow iff $\varphi(x^*,t) = x^*$ for all t. In such cases, $f(x^*) = 0$. An orbit through x is **periodic** of (minimal) period $T > 0$ iff the solution x at time t has the same value at time $t + T$, (i.e) $\varphi(x, t+T) = \varphi(x,t)$ for all t, and there is no $0 < s < T$ that satisfies $\varphi(x, t+s) = \varphi(x,t)$. A **periodic orbit** $\mathscr{J}$ is the set of points $\{y : y = \varphi(x,t), 0 \le t < T\}$ which is

a curve in phase space. A generalized notion of this is an invariant set. A set $M \in \mathbb{R}^n$ is called **invariant** under the flow $\varphi(x,t)$ if for any $x \in M$, we have $\varphi(x,t) \in M$ for all $t \in \mathbb{R}$. A set is **positive** (forward) or **negative** (backward) **invariant** if for all $x \in M, \varphi(x,t) \in M$ for all $t > 0$ or $t < 0$ respectively. That means trajectories beginning in an invariant set, remain in the invariant set for all $t \in \mathbb{R}$ [28, 95].

We define sets that are useful to understand asymptotic behaviour of a trajectory in a dynamical system in the long term. Firstly, a point p is called an $\omega-$ **limit point** for $x \in \mathbb{R}^n$, if there exists a sequence $\{t_n\}$ with $t_n \to \infty$ such that $\varphi(x,t_n) \to p$ as $n \to \infty$. Similarly, we can define an $\alpha-$ **limit point** with a sequence $\{t_n\}$ and $t_n \to -\infty$. Then, the ω-(resp. the α) **limit set** is the set all $\omega-$ (resp. α) **limit point** of trajectory through x tends p in forward (resp. backward) time,

$$\Lambda^+(x) = \{p \in \mathbb{R}^n : \exists \{t_n\} \text{ with } t_n \to \infty \text{ and } \varphi(x,t_n) \to p \text{ as } n \to \infty\},$$

$$\Lambda^-(x) = \{p \in \mathbb{R}^n : \exists \{s_n\} \text{ with } s_n \to -\infty \text{ and } \varphi(x,s_n) \to p \text{ as } n \to \infty\}.$$

1.2 Weakly coupled oscillators

The theory of coupled oscillators was pioneered by van der Pol [91, 92] but even before then, Huygens observed "an odd kind of sympathy" between two pendulum clocks [18]. There are many biological, chemical and physical motivations to study coupled oscillators. In term of biological examples, heartbeat models have been studied by van der Pol and van der Mark [93], and there have been studies on the synchronization of fireflies [99, 100] as coupled oscillators. Furthermore, the mechanism for the formation of a living organism is regarded as a fundamental issue in biology, called Morphogenesis. The first systematic theory of synchronization between biological clocks was presented by Winfree [99, 100], and there are now many researchers working in this area, for example: [23, 46, 58]. Murray [63] summarized many applications of oscillator techniques to biology. Besides, biological researchers have used oscillator models to understand the collective motion of fish schooling [70] and emergent behaviour of animal flocking [34]. On the other hand, Assenza and et al. [12] focused on social networks and the emergence of structural patterns out of synchronization

in systems with competitive interactions. Coupled chemical oscillations were studied by Kuramoto in [49] and Belousov-Zhabotinsky [36]. Electronic coupled oscillators have also used the oscillator theory, for example, van der Pol [91] considered relaxation oscillators and forced oscillators in a circuit with nonlinear resistance [92].

The theory of coupled oscillators can explain a large variety of phenomena in neuroscience [94]. For example, oscillators play a role in feature binding [83, 90]. It has been established that phase synchronization is essential in memory processes [24] and the generation of rhythmic motor output [84]. Meanwhile, serious diseases discussed in neural oscillations are neurological disorders [61], such as excessive synchronization during seizure activity in epilepsy, tremor experienced by patients with Parkinson's disease [89] and cortical coordination dynamics, and the disorganization syndrome in schizophrenia [16]. Furthermore, many problems in technology [77] concentrate on oscillatory activity and their effect on the control of external devices in brain-computer interfaces.

The theory of weakly coupled oscillators is well developed. This uses perturbation theory to investigate the dynamics [40] and reduces the dimension of phase space and allow us to understand behaviour such as cluster synchronization in coupled oscillators. However, in the weak coupling limit, certain qualitative dynamics cannot occur, for example, one can not find "oscillator death" whereby the network action of the oscillations is completely suppressed in one or more oscillators [22]. Hoppensteadt and Izkihevich [40] summarize some techniques for weakly coupled oscillators and apply them to neural systems. Guckenheimer and Holmes [33] use the averaging theorem to approximate dynamical systems that have rapidly varying phases.

1.3 Kuramoto's model and coupled phase oscillators

A self-sustained oscillator is a dynamical system (1.1) with a stable limit cycle in the phase space [42]. Let Γ be a continuous function that maps every point on the trajectory of a limit cycle to point on the unit circle, such that x_0 represents $\theta = 0$ and phase is point in $[0, 2\pi) = \mathbb{S}^1$. For an oscillator, we can choose this phase such that the phase has an equation

of motion

$$\dot{\theta} = \omega,$$

where $\dot{\theta}$ represents the rate of change of phase and ω the angular frequency. Note that this description characterises the oscillator only in terms of phase [99, 100]: the amplitude does not enter the description [42].

The dynamics of large populations of coupled oscillators have inspired many researchers. Winfree significantly developed this area [99, 100]. In [47], Kuramoto noticed that dynamical behaviour of a uniform system may have numerous coupled oscillators that reorganize themselves with time. Kuramoto [48, 49] introduced a model of self- sustaining oscillators which explains an interaction between every two phase oscillators in a $N-$globally coupled system. This model is described as a non-linear first order differential equation of finite global coupled phase oscillators,

$$\dot{\theta}_i = \omega_i + \sum_{j=1}^{N} g(\theta_j - \theta_i), \tag{1.2}$$

where $\theta_i \in [0, 2\pi) = \mathbb{T}$ and denotes the phase of the ith oscillator, and N is the total number of oscillators. The model often considered in the limit $N \to \infty$, and the $1/N$ factor is present to keep the model well- behaved in this limit, ω_i is the natural frequency of the ith oscillator that is distributed according to a probability density $s(\omega)$ (typically symmetric about some frequency Ω) and g is called the phase interaction or coupling function. Kuramoto studied the system (1.2) in the simplest case, where we can write interaction function as

$$g(\theta_j - \theta_i) = \frac{K}{N} \sin(\theta_j - \theta_i), \tag{1.3}$$

where $K \geq 0$ is a coupling constant and N is the number of oscillators. Then the system (1.2) becomes

$$\dot{\theta}_i = \omega_i + \frac{K}{N} \sum_{j=1}^{N} \sin(\theta_j - \theta_i). \tag{1.4}$$

Noted that the oscillators are identical if $\omega_i = \omega$, then any small coupling $K > 0$ leads to synchronization (phases have the same frequency) [40].

In [100] Winfree suggested visualizing the dynamics of the phases as points in the unit disk in the complex plane. As a result, the Kuramoto model can be written in terms of a

complex order parameter:

$$re^{i\psi} = \frac{1}{N}\sum_{j=i}^{N} e^{i\theta_j}, \tag{1.5}$$

where $r(t)$ with $0 \leq r(t) \leq 1$ measures the coherence of oscillators population, and ψ is the average phase, see Figure 1.1. We say that the order parameter describes the "mean field" of the system. The order parameter r is often depicted as an arrow from the center to the point $re^{i\psi}$ within the unit circle and each oscillator as a point moving around the unit circle. If r is a small value that corresponds to the system being incoherent (oscillators separate around the circle), while $r = 1$ implies the oscillators are in total synchronization (the oscillators rotate closer together with the same average phase $\psi(t)$).

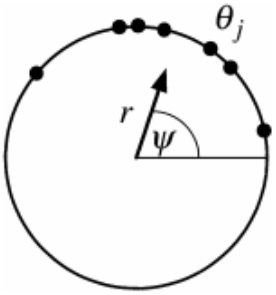

Figure 1.1: *Order parameter shows a synchrony relation between phase oscillators θ_j by r and the average phase ψ for (1.5). Reproduced from [87] with permission of the author.*

Taking equation (1.5) and multiplying both sides by $e^{-i\theta_i}$, we get

$$re^{i(\psi-\theta_i)} = \frac{1}{N}\sum_{j=i}^{N} e^{i(\theta_j-\theta_i)}, \tag{1.6}$$

and equating imaginary parts, we obtain

$$r\sin(\psi-\theta_i) = \frac{1}{N}\sum_{j=1}^{N} \sin(\theta_j-\theta_i). \tag{1.7}$$

Substituting this into the equation (1.4) we can write it in terms of the order parameter,

$$\dot{\theta}_i = \omega_i + Kr\sin(\psi-\theta_i), \qquad i = 1,2,...,N. \tag{1.8}$$

In this formulation each oscillator is coupled to the common average phase with coupling strength given by Kr. However, the phases θ_i move independently of each other. As a

consequence, the oscillator interacts with the others through the mean field $re^{i\psi}$. This way of imaging the moving oscillators around the circle greatly simplifies how we can think about synchronization. Note that full synchronization corresponds to $r = 1$.

Sakaguchi and Kuramoto studied interaction between oscillators depending on phase parameter α [78] by considering the coupling function,

$$g(\phi) = -\sin(\phi - \alpha). \tag{1.9}$$

This reduces to (1.3) in the special case $\alpha = 0$. Hansel, Mato and Meunier [37], inspired by coupling between neural oscillators, considered the more general interaction function with two parameters α and r that we consider in this work:

$$\begin{aligned} g(\phi) &= -\sin(\phi - \alpha) + r\sin(2x) \\ &= \cos(\phi + \beta) + r\sin(2x), \end{aligned} \tag{1.10}$$

with parameters r and α (or β). In Chapters four and five, we use β rather than $\alpha = \pi/2 - \beta$ because $r = \beta = 0$ is an integrable limit [1, 73].

In the limit $N \to \infty$, the sum in (1.2) is replaced by an integral, and the order parameter (1.5) can be written as an integral for infinity many oscillators. If we allow coupling to vary throughout the population then we can use this to investigate so- called chimera states [2, 17, 50, 52, 69]. In this work, we do not need to ues the order parameter because we consider a small network with a fixed number of oscillators [8, 73].

In 2002 Kuramoto and Battogtokh [50] extended the case of the phase oscillator model with global coupling to finite range nonlocal coupling with distributed natural frequencies [49, 87]. They brought attention to the fact that whole population of identical phase oscillators can separate into two groups with of qualitatively different dynamics: one consisting of synchronized oscillators and the other desynchronized as shown in [50, Figure 1]. They considered the system:

$$\frac{\partial}{\partial t}\phi(x,t) = \omega - \int_0^1 G(x - x')\sin(\phi(x,t) - \phi(x',t) + \alpha)\,dx', \tag{1.11}$$

where $\phi(x,t)$ is the phase of the oscillator at position x at time t, $0 \le x \le 1$ and a spatial coupling function or kernel G that varies with the distance.

$$G(x-x') = \frac{\kappa}{2}\exp(-\kappa|x-x'|).$$

In 2004 [2], Abrams and Strogatz studied the same system (1.11) of nonlocal coupled oscillators and used with different spatial coupling function function

$$G(x-x') = \frac{1}{2\pi}(1+A\cos(x-x')), \qquad 0 \le A \le 1 \text{ and } -\pi \le x \le \pi.$$

This provides nonlocal coupling between the oscillators and allowed them to solve analytically this system. They named this phenomenon “chimera" because the solution involves coherent and incoherent domains together which it is regarded as interesting and complicated. They imagined this solution as a chimera which is a mythical Greek monster. This animal has a lion's head and a goat's body and refers to anything with a strange or incredible shape. They were also able to discover bifurcations where the chimera state was born and vanishes [2, 3].

In [66] Omel'chenko et al. studied the behaviour of chimeras as a regular macroscopic pattern in space, with irregular motion in time. They considered a ring of N identical nonlocally coupled phase oscillators

$$\dot{\phi}_i(t) = \omega - \frac{2}{N}\sum_{j=1}^{N} G(x_k - x_i)\sin(\phi_i(t) - \phi_j(t) + \alpha),$$

where $\alpha \in (0, \pi/2)$, x_i are uniformly distributed of over $[-1,1]$ and every phase has spatial position $x_k = -1 + 2k/N$, $k = 1,2,...,N$ and the spatial coupling function function[97] is

$$G_{step}(x,r) = \begin{cases} 1/(2r) & \text{if } |x| \le r \\ 0 & \text{if } |x| > r. \end{cases}$$

In summary, there are different models of coupled phase oscillators depending on number of oscillators, coupling strength etc. These ideas for designing models make them more flexible to analyse and richly informative. This has motivated many studies of coupled systems in a wide range of disciplines.

1.4 Other examples of chimera states for phase oscillator systems

Dynamical states where coherence (synchrony) and incoherence (asynchrony) occur at the same time have been found in a wide variety of contexts [19, 44, 81, 82, 102]. Since their original discovery in coupled phase oscillators [50] and being named "chimeras" by Abrams and Strogatz [3], non-local interactions were originally regarded as essential for chimeras to emerge [32, 67]. However, chimera states have been found for systems with global coupling [65, 76, 79, 80], mean-field coupling [13] and even local coupling [14, 54]. Wolfrum and Omelchenko examined the detailed dynamical properties of chimera states in small populations of coupled phase oscillators [101]. However, exact solutions for chimera state have, in general, only been found at a population level [1]. There are a wide range of applications including chemical oscillations [49, 88], electronic circuits [26, 79], mechanical oscillators [60], brain dynamics [55] and optical experiments [35].

Recently, chimera states in a network of planar oscillators have been analysed by Laing [53]. His analysis uses amplitude and phase. In addition, chimera states have been analysed on the sphere surface. This analysis involves a demonstration of the existence of two distinct types of chimera states spot and spiral in a network of identical coupled oscillators [72]. Whether a particular system state is a chimera depends critically on the definition of coherence and incoherence. A particular approach was introduced by Ashwin and Burylko [8] who define a weak chimera as a type of invariant set with partial frequency synchronization. They showed (a) globally coupled identical phase oscillators cannot have weak chimera states and (b) there can be weak chimera state in some small networks of identical phase oscillators.

1.4.1 Definitions of a chimera state

Chimera states have been described in various ways. For example, the first definition was "an array of identical oscillators splits into two domains: one coherent and phase locked, the other incoherent and desynchronized" [2]. Another definition was "a chimera state

is a spatiotemporal pattern in which a network of identical coupled oscillators exhibits coexisting regions of synchronous and synchronous oscillation" [72]. A further definition is that "chimera states occur in a spatially homogeneous system, as regions of irregular incoherent motion coexist with regular synchronized motion, forming a self-organized pattern in a population of non locally coupled oscillators" [101]. In yet another paper, Laing inserted that "chimera states occur in networks of coupled oscillators, and are characterized by having some fraction of the oscillators perfectly synchronized, while the remainder is desynchronized" [53]. This motivated a precise definition of Ashwin and Burylko [8] that we give in Definition 3.1.

1.5 Motivation of this work

Since the start of study of coupled oscillators, numerical methods have played a crucial role in understanding the dynamics of networks and finding chimera states in dynamical networks. In most cases, chimera states have been found numerically for large numbers of oscillators [50, 53, 87]. Ashwin and Burylko [8] focused on a small number of oscillators and have numerically shown that there is a weak chimera state for the six oscillator system we study here. The motivation of this work is to give a rigorous proof of the existence of a weak chimera solution in this network and to study bifurcations of this chimera.

1.6 Essential concepts from dynamics

In the theory of nonlinear dynamical systems, there are essential concepts used to describe their properties and behaviour [28, 51, 57, 86, 95]. In order to introduce mathematical definitions of stability concepts, we consider the differential equation (1.1).

A point x for (1.1) is **Liapounov stable** or **stable** iff for all $\epsilon > 0$ and $y \in \mathbb{R}^n$; there exists $\delta > 0$ such that if $|\varphi(x, t_0) - \varphi(y, t_0)| < \delta$ then $|\varphi(x, t) - \varphi(y, t)| < \epsilon$ for all $t \geq t_0$, $t_0 \in \mathbb{R}$. This point is **quasi-asymptotically stable** iff there exists $\delta > 0$ such that if $|\varphi(x, t_0) - \varphi(y, t_0)| < \delta$ then $|\varphi(x, t) - \varphi(y, t)|$ converges to 0 as t goes to ∞. Finally, it is **asymptotically stable** or

attracting iff it satisfies both Liapounov stable and quasi-asymptotically stable [28]. When an equilibrium is Liapounov stable but not attracting it is called **neutrally stable** [86].

We now relate linear stability and asymptotic stability of nonlinear systems [57, 86]. Linearization about an equilibrium point x^* is a fundamental technique that is followed to analyse the nature of solutions for a nonlinear system close to this point. This follows from a study of the Taylor expansion for (1.1) around the equilibrium x^*. Let $x = x^* + \xi$, then we can use Taylor expansion to write

$$\dot{\xi} = f(x^* + \xi) = f(x^*) + D_f(x^*)\xi + O(|\xi|^2),$$

where $O(|\xi|^2)$ refers quadratic terms which are very small when ξ is small. Consequently, since x^* is an equilibrium then $f(x^*) = 0$, hence

$$\dot{\xi} = D_f(x^*)\xi + O(|\xi|^2), \tag{1.12}$$

where $D_f(x^*)$ is the **Jacobian matrix** at an equilibrium point that is a matrix of partial derivatives of f [86]. Note that

$$\dot{\xi} = D_f(x^*)\xi,$$

is called the **Linearization** at a fixed point, and we can get information about the stability of the original system (1.1) by looking at how the perturbation grows or decays as time goes on. For example, if all eigenvalues are $\lambda_i > 0$ or $\lambda_i < 0$ (where λ_i are eigenvalues of $D_f(x^*)$), then the perturbation $\xi(t)$ grows or decays exponentially [86]. Now, we briefly state stability for periodic orbits.

If $\mathscr{J}$ is a periodic orbit for period T of (1.1) and $y \in \mathbb{R}^n$ on the $\mathscr{J}$, then $\varphi(x, T) = y$. Hence, we can use the notation of the distance between a point and a set to define a neighbourhood $N(\mathscr{J}, \epsilon)$ of the periodic orbit $\mathscr{J}$ is

$$N(\mathscr{J}, \epsilon) = \{x \in \mathbb{R}^n : \ |x - y| < \epsilon \ \text{ for some } y \in \mathscr{J}\}.$$

A periodic orbit $\mathscr{J}$ is **Liapounov orbitally stable** if for all $\epsilon > 0$ there exists $\delta > 0$ such that if $|\varphi(x, t_0) - \varphi(y, t_0)| < \delta$ then $\varphi(x, t) \in N(\mathscr{J}, \epsilon)$ for all $t \geq t_0$. Also, it is **asymptotic orbitally stable** if it is Liapounov orbitally stable and there exists $\delta > 0$ such that if $x \in N(\mathscr{J}, \delta)$ then $d(\varphi(x, t), \mathscr{J}) \to 0$ as $t \to \infty$ [28, 95].

1.6.1 Hyperbolic invariant sets and structural stability

An equilibrium x^* of (1.1) is **hyperbolic** for a vector field (resp. map) iff $D_f(x^*)$ has no eigenvalues with zero real parts (resp. has no multipliers on the unit circle) [28, 95]. If x^* is hyperbolic then it is persistent under sufficiently small perturbations of (1.1).

Initially, we concentrate on classification of hyperbolic solutions for an equilibrium. Suppose that x^* is a hyperbolic equilibrium point. Then x^* is a **sink** or **stable node** if all eigenvalues of $D_f(x^*)$ have strictly negative real part and a **source** or **unstable node** if all eigenvalues of $D_f(x^*)$ have strictly positive real part. Otherwise, x^* is a **saddle** point, i,e. if some, but not all, of the eigenvalues have positive and negative real part. Finally, if the eigenvalues of linearization are purely imaginary, then x^* is the non-hyperbolic point and called a **center** [95]. A periodic orbit $\mathscr{J}$ with minimal period T is a **hyperbolic periodic orbit** if one Floquet multiplier for the periodic orbit has modulus one and the remaining Floquet multipliers [28] do not have modulus one.

The neighbourhood of flows with a hyperbolic equilibrium will have a similar nearby hyperbolic equilibrium: we say the equilibrium persists. However a nonhyperbolic equilibrium is not persistent under a small perturbation of the vector field. As a consequence, there is a topological equivalence between the flow near a hyperbolic fixed point of a nonlinear system and the linearization. This is expressed in the next theorem:

Theorem 1.1. *[28, Theorem 4.9] If x^* is a hyperbolic equilibrium point for (1.1) then on some neighbourhood of this hyperbolic point there is a continuous invertible map H which takes orbits of the nonlinear flow onto orbits of the linearized flow $e^{(tD_f(x^*))}$ and preserves the direction of flow on these orbits.*

An equilibrium is said to be **structurally stable** if the topology of nearby orbits does not change under an arbitrarily small C^1 perturbation of the system. Note that hyperbolic equilibria are structurally stable, while orbits nonhyperbolic equilibria such as centres can change considerably even for arbitrarily small perturbations [57, 95].

1.6.2 Bifurcation theory

Consider a first-order autonomous differential equation with one parameter as,

$$\dot{x} = f(x, \mu), \tag{1.13}$$

where $x \in \mathbb{R}^n$ and $\mu \in \mathbb{R}$ is a real parameter. The qualitative behaviour orbits of the flow can change owing to variations in the value of a parameter μ. These behavioural changes of the dynamics are called **bifurcations**, and a parameter value at which they occur is called a **bifurcation point**. Formally, bifurcation theory is the study of the qualitative changes that occur close to non-hyperbolic solutions of a dynamical system as a result of varying the parameters [28]. There are many ways of understanding possible changes that occur in differential equations, ranging from an analytic description to a topological feature of a vector field, for example, the number of equilibrium points or periodic orbits. In this section, we review some simple techniques to describe bifurcations of an equilibrium point and limit cycle in a continuous and discrete dynamic. The theory for bifurcations of fixed points of maps is very similar to the theory for vector fields. Therefore, we will not include as much detail about bifurcations of fixed points but merely highlight the differences when they occur.

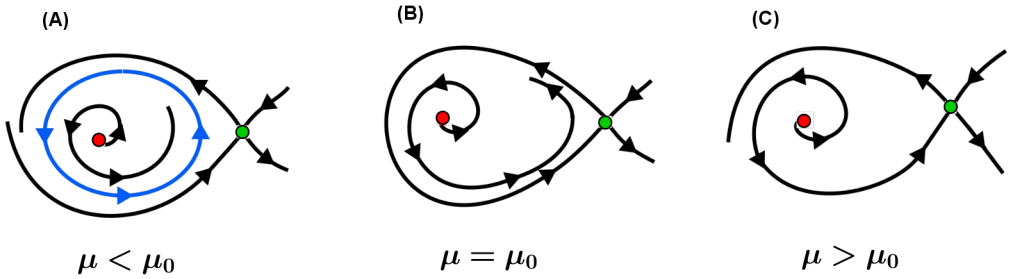

Figure 1.2: *Three sketches represent phase portraits of homoclinic bifurcation of a planar system. Before this bifurcation when $\mu < \mu_0$, the blue curve shows a stable periodic orbit and the red/ green points correspond to unstable focus and saddle point respectively (Panel (A)). The homoclinic bifurcation happens when a stable periodic orbit hits the green saddle point and vanishes at $\mu = \mu_0$: there is a trajectory that begins and ends at the same point (the green saddle point)in Panel (B). The right panel shows a phase portrait after this bifurcation, there is a trajectory that connects between the green saddle point and the unstable red focus point when $\mu > \mu_0$.*

1.6.3 Types of bifurcation

Bifurcations may involve equilibria, periodic orbits or both of them at the same time. The information in this subsection can be found in many references, for example, [28, 51, 86, 95]. Bifurcation involving only equilibria occur at non hyperbolic points (x_0, μ_0), where the Jacobian matrix has eigenvalues with zero real part at this point. The most common bifurcation is a **saddle node bifurcation**, where two equilibria (one is a stable node, and another is the saddle) collide to create a linearly degenerate point before they vanish as the parameter is varied. Another type of bifurcation is a **transcritical** in which two equilibria exist at all nearby parameters except at the bifurcation point where they come together. It occurs when two points (stable and unstable) swap their stability as a parameter is varied. Finally, a **pitchfork bifurcation** can be found in the presence of symmetries. In this bifurcation, the number of equilibria changes from one to three. There are two different types of pitchfork bifurcation; a **supercritical bifurcation** in which there are stable branches on both sides of the bifurcation, and a **subcritical bifurcation** where there are unstable equilibria on both sides of the bifurcation.

Another type of a local bifurcation involves both an equilibrium and a limit cycle. The **Andronov-Hopf bifurcation** for a vector field occurs when an equilibrium has a pair of complex conjugate eigenvalues of $D_f(x, \mu)$ that pass through the imaginary axis. Then the equilibrium switches its stability, and a periodic solution appears. Similar to the pitchfork there are two types: **supercritical and subcritical Hopf bifurcation** depending on branch stabilities. A **Saddle node bifurcation of periodic orbits** involves two limit cycles. As a parameter is varied, the limit cycles coalesce and create half stable limit cycle then annihilate. The change in stability of limit cycle is associated with the appearance of two similar limit cycles. A bifurcation that involves three limit cycles coming together and forming one limit cycle is called a **pitchfork bifurcation of periodic orbits**.

1.6.4 Global bifurcation theory

The previous subsection considers only bifurcations with changes near an equilibrium point or a periodic orbit. There are however other bifurcations that can create large periodic solutions and that are not reducible to a local analysis.

An interesting example of such bifurcations involve **saddle connections**. Bifurcations of a **Homoclinic orbit** occur if there is a connection of trajectory to a saddle point (an orbit $\varphi(x,t) \to x_0$ as $t \to \mp\infty$) where x_0 is an equilibrium of the flow. Shown in Figure 1.2, this bifurcation occurs at a parameter μ_0 in the two dimensional phase space. Homoclinic bifurcation reveals changes to the invariant sets as a parameter is varied. Let μ be a parameter such that for $\mu > \mu_0$ there are three objects: an unstable focus (the red point) inside a stable periodic orbit (blue curve) that closed to a saddle point (the green point) outside the periodic orbit (see Figure 1.2(A)). This saddle point has two branches (stable and unstable manifolds) as sketched in (A). At $\mu = \mu_0$, a homoclinic orbit is created at a collision of the limit cycle with the saddle, and the branches (stable and unstable manifold) of the saddle point are connected together (Figure 1.2(B)). A small perturbation of the system can destroy a homoclinic orbit because it is structurally unstable according to Peixoto's [28, Theorem 4.13] that happen at $\mu < \mu_0$ as sketched in Figure 1.2(C).

More complex global bifurcations are associated with a **heteroclinic path** in phase space which joins different hyperbolic equilibrium points. If a trajectory connects one saddle point to another or saddle to itself is called **saddle connection**, for example, if x_0 and y_0 are saddle points then the flow $\varphi(x,t) \to x_0$ as $t \to \infty$ and $\varphi(x,t) \to y_0$ as $t \to -\infty$, [51].

1.6.5 Chain recurrent and invariant sets

Recurrence is a topological property of objects in the dynamical system. It describes aspects of the eventual dynamical behaviour of the orbits of a map or flow. Both equilibria and periodic orbits display recurrence in the sense that they return to their initial condition infinitely often. There are different possible definitions for the recurrence according to type of a flow. In [4], Alongi and Nelson discussed six types of recurrence and relate their

properties. In this thesis, we consider the following chain recurrence.

Definition 1.1. *[4, Definition 2.7.1] Suppose $x, y \in X$ and $\epsilon, T > 0$, and $\varphi(x,t)$ is a flow on a metric space (X,q). We say there is $(\epsilon,T)-$**chain** from x to y with respect to $\varphi(x,t)$, if there is a finite subset $x = x_0, x_1, ..., x_{n-1}, x_n, y_n = y$ of X and $t_i \in [T,\infty)$, $i = 0,1,2,..,n$ such that*

$$q(\varphi(x_i,t_i),y_i) < \epsilon \quad for \ \ i = 1,2,...,n-1, \ and \ \ x_{i+1} = y_i.$$

Note that, the above definition is for forward time. Moreover, this chain is automatically considered as an $(\epsilon,T)-$chain from y to x for the time reversed flow. Under the same a flow φ_t and metric q, we define three important notions that depend on a direction of the flow [4, 10]. Firstly, **forward chain limit set** Ω_+ of x is the set all $y \in X$ such that there is an $(\epsilon,T)-$chain from x to y for the flow φ_{+t} for all ϵ and $T > 0$. Also, for the reversed time, **backward chain limit set** Ω_- of x is the set all $y \in X$ such that there is an $(\epsilon,T)-$chain from x to y for the flow φ_{-t} for all ϵ and $T > 0$. Additionally, there is an equivalent relation between x and y such that $x, y \in X$, if there is two forward chain limit sets $\Omega_+(x)$ and $\Omega_+(y)$ for (resp. x, y), then these points are **chain equivalent** $\sim$ if $x \in \Omega_+(y)$ and $y \in \Omega_+(x)$. We can say $x \in X$ is **chain recurrent point** if $x \sim x$. The set of all chain recurrent points of φ_t is called **chain recurrent set**. We use this in our definition of a weak chimera in chapter three.

1.6.6 Poincaré section

The French mathematician Henri Poincaré (1854-1912) set up a connection between continuous system and its discrete dynamics. Poincaré section allows one to study maps induced by a flow [57] in a natural way. We will use this technique in Chapter five. Consider differential equation (1.1), and suppose that there are a periodic orbit $\mathscr{J}$ and a point $x_0 \in \mathscr{J}$. The aim from this method reduces the n-dimensional phase space into a $(n-1)-$ dimensional surface. Then, it is possible to find surface of a local cross-section $\Sigma \subset \mathbb{R}^n$ of dimension $n-1$ called a **Poincaré section**. It intersects transversely the orbit $\mathscr{J}$ at x_0. A trajectory starting at $x_0 \in \Sigma$ returns to the same point x_0. Nearby points also return nearby at the **first return**. We represent this process as a map P. Suppose x_0 has a sufficiently small neighbourhood U in

Σ and define the map $P : U \to \Sigma$ by,

$$P(x) = \varphi(x, \tau(x)),$$

where $\phi(x, \tau(x)) \in \Sigma$, $\phi(x, T) \notin \Sigma$ for $0 < T < \tau(x)$, $\tau(x)$ is the time of first return of point x to the section Σ. This map P is called the **first return map** or **Poincaré map** [28, 95]. The fixed point x_0 of Poincaré map satisfies $P(x_0) = x_0$ which correspond to periodic orbit for (1.1).

1.6.7 Numerical simulation continuation and bifurcation analysis

Generally, a mathematical model of a dynamical system involves two quantities: phase space variables and parameters that change the behaviour of a dynamical system. For example, the Kuramoto model with the coupling function is a nonlinear dynamical system (1.10) with two parameters α and r. Such systems are often difficult to solve analytically, even if we restrict to equilibria. Therefore, numerical methods are an important technique to approximate solutions by numerical integration. There are many packages that can be used to numerically approximate solutions, plot phase portrait and time series.

An algorithm to find equilibria or periodic solutions and examine how they change over a range of values for parameters is called numerical continuation. This method involves calculating the stability of equilibrium points or limit cycles for a solution when parameters are varied. Numerical continuation deals with a nonlinear system has the similar form of (1.13) such that $f(y, \mu) = 0$, and choosing an observable $F : \mathbb{R}^n \to \mathbb{R}$, $F(x) = y$, where we plot the bifurcation diagram with coordinates (y, μ) [51]. This diagram displays qualitative information about ODE at every value of a parameter, where y become as a function of μ. Also, it has equilibria curve that its points satisfy $f(y, \mu) = 0$.

Several continuation software packages have been developed to support the analysis of bifurcation, for example, MATCONT, AUTO, XPPAUT. In addition, the lectures [20] explain numerical methods that are used in these packages software. Several books [21, 68] provide theory and practical examples of continuation. In this thesis, we use XPPAUT to plot bifurcation diagrams and MATLAB and MAPLE for simulations for the model.

1.7 Outline

This thesis is organized into seven chapters. This chapter describes briefly some essential background for this work. We introduce some notions and definitions for dynamical systems, such as local and global bifurcations. A literature review is presented about weakly coupled oscillators chimeras, the Kuramoto model and coupling function. We mention some examples and definitions for chimera states. We use the Poincaré section to explain the connection between continuous and discrete dynamics. Also, we refer to some methods used to simulate and analyse results of this work.

Chapter two gives some background information beginning with a description of symmetry groups, isotropy subgroups and fixed point subspaces. We consider equivariance which is a property of a dynamical system that means the elements of group commute with a nonlinear vector field. This chapter highlights two approaches to find invariant subspaces in coupled systems. The first one uses isotropy subgroups to get a flow invariant subspace and the second considers balance colourings to get a flow invariant subspace. These balanced colourings may be not associated with any symmetry in which case we call the balanced colouring exotic. We consider exotic invariant subspace to find chimaera states in the next chapter.

Chapter 3 concentrates on bifurcations of chimera states for a system of six coupled phase oscillators studied in [8]. The chapter starts with some background on the existence of chimera states. Then, we use invariant subspaces to reduce the system of six coupled oscillators to a planar system. We also present a numerical bifurcation analysis of the chimera in this system. To do this, we use the numerical continuation to plot bifurcation diagrams and study stability.

Chapter 4 is restricted to find chimera states for a particular value of the parameters. We use an analytical approach to prove that there is an integral of the motion of this system of coupled phase oscillators when coupled parameters β and r equal zero. We prove some lemmas to describe the motion of flow. Finally, the main topic for this chapter is to prove that there is an infinite number of chimera states for this system when there is an integral of the motion.

The analysis of chimera states is extended in chapter 5 for the two parameters β and r away from zero. We translate the parameters to the original to study stability and bifurcation numerically for a chimera with sufficiently small parameters. In our study, the function of the first return map is constructed to approximate chimera states near the integral motion. Firstly, we use the Poincare map to find analytically chimera states at specific of level curve and parameters. Then, the numerical integral is employed to prove approximately chimera states. We find this result for various values of parameters that have a remarkable effect on the number of chimeras. Also, this chapter introduces comparing between this approximate findings and continuation results in chapter three to reveal the similarities between values of bifurcation points for both methods.

In chapter 6, we consider another invariant subspace A_6 to prove the existence of chimera states by using numerical simulation. This subspace was suggested by Yuri Maistrenko (pers. comm). We rewrite the system of six coupled phase oscillators within A_6. Then, a reduction of this system is by phase differences to get an ODE as a flow on a circle. The discussion of dynamical of this equation help us to determine regions where chimera states exist. Rewriting the full system of six oscillators in term of phase differences allows us to study the dynamics near this bifurcation point. The sign of eigenvalues provides information about the stability of the bifurcating solutions in A6. We find numerically there are chimera states within A6 that are stable in the full system.

In chapter 7, we summarise our work and present a brief review of the primary results and some possible future works. Some appendices include MAPLE code is used to solve an integral equation for the chapter 5.

Note 1. *The material in chapters 4 and 5 is under revision for publication in a journal, under the title "Existence and stability of chimera states in a minimal system of phase oscillators".*

CHAPTER 2

SYMMETRIES AND THE DYNAMICS OF COUPLED SYSTEMS

We consider dynamical systems that consist of a number of simple systems coupled together as a network. Symmetries are of great interest in applications and impose interesting structures on the dynamics of such coupled systems. In the particular case of symmetrically coupled systems, there are flow invariant subspaces that can be characterized by the symmetries. Note, these flow invariant subspaces constrain and provide a framework to understand the dynamics. In 1992 Ashwin and Swift [11] introduced a strategy for symmetrically coupled oscillators to find flow-invariant subspaces by characterizing their isotropy subgroups and fixed-point subspaces. Later, Antoneli and Stewart [5] noticed that flow invariant subspaces can also arise from balanced colouring for the network that are not fixed-point space colourings and these called exotic balanced colourings. We introduce both methods in this chapter.

A dynamical system has a symmetry if the structure of a system of ODEs is unchanged under some transformations of the variables. The set of transformations form a group [30]. Therefore section 2.1 states some background about transformation under composition groups and group representation. Section 2.2 discusses some tools for symmetries in the system. We introduce coupled phase oscillators as a normal form for coupled oscillators and discuss spatio-temporal symmetries for different groups in section 2.3. Finally, section

2.4 uses symmetries in a network to explain the relation between symmetry and synchrony.

2.1 Group and representation theory

Representation theory [25, 43] studies the action of a group on a vector space. Here, we concentrate on specific aspects of this theory that can be used to study the symmetry properties of a dynamical system [29, 30]. The map $f : G \rightarrow H$ is called a **group homomorphism** between groups $(G,\cdot)$ and $(H,*)$ if $f(a\cdot b) = f(a) * f(b)$ for all $a,b \in G$. This map is called a **group isomorphism**, if it is a homomorphism and bijective. Note that if there is an isomorphism between the groups $(G,\cdot)$ and $(H,*)$, we say that $(G,\cdot)$ and $(H,*)$ are isomorphic and write $(G,\cdot) \cong (H,*)$.

Many interesting examples of groups are transformation groups. Let V be a vector space over $\mathbb{R}$ or $\mathbb{C}$. A **general linear group** $GL(V)$ over V is the group of all the invertible linear transformations of V [27]. If $V = \mathbb{R}^n$ then we say that $GL_n(\mathbb{R})$ is a general linear group of dimension n over the field $\mathbb{R}$. Any matrix group on $\mathbb{R}^n$ is a subgroup of $GL_n(\mathbb{R})$. We will concentrate on compact Lie groups Γ which have the structure of a differentiable manifold and can be thought of as closed subgroups of $GL_n(\mathbb{R})$. Compact Lie groups can be classified as: continuous or finite. The main finite groups [27, 29, 75] that we shall consider the following:

1. A group G is called **cyclic** of order $n \in N$ if there exists an element g belonging to G such that $G = \langle g\rangle = \{e, g, g^2, ..., g^{n-1} : g^n = e\}$. The element g is called a **generator** of the cyclic group because every element in the group can be written as a power of g. This group is represented by the symbol Z_n. Note that this is isomorphic to the group of rotation by multiples of $\frac{2\pi}{n}$ about the origin on the plane.

2. The full permutation group of any finite set A is called the **symmetry group or permutation group of** A, and it is represented by the symbol $S(A)$. In the special case $A = \{1,2,..n\}$, we write $S_n = S(A)$ and note the number of elements of S_n is $n!$.

3. For every positive integer $n \geq 3$, the regular polygon with n sides has a group of symmetries, called **Dihedral group**, which is generated by two elements σ (rotation) and τ (reflection). This group is denoted by D_n such that $D_n = \{e, \sigma, ..., \sigma^{n-1}, \tau, \sigma\tau, ..., \sigma^{n-1}\tau : \tau^2 = e, \sigma^n = e \text{ and } \sigma\tau = \tau^{n-1}\sigma\}$. Note that if $n \geq 3$ then D_n is not a commutative or cyclic group. D_n has order $2n$, and the group is isomorphic to rotations and reflections in the plane that preserve a regular $n-gon$.

Some examples of compact Lie continuous groups [27] are:

1. Recall that an $n \times n$ matrix B is called **orthogonal** in $\mathbb{R}^n$ if it is invertible and $B^{-1} = B^T$ or $(BB^T = I)$. These matrices form a subgroup of the group of $GL_n(\mathbb{R})$, called the **orthogonal group** and denoted $O(n)$.

2. A **special orthogonal group**, $SO(n)$ consists of all orthogonal matrices with determinant +1. Note $\dim(SO(n)) = n-1$. When $n = 2$, the special orthogonal group $SO(2)$ consists of counterclockwise rotations about the origin,

$$B = \begin{bmatrix} \cos\theta & -\sin\theta \\ \sin\theta & \cos\theta \end{bmatrix}$$

in the plane, and is isomorphic to $\mathbb{S}^1 = \mathbb{T}^1$.

3. The n-dimensional torus is $\mathbb{T}^n = (\mathbb{S}^1)^n$, such that $\mathbb{T}^n = \{(\theta_1, \theta_2, ..., \theta_n) : \ \theta_i \in \mathbb{S}^1, i = 1, 2, ..., n\}$. This acts on $\mathbb{C}^n$ by the diagonal matrix,

$$B = \begin{bmatrix} e^{i\theta_1} & 0 & \dots & 0 \\ \vdots & \vdots & \ddots & \vdots \\ 0 & 0 & \dots & e^{i\theta_n} \end{bmatrix}$$

which can be seen as an action on $\mathbb{R}^{2n}$.

We are interested in how these groups act as a linear transformation on a vector field. A **linear action** of a compact Lie group Γ on the vector space V is a smooth homomorphism $\rho : \Gamma \to GL(V)$ [29]. If we define $\gamma.v = \rho(\gamma).v$ for $\gamma \in \Gamma$, then ρ is a homomorphism under the following conditions:

1. $(\gamma\delta)v = \gamma(\delta v)$, for all $\gamma, \delta \in \Gamma$ and $v \in V$.

2. $ev = v$ where e is the identity element of Γ, for all $v \in V$.

Note that the group $\rho(\Gamma)$ is a group of matrices and a subgroup of $GL(V)$.

Equivalence relations play an important role in group theory. A relation $\sim$ on a set A is called an **equivalence relation** if its elements satisfy three conditions, reflexive, symmetric and transitive [27]. A particular example is called the **conjugacy relation**. For $a, b \in G$ we say that $a \sim b$ or a is **conjugate** to b in G, if there exists an element $x \in G$ such that $b = xax^{-1}$. It partitions any group into classes called **conjugacy classes**, such that if $a \in G$ then the conjugacy class of a is $[a] = \{x \in G : x \sim a\}$ [38].

2.2 Symmetries of dynamical systems

Golubitsky et al. [30] summarized ways to utilize group theory for analysing the bifurcation of ordinary differential equations with symmetry. Approximate symmetries can be seen in many natural phenomena and so they are often present in mathematical models. Once we obtain general results for arbitrary symmetries, they are then also applicable to other phenomenon. Moreover, they noted that bifurcation for a system with symmetry can be quite different to bifurcations for a system without symmetry. Golubitsky et al. gave some observations and definitions to study symmetry that will be stated here briefly. As in (1.1) suppose that

$$\frac{dx}{dt} = f(x), \tag{2.1}$$

is a system of ODEs for $x \in \mathbb{R}^n$, where $f : \mathbb{R}^n \to \mathbb{R}^n$ is smooth, and let Γ be a group acting linearly on $\mathbb{R}^n$. If

$$f(\gamma x) = \gamma f(x),$$

for all $x \in \mathbb{R}^n$ and $\gamma \in \Gamma$, then we say Γ is the symmetry group for (2.1) and this system is called Γ – **equivariant**. This means that the nonlinear vector field f commutes with the linear action of Γ. One consequence is that if $x(t)$ is a solution for (2.1) then so is $\gamma x(t)$. We can apply this notion to a steady-state solution. If $x(t) = x_0$ is an equilibrium point for

(2.1) then there are two possibilities. Firstly, if $\gamma x_0 \neq x_0$, there γx_0 is a new equilibrium point. Secondly, if $\gamma x_0 = x_0$, then γ is a symmetry of the equilibrium [30].

A similar result can be observed for a periodic solution. If $x(t)$ is a $T-$periodic solution of (2.1) then $\gamma x(t)$ is also a periodic solution. Hence, either there is a new periodic solution due to the trajectories of $x(t)$ and $\gamma x(t)$ being separated or we can say that these trajectories are identical, meaning that $x(t)$ and $\gamma x(t)$ are different because of a phase shift, that is

$$x(t) = \gamma x(t - t_0) \qquad \text{for some} \quad t_0 \in (0, T).$$

As a result, a symmetry of periodic solution $x(t)$ is the pair (γ, t_0) which has both a spatial component γ and a temporal component t_0, that will be stated later.

Although [30] consider symmetries of ODEs on $\mathbb{R}^n$, it is possible to generalize this to ODEs on a manifold M. In this case, the symmetry of elements belonging to manifold M is expressed as the actions γ of group Γ acts on a manifold M. The set of all elements $\gamma \in \Gamma$ that leaves $x \in M$ invariant is called an **isotropy subgroup** Σ_x of x. Thus, for any $x \in M$, we can define $\Sigma_x = \{\gamma \in \Gamma : \gamma x = x\}$. Note that the isotropy subgroup is defined for any point $x \in M$, whether or not it is an equilibrium. Similarly, the set of points in M that are invariant under the action of $\Sigma \subseteq \Gamma$ is called a **fixed point subspace** Fix(Σ) of Σ. That is Fix(Σ) = $\{x \in M : \gamma x = x \text{ for all } \gamma \in \Sigma\}$.

If $x \in$ Fix(Σ), then $\Sigma \leq \Sigma_x$, which means that the isotropy of the points in Fix(Σ) can be larger than Σ [29]. Note that the action of the group has no effect on the fixed-point subspace of that group. The set $Orb(x) = \{\gamma x : \gamma \in \Gamma\}$ refers to all images of an element $x \in M$ under the action of Γ. This set is the **group orbit** of the action of Γ on $x \in M$. The following lemma compares the isotropy subgroups of points on the same orbit.

Lemma 2.1. *[30, Lemma 1.1] There are conjugate isotropy subgroups for all points on the same group orbit of* Γ. *More precisely, for any* $x \in M$ *and* $\gamma \in \Gamma$ *then,*

$$\Sigma_{\gamma x} = \gamma \Sigma_x \gamma^{-1}.$$

Lemma 2.2. *[29, Theorem 1.17] Let* $f : \mathbb{R}^n \to \mathbb{R}^n$ *be* $\Gamma-$*equivariant and* $\Sigma \subset \Gamma$ *be a subgroup. Then*

$$f(Fix(\Sigma)) \subset Fix(\Sigma).$$

Proof. Let $v \in \mathbb{R}^n$ and $\sigma \in \Sigma$. Then $\sigma v = v$ implies that
$\sigma f(v) = f(\sigma v) = f(v)$, so that $f(v) \in Fix(\Sigma)$. ■

The above lemma implies that the fixed-point spaces Fix(Σ) are flow-invariant for any Γ−equivariant system.

2.3 Oscillators and reduction normal form

An **oscillator** [11] is a dynamical system that has an asymptotically stable limit cycle $\{\gamma(t)\}$ and is described by an ODE:

$$\dot{x} = g(x, \lambda), \tag{2.2}$$

where $x \in X$ is the phase space of the oscillator, and $\lambda \in \mathbb{R}$ is a parameter.

Definition 2.1. *[11, Definition 2.2] A **network of weakly coupled identical oscillators** $\mathscr{C}^k$ is a dynamical system corresponding to an ODE that has two parameters λ and ϵ and is formed as:*

$$\dot{x} = f(x, \lambda, \epsilon), \tag{2.3}$$

where $x = (x_1, x_2, ..., x_n) \in X^n$ is the phase space variable, $\lambda \in \mathbb{R}$ is the bifurcation parameter and $\epsilon \in \mathbb{R}$ is the coupling interaction parameter. We assume :

- *f is jointly $\mathscr{C}^k$ in x, λ, and ϵ.*
- *$f(x, \lambda, 0) = (g(x_1, \lambda), g(x_2, \lambda), ..., g(x_n, \lambda))$ for some g on X^n that is an identical oscillator with limit cycle $\{\gamma(t)\}$ in each of the components.*

We can deduce from the definition that if $\epsilon = 0$ then the oscillators are uncoupled. This means that, for (2.2), each system has an asymptotically stable limit cycle (i.e. trajectories within a sufficiently close neighbourhood of each $x_i \in \gamma(t)$ is attracted to the limit cycle for all $t > 0$). Because the limit cycle is regarded as a 1−torus, then $\underline{x} = (x_1, x_2, ...x_n)$ will be attracted to an n−torus defined by $\{x_i = \gamma(t + \theta_i) : \Theta \in \mathbb{T}^n\}$, where $\Theta = (\theta_1, \theta_2, ..., \theta_n)$ is defined as the coordinate of n-dimensional system for $\epsilon = 0$ on the invariant n−torus.

If ϵ is small enough then normal hyperbolicity [39, 40] implies persistence of the $n-$torus as an asymptotically attracting invariant manifold. More precisely, for $\epsilon = 0$, all periodic solutions with period 2π (identical oscillators) have n Floquet multipliers which are equal to one (neutrally stable), and the rest of the multipliers are within the unit circle (by assumption). We note from [40, Theorem 4.1] that the torus is persistent under sufficiently small perturbation.

The equation (2.3) is $\Gamma-$equivariant if f commutes with $\Gamma < S_n$ on a system which is described as $(x_1, x_2, ..., x_n, \epsilon) \to (x_{\sigma(1)}, x_{\sigma(2)}, ..., x_{\sigma(n)}, \epsilon)$ for all $\sigma \in \Gamma$,

This means that we can reduce a $\Gamma-$equivariant network of weakly coupled systems (2.3) such that each uncoupled system equation $\epsilon = 0$ has a stable limit cycle flow generated by [40, Theorem 9.1],

$$\dot{\Theta} = \mathbf{1} + \epsilon F(\Theta, \lambda) + O(\epsilon^2), \tag{2.4}$$

where F is $\Gamma-$equivariant and $\mathscr{C}^{k-1}$ on the $n-$torus that represents the dynamics of the equation (2.3) in phase coordinates. Ashwin and Swift [11] used averaging to introduce an extra symmetry and so approximate the right hand side of the system as follows [40, Theorem 9.4].

Definition 2.2. *[11, Definition 2.4] Let the average of the function F over one period be*

$$G(\Theta, \lambda) = \frac{1}{2\pi} \int_0^{2\pi} F(\Theta + t\mathbf{1}, \lambda)\, dt. \tag{2.5}$$

Then the averaged system obtained from Equation (2.4) is

$$\dot{\Theta} = \mathbf{1} + \epsilon G(\Theta, \lambda) + O(\epsilon^2). \tag{2.6}$$

For $\epsilon \ll 1$, the dynamics of the equation (2.4) can be shown to be $\epsilon-$close to those of equation (2.6) for time of order $O(\epsilon^{-1})$ [62]. The next theorem proves that the new system (2.6) has an additional symmetry to (2.4), namely it is invariant under the action of $\mathbb{T}^1$ given by

$$\theta_i \mapsto \theta_i + \varphi \quad \text{for} \quad \varphi \in \mathbb{T}^1.$$

Theorem 2.3. *If $\theta_i(t) \in [0, 2\pi)^N, i = 1, 2, 3, ..., n$ is a solution for system (2.6), then $\theta_i(t) + \varphi$, ($\varphi \in [0, 2\pi)$ is a constant) is also a solution.*

Theorem 2.3 implies that after the system is reduced to (2.6), we have $\Gamma \times \mathbb{T}^1$-equivariant flow on $\mathbb{T}^n$, or equivalently a Γ-equivariant flow on the phase differences $\mathbb{T}^{n-1}$.

2.3.1 Spatio-temporal symmetries oscillators network

We summarize a framework for analysis of arbitrary symmetric networks of weakly coupled oscillators [11]. By using the symmetry of the networks, Ashwin and Swift found dynamically invariant regions in the phase space which exist only due to spatial-temporal symmetry. Here, we discuss some definitions and results from [11].

The system (2.6) can be written as n phase equations

$$\dot{\theta}_i = 1 + \epsilon G_i(\Theta, \lambda), \qquad i = 1, 2, ..., n, \tag{2.7}$$

which is assumed equivariant under the action of $\Gamma \times \mathbb{T}^1$ on $\mathbb{T}^n$ defined by $[(\sigma,\omega)(z)]_i = \omega z_{\sigma(i)}$ for all i, any $(\sigma,\omega) \in \Gamma \times \mathbb{T}^1$ and $z_j = e^{i\theta_j}$. This action has many different fixed point subspaces that are one-dimensional (i.e. they have a maximal isotropy) and there is no point that is fixed by all elements of this action. Also, this action has spatial and temporal symmetry, suppose Γ is a subgroup of S_n. The **spatial projection π_s on Γ is an** isomorphism [30] when restricted to any isotropy subgroup $\Sigma < \Gamma \times \mathbb{T}^1$, defined by $\pi_s(\Sigma) = \{\sigma : (\sigma,\omega) \in \Sigma\}$ for any $\Sigma \subseteq \Gamma \times \mathbb{T}^1$. Note that two elements of Σ are the same if they have the same spatial symmetry. Then, we can write any element belongs to an isotropy subgroup $\Sigma < \Gamma \times \mathbb{T}^1$ as $(\sigma, \omega(\sigma))$, with $\sigma \in \pi_s(\Sigma)$ [11, Definition 3.1]. The **temporal symmetry** π_t on $\mathbb{T}^1$ is a homomorphism. If $\pi_t(\Sigma)$ is nontrivial, we call Σ a **twisted isotropy subgroup** [30, p300]. Also, Ashwin and Swift showed that the image of a temporal projection for any isotropy subgroup must have order m dividing the number of oscillators n in the network [11, Lemma 3.1]. In the next subsection, we introduce the isotropy structure of $S_n \times \mathbb{T}^1$- equivariant ODE on $\mathbb{T}^n$ using [11].

2.3.2 The isotropy subgroups $S_n \times \mathbb{T}^1$

There is a one-to-one correspondence between conjugacy classes of isotropy subgroups and different ways of writing $n = m(k_1 + k_2 + ... + k_\ell)$, where ℓ, m and k_j are integers, with

$k_1 \geq k_2 \geq ... \geq k_\ell \geq 1$, as shown in [11].

Theorem 2.4. *[11, Theorem 3.1] Every isotropy subgroup of $S_n \times \mathbb{T}^1$ is conjugate to a subgroup of the form $\Sigma_{\boldsymbol{k},m}$ which is defined as :*

$$(S_{k_1} \times S_{k_2} \times ... \times S_{k_\ell})^m \otimes Z_m, \tag{2.8}$$

where $n = mk$ and $k = k_1 + k_2 + ... + k_\ell$. The fixed point subspace $Fix(\Sigma_{\boldsymbol{k},m})$ is an $\ell-$dimensional torus and this torus $\mathbb{T}^\ell$ is subset from $\mathbb{T}^n$.

From the above theorem, each partition of the oscillators is divided into m collections, with each having k oscillators. They are rotated by a phase shift of $2\pi/m$. Moreover, another partition in each collection divides it into ℓ sets of k_i phase-locked oscillators (two oscillators $\theta_i(t)$ and $\theta_i(t)$ are phase-locked if $|\theta_i(t) - \theta_i(t)|$ is bounded for all $t > 0$). This partition has $(S_{k_1} \times S_{k_2} \times ... \times S_{k_\ell})$ symmetry. The coordinates of the fixed-point space is

$$((z_1, z_1, ..., z_1, z_2, z_3, ..., z_\ell), (z_1\omega^k, z_2\omega^k, ..., z_\ell\omega^k), ..., (z_1\omega^{-k}, z_2\omega^{-k}, ..., z_\ell\omega^{-k})),$$

where $\omega = e^{2\pi i/n}$ and that $\omega^{(m-1)k} = \omega^{-k}$. Because all fixed point subspaces are diffeomorphic to $\{(z_1, z_2, ..., z_l) : |z_i| = 1\}$, they are $\ell-$dimensional tori. The permutation groups within $\Sigma_{\boldsymbol{k},m}$ commute because the permutations S_{k_i} are disjoint sets. However, there is a semidirect product between Z_m and the permutations due to the fact that the phase shift does not commute with them. As an example of an application of Theorem 2.4, we consider the next example 2.1 with a network which has $n = 8$. This is similar to the example $n = 9$ in Ashwin and Swift [11].

Example 2.1. *Consider a network which has $n = 8$ oscillators and $S_8 \times \mathbb{T}^1$ symmetry. According to Theorem 2.4, it can be written as $n = 8 = 4 \times 2$ then $m = 4$, $k = 2$, $k_1 = 1$, $k_2 = 1$ and $\ell = 2$. Since $m, \ell > 1$ we get the smallest a nontrivial isotropy subgroup. The two-dimensional torus of points $((a, b), (a\omega^2, b\omega^2), (a\omega^4, b\omega^4), (a\omega^6, b\omega^6)) \in \mathbb{T}^8$ has isotropy $(S_1 \times S_1)^4 \otimes Z_4$. The corresponding fixed-point subspace is*

$$\{(a, b, a\omega^2, b\omega^2, a\omega^4, b\omega^4, a\omega^6, b\omega^6) : (a, b) \in \mathbb{T}^2\}.$$

$n = m \times k$	Number of blocks	Number of elements	Dim	Isotropy	Fixed point spaces
$n = 8 = 2 \times 4$	$m = 2$	$\kappa = 4, \kappa_1 = 1, \kappa_2 = 3$	$\ell = 2$	$(S_3 \times S_1)^2 \otimes Z_2$	$\{(a,a,a,b,-a,-a,-a,-b) : (a,b) \in \mathbb{T}^2\}$
$n = 8 = 2 \times 4$	$m = 2$	$\kappa = 4, \kappa_1 = 1, \kappa_2 = 1, \kappa_3 = 2$	$\ell = 3$	$(S_2 \times S_1 \times S_1)^2 \otimes Z_2$	$\{(a,a,b,c,-a,-a,-b,-c) : (a,b,c) \in \mathbb{T}^3\}$
$n = 8 = 2 \times 4$	$m = 2$	$\kappa = 4, \kappa_1 = 2, \kappa_2 = 2,$	$\ell = 2$	$(S_2 \times S_2)^2 \otimes Z_2$	$\{(a,a,b,b,-a,-a,-b,-b) : (a,b) \in \mathbb{T}^2\}$

Table 2.1: *This table shows a few possible isotropy subgroups of $S_8 \times \mathbb{T}^1$ and their fixed-point spaces for $n = 8$.*

This fixed-point subspace is represented in Figure 2.1 with other three possibilities to get isotropy subgroups when $n = 2 \times 4$ which are listed in Table 2.1.

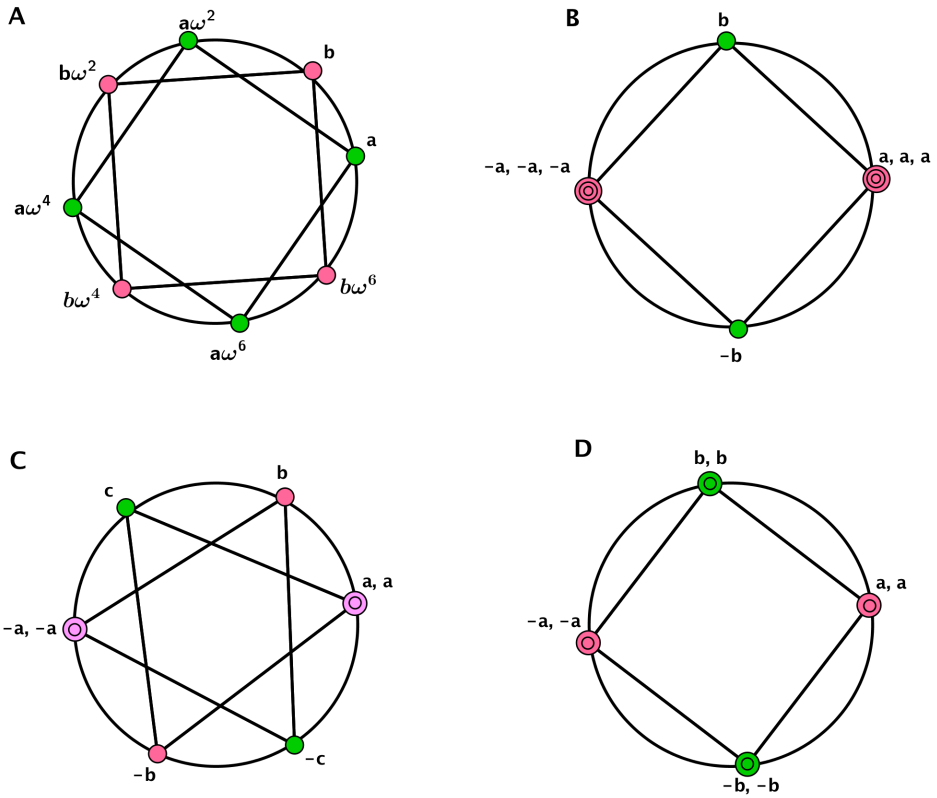

Figure 2.1: *This figure visualizes possible symmetries of periodic solutions for $S_8 \times \mathbb{T}^1$ symmetry, which are listed in Table 2.1. Four fixed point subspaces for an isotropy subgroup of eight oscillators are represented on the unit circle in the complex plane. **A** illustrates that there is no symmetry of phase oscillators and represents them by single phases a, b with green and pink dots. **B** shows triple symmetry phases with pink dots which corresponds to conjugation and single phases with the green dot. **C** is slightly different from **B**, it shows double phases with purple dots and two singles phases with green and pink dots. Finally, in **D**, there are two double phases with green and pink dots.*

2.3.3 The isotropy subgroups of $\Gamma \times \mathbb{T}^1$

We will describe computation of the isotropy structure of $\Gamma \times T^1-$equivariant systems for any $\Gamma < S_n$ using a result in [11]. The first step is to list generators of all subgroups of Γ, then find the possible twist homomorphism associated with each of these generators. One of the important properties of a group which is useful for indistinguishable oscillators is **transitivity**. The group Γ is transitive if there is an element $\sigma \in \Gamma$ that has a spatial symmetry $i = \sigma(j)$ for all i, j in $\{1,2,...,n\}$. A transitive network is **indistinguishable** in that any oscillator can do the job of any other oscillator. In other words, if the symmetry group of a network is transitive, then the oscillators are indistinguishable [11, definition 3.2].

This property enables us to determine the system using an equation for only one oscillator. Moreover, $\{(a,a,...,a)\}$ is a fixed-point space of $\Gamma \times T^1$ if and only if Γ is transitive. One can get indistinguishable oscillators within various symmetry groups, for example S_n, Z_n, D_n groups.

We next review isotropy subgroups for two symmetry groups discussed in [11].

The Isotropy structure of $Z_n \times \mathbb{T}^1$

Consider a ring of oscillators with a specific orientation, and label the elements in the group Z_n to label the oscillators 1 to n around the ring. This means that we pick a generator of Z_n that is an $n-$cycle, $\sigma = (1,...,n)$.

Theorem 2.5. *[11, Theorem 4.1] Let the isotropy subgroups of $Z_n \times \mathbb{T}^1$ be one-to-one correspondence with two integer positive numbers m and p where $n = mk$ and $p \in \{0,1,2,...,m-1\}$. Under spatial projection, the isotropy subgroups $Z_m(p)$ are isomorphic to a cycle group Z_m and are generated by (σ^k, ω^{kp}). Then, the fixed-point subspaces of $Z_m(p)$ can be written as,*

$$Fix(Z_m(p)) = \{z \in \mathbb{T}^n : z_j = a_j \omega^{jp}\}, \qquad \text{such that} \quad a_j = a_i \text{ if } j = i (mod\ k),$$

which have dimension $k \in \mathbb{T}^n$.

Note that if $p \neq 0$ then the isotropy subgroups have temporal projection. There is no conjugate between the subgroups of Z_n, if they have different p. These isotropy subgroups can be partially ordered in the lattice according to [11, Lemma 4.1]. For example, we illustrate the isotropy subgroups for $Z_4 \times T^1$ as lattice in Figure 2.2.

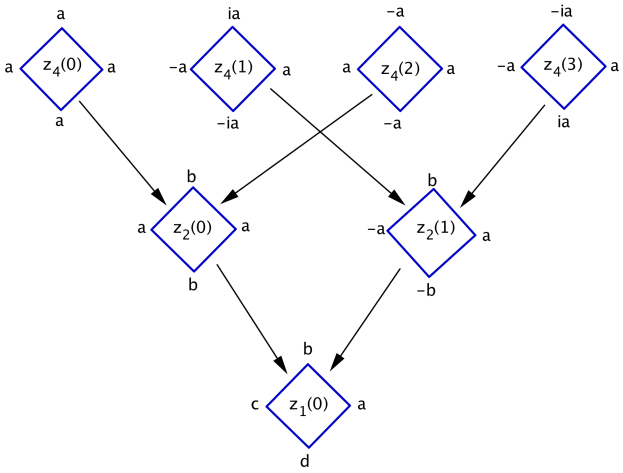

Figure 2.2: *This figure shows the fixed-point subspace for* $Z_4 \times \mathbb{T}^1$. *Their partial order is shown by isotropy lattice of symmetry subspaces of* $Z_4 \times \mathbb{T}^1$, *[11, Figure 3].*

The Isotropy structure of $D_n \times \mathbb{T}^1$

The symmetry of an oscillator ring with no preferred direction is isomorphic to the symmetries of a regular $n-$gon including reflection, D_n. Recall that this group is defined by,

$$D_n \equiv \langle \{\sigma, \tau\} | : \ \sigma^n = \tau^2 = 1, \ \sigma\tau\sigma = \tau \rangle,$$

where $\tau = (1)(2,n)(3,n-1)$ ... and $\sigma = (1,2,...,n)$. Note that, τ fixes 1 and $n/2$ if n is even, whereas τ fixes only 1 if n is odd. The classification of isotropy subgroups for the action of $D_n \times \mathbb{T}^1$ is achieved by two steps. Firstly, we determine all subgroups of D_n. As known, the subgroups of D_n are conjugate to one (or more) of the following subgroups:

$$D_m(k) \equiv \langle \{\sigma^k, \tau\} \rangle = \langle \{\sigma^{k-1}\tau, \tau\} \rangle,$$

$$D_m(k\sigma) \equiv \langle \{\sigma^k, \tau\sigma\} \rangle = \langle \{\sigma^{k-1}\tau, \tau\sigma\} \rangle,$$

$$Z_m \equiv \langle \{\sigma^k\} \rangle,$$

where $mk = n$, for more details see [11]. Secondly, finding all twisted subgroup are of $D_n \times \mathbb{T}^1$, as illustrated in the next lemma.

Lemma 2.6. *[11, Lemma 4.2] All twisted isotropy subgroups of $D_n \times \mathbb{T}^n$ are conjugate to one of the following:*

$$D_m(+-) \equiv \langle\{(\sigma^{k-1}\tau, 1), (\tau\sigma, -1)\}\rangle, \quad (m \text{ must be even})$$

$$D_m(--) \equiv \langle\{(\sigma^{k-1}\tau, -1), (\tau\sigma, -1)\}\rangle, \quad (k \text{ must be even})$$

$$Z_m(p) \equiv \langle\{(\sigma^k, \omega^{pk})\}\rangle, \quad \text{where } p \in \{1, 2, ..., [m/2]\}.$$

The isotropy subgroups of $D_n \times \mathbb{T}^n$ and their fixed point space are defined in [11, Table 2], where $mk = n$ runs through all binary factorization of n. In 2015 [8], Ashwin and Burylko reformulated this table for $n = 6$, as we discuss in the next chapter.

2.4 Synchrony and symmetry in networks

Symmetry groups can be used to formulate a theory that can be very helpful for studying coupled dynamical systems. There are substantial effects of network symmetries on equilibria, periodic orbits, heteroclinic cycles, and chaotic attractors. Particular aspects that can usefully be understood using symmetries include synchrony and bifurcations.

2.4.1 Tools for symmetric networks

Stewart, Golubitsky and Pivato [85] introduced a new framework to understand coupled cell system dynamics in term of their architecture. Dynamical systems (in the continuous states of the coupled ODEs) are represented by a network $\mathcal{N}$ which is regarded as a directed graph [64, 98]. This graph has nodes and edges which are classified according to labels or "types" and correspond to cells and couplings respectively. Identical internal dynamics of the cells mean these cells have the same label; identical couplings is a property for arrows with the same label. Every cell c has a phase space P_c, and the cartesian product $P = \prod_c P_c$ refers to the total phase space of the network. Therefore, we can say that points $x \in P$ have coordinates x_c.

We give a definition of coupled cell networks based on equivalence relations between cells, as follow.

Definition 2.3. *[5, Definition 2.1.] A **coupled cell network** $\mathcal{N}$ consists of:*

1. *A finite set of $\mathcal{D} = \{1, 2, 3, ...N\}$ of **cells** or **nodes**.*
2. *A finite set $\mathcal{E}$ of **edges** or **arrows**.*
3. *A **cell-equivalence** is an equivalence relation between cells in $\mathcal{D}$ and is denoted by $\sim_C$. The type or cell label of cell c is its $\sim_C$- equivalence class.*
4. *An **edge-equivalence** is an equivalence relation on edges in $\mathcal{E}$, and is denoted by $\sim_E$. The type or coupling label of edge e is its $\sim_E$- equivalence class.*
5. *For $e \in \mathcal{E}$, there are two maps $\mathcal{H}, \mathcal{T} : \mathcal{E} \to \mathcal{D}$ such that $\mathcal{H}(e)$ is a **head** of e and $\mathcal{T}(e)$ is a **tail** of e.*

Also, we require a consistency condition that If there are two arrows $e_1, e_2 \in \mathcal{E}$ such that $e_1 \sim_E e_2$, then $\mathcal{H}(e_1) \sim_C \mathcal{H}(e_2)$, $\mathcal{T}(e_1) \sim_C \mathcal{T}(e_2)$.

In this definition, if $\mathcal{T}(e)$ is the same as $\mathcal{H}(e)$, then an arrow is a self-connection. If distinct arrows $e, \acute{e}$ have $\mathcal{T}(e) = \mathcal{T}(\acute{e})$ and $\mathcal{H}(e) = \mathcal{H}(\acute{e})$ then multiple arrows. Associated with each cell $c \in \mathcal{D}$, some notions can be used to prove the equivalence between cells.

An input of all edges to cell $c \in \mathcal{D}$ is called the **input set** of c and written $I(c) = \{e \in \mathcal{E} : \mathcal{H}(e) = c\}$. There is an **input equivalence** $\sim_I$ between these input arrows on $\mathcal{D}$ [31]. One can say $c \sim_I d$, if and only if there exists a bijection $\beta : I(c) \to I(d)$ such that for every $i \in I(c)$, $i \sim_E \beta(i)$. Any such bijection β is called an input isomorphism from cell c to cell b. The set $B(c, d)$ denotes the collection of all input isomorphisms from cell c to cell d [5].

2.4.2 Balanced equivalence relations and symmetric networks

We now discuss an important type of equivalence relation between cells and edges in $\mathcal{N}$. In [5], note that, an equivalence relation $\bowtie$ on $\mathcal{D}$ can be viewed as a "colouring" of cells, that means $c \bowtie d$ iff c and d have the same colour. An equivalence relation $\bowtie$ on $\mathcal{D}$ is **balanced** if for every cell $c, d \in \mathcal{D}$ with $c \bowtie d$, then there exists bijection $\beta \in B(c, d)$ such that

$\mathscr{T}(i) \bowtie \mathscr{T}(\beta(i))$ for all $i \in I(c)$ [5, Definition 2.5]. In addition, the equivalent relation is a **balanced coloring** if the equivalent cells receive the same colour input.

A unique partition ($\bowtie$-equivalence class) of $\mathscr{D}$ is determined by the equivalence relation $\bowtie$ on $\mathscr{D}$. This is shown in Figure 2.3, where the cells that receive the same colour belong to the same equivalence class. Conversely, a unique equivalence relation can be found by any partition. Any equivalence relation $\bowtie$ on the set of cells of a network corresponds to a **polydiagonal**, which for an equivalence relation $\bowtie$ is the set for all $x \in P$ such that $c \bowtie d$ implies that $x_c = x_d$. This written as,

$$\triangle_{\bowtie} = \{x \in P : c \bowtie d \Rightarrow x_c = x_d\}.$$

The set $\triangle_{\bowtie}$ is said to be a **balanced polydiagonal** if $\bowtie$ is balanced. This depends only on network structure and not on the details of the ODEs. If cells have the same colour then they identical dynamics within the balanced polydiagonal as so it can be regarded as a "pattern of synchrony". The dynamical meaning of **synchrony** is $x_c(t) = x_d(t)$ for all times t on a trajectory $x(t)$ of an admissible vector field f if and only if there is an equivalence relation $c \bowtie d$ on set $\mathscr{D}$. The implication of the above discussion is that the general network architecture can be employed to create universal possibilities for synchrony by polydiagonal.

Antoneli and Stewart [5] discussed networks $\mathscr{N}$ that have a group of symmetries Γ. More precisely, the set of permutations of the cells that preserve the network structure (including types of cells and arrows) is the group $\Gamma = Aut(\mathscr{N})$ that is the automorphism group of the network. Also, the permutations for cells coordinates of P occurs due to Γ group's action. The consequence of this is that every admissible vector field in the sense of ([85] Definition 4.1) is $\Gamma-$equivariant for this group.

Connections between the notions of fixed-point space $\Sigma \subset \Gamma$ and balanced polydiagonal are also explained. Because equivalence classes of the relation $\bowtie$ are the same as $\Sigma-$orbits, it is easy to prove that every fixed-point space of a subgroup $\Sigma \subset \Gamma$ is a balanced polydiagonal. The converse is incorrect, for example, consider a coupled cell network with four cells and a trivial symmetry group illustrated in Figure 2.3. The shape of cell symbol (circle, square, triangle) points to the type of cell and the arrow (solid, dotted, shape and colour of arrowhead) refers to the arrow. Colours of the cells indicate equivalent classes which are {1},

{2, 3}, {4}. An admissible vector field corresponding to a class of differential equations with this network has the form

$$\begin{aligned} \dot{x_1} &= f(x_1; x_3, x_4) \\ \dot{x_2} &= g(x_2; x_1) \\ \dot{x_3} &= g(x_3; x_1) \\ \dot{x_4} &= h(x_4; x_2, x_3) \end{aligned} \tag{2.9}$$

where f, g, h are arbitrary functions, $x_1 \in P_f$, $x_2, x_3 \in P_g$ and $x_4 \in P_h$ such that P_f, P_g and P_h are phase spaces. Because cells 2 and 3 have the same colour and input, the equivalence relation gives ~~to~~ balance polydiagonal

$$\Delta_{\bowtie} = \{(u, v, v, w) : u \in P_f, v \in P_g, w \in P_h\}.$$

As a result, networks with trivial symmetry group can possess nontrivial balanced equivalence relations [85]. Networks with nontrivial symmetry can also possess "exotic" balanced polydiagonals which do not give rise to fixed-point spaces, (more details are shown in the subsection 2.4.3).

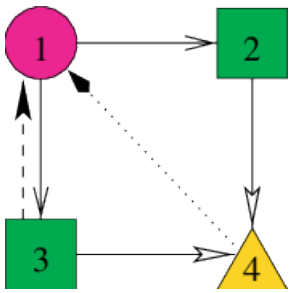

Figure 2.3: *This figure shows a network of four with coupled cells. This network has trivial symmetry. As seen, the cells are classified according to shape (circle, square, triangle), and form of arrow (solid, dotted, shape and color of arrowhead), Figure(4)[5].*

The next theorem articulates the main property of a balanced equivalence relation which leads to a flow-invariant polydiagonal, as well as the converse. There are typically many possible balance equivalence relations, just as there are many fixed point subspaces.

Theorem 2.7. *[5, Theorem 2.6] Suppose that $\bowtie$ is an equivalence relation on the cells of a coupled cell network. Then the polydiagonal $\Delta_{\bowtie}$ is flow-invariant if and only if the equivalence relation is balanced.*

A pattern of synchrony is one of dynamical consequences of flow-invariance. It is created when there exist trajectories $x(t)$ of the ODE such that $c \bowtie d \Rightarrow x_c(t) = x_d(t),\ t \in \mathbb{R}$. Such trajectories arise when initial conditions $x(0)$ lie in $\Delta_{\bowtie}$. In this case, the whole trajectory lies in $\Delta_{\bowtie}$ for all positive and negative times, and is a trajectory of the restriction $f|\Delta_{\bowtie}$. The associated dynamics can be steady-state, periodic, or even chaotic, depending on f and its restriction to $\Delta_{\bowtie}$.

2.4.3 Symmetry group of networks

For a general network, [5] is devoted to finding an equivalent relation from subgroups of the automorphism group $Aut(\mathcal{N})$. Antoneli and Stewart considered global symmetries of networks as subgroups of $Aut(\mathcal{N})$. Also for simplicity, they do not allow self-connections or multiple arrows in the network.

Definition 2.4. *[5, Definition 3.1] An **automorphism** of a coupled cell network $\mathcal{N}$ with cells $\mathscr{D}$ and arrows $\mathscr{E}$ consists of two bijective maps $\sigma_{\mathscr{D}} : \mathscr{D} \to \mathscr{D}$ and $\sigma_{\mathscr{E}} : \mathscr{E} \to \mathscr{E}$, that satisfy the four conditions:*

(1) $\sigma_{\mathscr{D}}(\mathscr{H}(e)) = \mathscr{H}(\sigma_{\mathscr{E}}(e))$, *for all* $e \in \mathscr{E}$.

(2) $\sigma_{\mathscr{D}}(\mathscr{T}(e)) = \mathscr{T}(\sigma_{\mathscr{E}}(e))$, *for all* $e \in \mathscr{E}$.

(3) $i \sim_{\mathscr{D}} \sigma_{\mathscr{D}}(i)$, *for all* $i \in \mathscr{D}$

(4) $i \sim_{\mathscr{E}} \sigma_{\mathscr{E}}(i)$, *for all* $e \in \mathscr{D}$.

A group that contains the set of all automorphisms of $\mathcal{N}$ under composition operation is called the automorphism group, or symmetry group of $\mathcal{N}$, and is denoted by $Aut(\mathcal{N})$.

Using subgroups of the automorphism group $Aut(\mathcal{N})$ of $\mathcal{N}$, one can build balanced equivalence relations on $\mathcal{N}$. Suppose that there is a subgroup $\Omega \subseteq Aut(\mathcal{N})$ and the projection of Ω into $Aut_{\mathscr{D}}(\mathcal{N})$ is $\Omega_{\mathscr{D}}$. The relation $\bowtie_\Omega$ is defined by

$$c \bowtie_\Omega d \Leftrightarrow \exists\ \omega \in \Omega : \omega_{\mathscr{D}}(c) = d.$$

Then the $\bowtie_\Omega$ −class represents the $\Omega_{\mathscr{D}}$−orbits of cells, as well as identifying a balanced polydiagonal

$$\triangle_\Omega = \triangle_{\bowtie_\Omega} = Fix(\Omega),$$

where $Fix(\Omega)$ refers to fixed-point space of Ω which acts on the total phase space P. As a proposition, if Ω is any subgroup of $Aut(\mathcal{N})$, then $Fix(\Omega)$ is a balanced polydiagonal.

Definition 2.5. *[5, Definition 3.4] Suppose that a network $\mathcal{N}$ has a balanced equivalence relation $\bowtie$ and automorphism group $Aut(\mathcal{N})$. If $\triangle_\bowtie = Fix(H)$ for some subgroup $H \subset Aut(\mathcal{N})$, we can say that $\bowtie$ is a **fixed-point colouring**, otherwise we say that $\bowtie$ it is **exotic**.*

We now consider a simple example of a symmetric network possessing exotic balanced colourings; that is, balanced colourings that are not fixed-point colorings.

Example 2.2. *[6] It is not true that in a group network, every balanced polydiagonal is the fixed-point space of a subgroup of that group. A simple example occurs for the alternating group A_4 acting on $C = 1,2,3,4$ in its natural permutation action, as shown in Figure 2.4. This action can be visualized as the group of rotations of a regular tetrahedron with vertices labelled 1, 2, 3, 4. The polydiagonal $\triangle_\bowtie = \{x,x,z,w\}$ for which $1 \bowtie 2$ is easily seen to be balanced. However, it is not the fixed-point space of any subgroup of A_4. The only rotations of the tetrahedron that fix the set $1,2$ are the identity and the rotation $(12)(34)$ of order 2. The fixed-point spaces related to these rotations are (x,y,z,w) and (x,x,z,z). However, $Aut(\mathcal{N}_{A_4}) = S_4$, and is a fixed-point colouring derived from a subgroup of S_4 that is not contained in A_4, namely the Z_2 subgroup generated by the reflection (12).*

Also, Antoneli and Stewart [5] show that in general the fixed point subspaces of group Γ are only the flow-invariant subspaces. They prove this in the next theorem which does not include any explicit network structure.

Theorem 2.8. *[5, Theorem 4.1] Suppose a finite group* Γ *acts linearly on a finite-dimensional real vector space* X*. Then, the fixed-point spaces of an isotropy subgroup of* Γ *are the only subspaces of* X *that are flow-invariant for all* $\Gamma-$*equivariant vector fields.*

For particular admissible vector fields there may be other flow-invariant subspaces, but these depend on particular properties of the vector field.

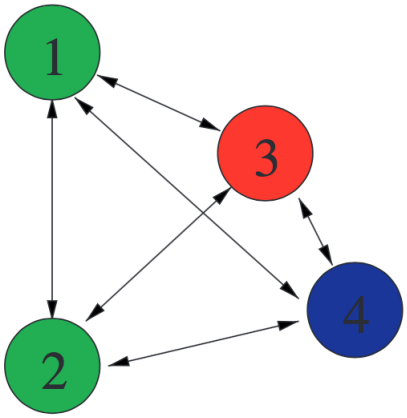

Figure 2.4: *Exotic balanced polydiagonal on a symmetric network* (A_4) *that is not a fixed-point space for any subgroup of* (A_4)*, Figure(4)[6].*

In a summary, we have two techniques to find flow invariant subspaces. Symmetrically coupled oscillators have fixed-point spaces that are flow-invariant [11]. Antoneli and Stewart [5] show networks can have exotic balanced polydiagonals that are not fixed-point subspaces but depend on special properties of the network. They discuss balanced colouring equivalence relations. Additionally, they concentrated on studying an example of symmetric networks that have exotic balanced polydiagonals that are not a fixed-point subspaces.

Invariant subspaces help us to understand how symmetries constrain dynamics for coupled oscillators and fixed-point subspaces will be fundamental to the rest of the thesis.

CHAPTER 3

WEAK CHIMERA AND BIFURCATIONS OF A SIX-OSCILLATOR SYSTEM

In this chapter, we consider a network of six phase oscillators studied in [8] where weak chimera solutions were found. Here we make a suitable change of coordinates for the phase portrait and analyse bifurcations at specific values of parameters. Section 3.1 presents briefly a literature review about the existence of weak chimera states on modular and non-modular networks. Section 3.2 studies a generalized Kuramoto model for six phase oscillators system within a particular invariant subspace. This section explains the reduction for a system of six coupled phase oscillators for a non-modular network. We numerically find weak chimeras and investigate the bifurcation diagrams for this six oscillator network, as illustrated in Section 3.3. Section 3.4 investigates the effects of parameter, phase and time-reversal symmetries on bifurcation diagrams.

3.1 Definition and existence of a weak chimera state

As discussed in sections 1.3 and 1.4, many factors play an essential role in the existence of weak chimera state, for example, a network structure (global, local, nonlocal, modular,

size), the number of oscillators (high, low), the coupling strength (weak, strong) and the type of oscillators (indistinguishable, identical, homogeneous, etc.). Different studies assumed different conditions to prove the appearance of weak chimera states. For instance, the first observation of the chimera state in a system of infinitely many nonlocally coupled phase oscillators was presented by Kuramoto and Battogtokh [50]. In 2004, Abrams and Strogatz [2] called this phenomenon "chimera states" and investigated chimeras in a one-dimensional ring of nonlocally coupled oscillators. In 2008, chimeras were found in a network of identical global coupled oscillators [1]. Laing introduced the first analysis for the existence of chimera states in two dimensional networks of coupled oscillators [53]. Asymptotic methods were used by Panaggio and Abrams to identify under any condition that one can find chimera states in the surface of a two-dimensional torus [71]. In 2015 the same previous authors worked to prove the existence of chimeras consisting of spots and spirals of desynchrony on the surface of a sphere [72]. Sethia and Sen [80] showed that both the weak coupling approximation and nonlocal coupling are not essential conditions for the existence of chimera states.

Ashwin and Burylko [8] introduced the notion of a weak chimera for finite networks of indistinguishable phase oscillators for reasons discussed in Section 1.4. They defined a weak chimera state as an invariant set that contains a form of partial frequency synchronization. We will introduce a precise definition of weak chimera states in the next section. In the same paper, it was also shown that weak chimeras can not occur in networks of the identical phase oscillators if there is globally and identically coupled or if the system size too small. In particular, [8, Theorem 1] states that it is not possible that weak chimera states exist for fully symmetric coupling of N identical phase oscillators because in such a case, all trajectories are frequency synchronized. In the same reference, the authors identified conditions for the appearance of attracting weak chimera states in the system of indistinguishable phase oscillators. These conditions mean that networks must have at least four oscillators, at least two different coupling strength. They investigate systems where the coupling function has at least two Fourier components (i.e., coupling functions of the form (1.10)).

Moreover, the paper [8] classifies networks into two types. The first type consists of

modular networks which means that networks can be decomposed into a number of smaller subnetworks. This type is used in [8] to explains the appearance of weak chimera states in systems of four, six or ten oscillator modular networks (see Figure 3.1). Bick and Ashwin [15] considered an example of weak chimeras in modular networks with non-zero coupling between clusters of oscillators. The second type consists of non-modular networks with non-global coupling structures (see Figure 3.2). Ashwin and Burylko [8] also found attracting weak chimera states in the second type of networks.

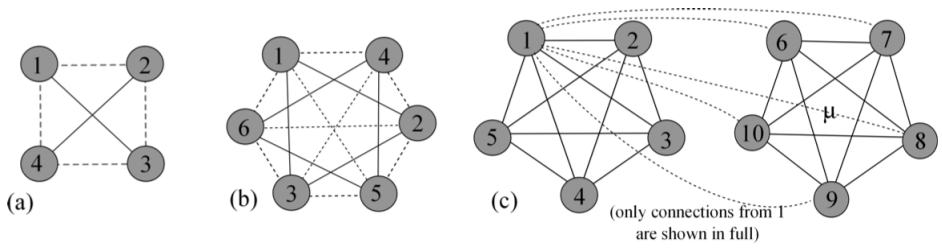

Figure 3.1: *Networks of (a) four, (b) six and (c) ten indistinguishable oscillators with modular structure robust weak chimera state. This figure shows two types of coupling, the solid line has a bidirectional coupling with strength equal 1 whereas the dashed line indicates bidirectional coupling with strength* ϵ *[8].*

3.2 Weak chimera in six- oscillators networks

In [8] Ashwin and Burylko numerically show that there is a weak chimera state in a finite non-modular network of six oscillators (i.e. the network is bidirectionally coupled with strength 1). They considered a generalized Kuramoto model of N coupled phase oscillators as,

$$\dot{\theta}_i = \omega_i + \sum_{j=1}^{N} K_{ij}\, g(\theta_i - \theta_j), \tag{3.1}$$

where $(\theta_1, \ldots \theta_N) \in \mathbb{T}^N = [0, 2\pi)^N$ and ω_i is the natural frequency of the oscillator θ_i, K_{ij} is the coupling strength, and g is the coupling function for Hansel-Mato-Meunier [9, 37] with two parameters α and r. Recall we have

$$g(\phi) = -\sin(\phi - \alpha) + r\sin(2\phi). \tag{3.2}$$

This is called Kuramoto-Sakaguchi coupling [78] for $r = 0$. The average frequency [45] of the ith oscillator in the system (3.1) is defined as

$$\Omega_i = \lim_{T\to\infty} \frac{\theta_i(T)}{T}, \tag{3.3}$$

and the frequency difference [8] between two oscillators i and j is :

$$\Omega_{ij} = \lim_{T\to\infty} \frac{1}{T}[\theta_i(T) - \theta_j(T)]. \tag{3.4}$$

We define two oscillators as i and j as frequency synchronized if $\Omega_{ij} = 0$, and as not frequency synchronized, otherwise. The formal definition of a weak chimera state is formulated as follows in [8]. The next definition describes a weak chimera in a finite system.

Definition 3.1. *[8] A set $A \subset \mathbb{T}^N$ for a coupled N phase oscillator system is a **weak chimera state** if it is a connected chain-recurrent flow-invariant set such that for each trajectory in A there are distinct oscillators i, j and k such that $\Omega_{ij} \neq 0$ and $\Omega_{ik} = 0$.*

After that, we do not consider any other chimera state in this thesis, from this point on we will simply refer to weak chimera as a chimera. It is not surprising to find chimera states in coupled phase oscillator networks with different natural frequencies of oscillators or non-local coupled networks. However, the interesting case is a chimera state in coupled indistinguishable phase oscillator networks. Indistinguishable oscillators which have the same number and strength of input [11]. For example in Figure 3.2, there are three coupled structures of six indistinguishable oscillators. Here, we concentrate in a network of six indistinguishable oscillators (Figure 3.2(a)). Let the coupled oscillator network of this figure be governed by

$$\dot{\theta}_i = \omega + \sum_{|j-i|=1,2} g(\theta_i - \theta_j), \tag{3.5}$$

with the coupling (3.2) and indices taken modulo 6, where phase oscillators $\theta_i \in [0, 2\pi) = \mathbb{T}$ and ω is the constant natural frequency of θ_i.

We can expand the system (3.5) to get

$$\begin{aligned}
\dot{\theta_1} &= \omega + g(\theta_1-\theta_2) + g(\theta_1-\theta_3) + g(\theta_1-\theta_5) + g(\theta_1-\theta_6),\\
\dot{\theta_2} &= \omega + g(\theta_2-\theta_1) + g(\theta_2-\theta_3) + g(\theta_2-\theta_4) + g(\theta_2-\theta_6),\\
\dot{\theta_3} &= \omega + g(\theta_3-\theta_1) + g(\theta_3-\theta_2) + g(\theta_3-\theta_4) + g(\theta_3-\theta_5),\\
\dot{\theta_4} &= \omega + g(\theta_4-\theta_2) + g(\theta_4-\theta_3) + g(\theta_4-\theta_5) + g(\theta_4-\theta_6),\\
\dot{\theta_5} &= \omega + g(\theta_5-\theta_1) + g(\theta_5-\theta_3) + g(\theta_5-\theta_4) + g(\theta_5-\theta_6),\\
\dot{\theta_6} &= \omega + g(\theta_6-\theta_1) + g(\theta_6-\theta_2) + g(\theta_6-\theta_4) + g(\theta_6-\theta_5).
\end{aligned} \tag{3.6}$$

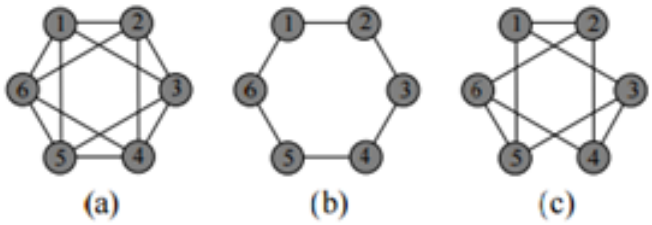

Figure 3.2: *Three ways of coupling six oscillators into a network of indistinguishable oscillators (a) Non-global coupling a system of six oscillators. (b) Local coupling in a system of six oscillators. (c) Each oscillator is linked with three different oscillators in a system of six oscillators [8].*

In 1992, Ashwin and Swift presented Table 2 in [11] which illustrated fixed point subspaces for $D \times \mathbb{T}^1$ with finite number n of oscillators. Then, in 2015, Ashwin and Burylko restricted this table to the six oscillators ($n = 6$) and noted for this system there are additional invariant subspaces, exotic sets [8, Table I]. These subspaces are not invariant due to symmetries, but are invariant as a consequence of exotic balanced polydiagonal between equivalent oscillators [5]. We summarize in Table 3.1 the invariant subspaces and symmetry-forced subspace for the system (3.5)(for more information see [8, Table I]). The balanced colouring $\bowtie$ on networks A_1, A_2 determines the quotient network III in Figure 3.3. After restricting the six oscillators to the subspace A_1 we get

$$(\theta_1,\theta_2,\theta_3,\theta_4,\theta_5,\theta_6) = (\phi_1,\phi_2,\phi_3,\phi_1,\phi_3,\phi_2). \tag{3.7}$$

Subgroups Σ	Fixed-point space	Dim
D_6	(a,a,a,a,a,a)	1
D_6^-	$(a,a+\pi,a,a+\pi,a,a+\pi)$	1
Z_6^1	$(a,a+\xi,a+2\xi,a+3\xi,a+4\xi,a+5\xi)$	1
Z_6^2	$(a,a+2\xi,a+4\xi,a,a+2\xi,a+4\xi)$	1
D_3	(a,b,a,b,a,b)	2
Z_3	$(a,b,a+2\xi,b+2\xi,a+4\xi,b+4\xi)$	2
D_2	(a,b,a,a,b,a)	2
D_2^-	$(a,b,a,a+\pi,b+\pi,a+\pi)$	2
Z_2^1	(a,b,c,a,b,c)	3
Z_2^2	$(a,b,c,a+\pi,b+\pi,c+\pi)$	3
A_0	(a,b,c,a,d,e)	5
A_1	(a,b,c,a,c,b)	3
A_2	(a,b,b,a,c,c)	3
A_3	$(a,b,c,a+\pi,c+\pi,b+\pi)$	3
A_4	$(a,b,b+\pi,a+\pi,c+\pi,c)$	3
A_5	$(a,a+\pi,b,a,a+\pi,b)$	2
A_6	$(a,a+\pi,b,a,a+\pi,b+\pi)$	2
A_7	$(a,a+\pi,b,a+\pi,a,b)$	2

Table 3.1: *Isotropy subgroups and their fixed point spaces for the six oscillator system in Figure 3.2(a) with $\xi = \pi/3$ and arbitrary phases a,b,c,d,e and f. This table is divided into two sets of isotropy subgroups (green and yellow). Invariant sets due to symmetry are marked in green and exotic balanced polydiagonal in yellow [8].*

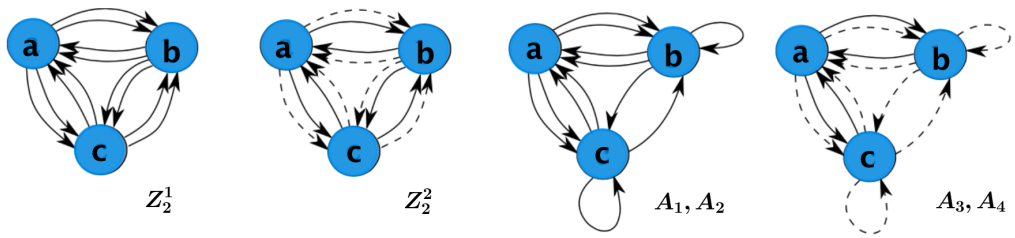

Figure 3.3: *Quotient networks of the subgroups that have listed in Table 3.1 and correspond to the nearest and next nearest neighbour coupling in Figure 3.2(a), There are two types of the arrows: solid and dashed. Solid means an input between the original phases. Dashed denotes an input with phase-shift by π. As seen that symmetry D_3 is in the quotients for Z_2^1 and Z_2^2 and symmetry Z_2 is in the quotients for A_3 and A_4.*

Then, there was found a weak chimera state that is stable in the invariant subspace A_1

[8]. After rewriting the system (3.6) in the subspace A_1 using (3.5), we get

$$\begin{aligned}\dot{\phi_1} &= \omega + 2g(\phi_1-\phi_2) + 2g(\phi_1-\phi_3),\\ \dot{\phi_2} &= \omega + 2g(\phi_2-\phi_1) + g(\phi_2-\phi_3) + g(0),\\ \dot{\phi_3} &= \omega + 2g(\phi_3-\phi_1) + g(\phi_3-\phi_2) + g(0).\end{aligned} \tag{3.8}$$

The quotient network (3.8) can be written using phase differences. Defining $\xi = \phi_1 - \phi_3$, $\eta = \phi_2 - \phi_3$, and $\xi - \eta = \phi_1 - \phi_2$, we obtain

$$\begin{aligned}\dot{\xi} &= 2g(\xi-\eta) + 2g(\xi) - 2g(-\xi) - g(-\eta) - g(0),\\ \dot{\eta} &= 2g(\eta-\xi) + g(\eta) - 2g(-\xi) - g(-\eta).\end{aligned} \tag{3.9}$$

The special case of (3.2, 3.9) where $\alpha = \pi/2$ and $r = 0$ is

$$\begin{aligned}\dot{\xi} &= 2\cos(\eta-\xi) - \cos(\eta) - 1,\\ \dot{\eta} &= 2\cos(\eta-\xi) - 2\cos(\xi),\end{aligned} \tag{3.10}$$

which was used in [8] to give a numerical observation of neutrally stable weak chimera states within A_1 (see Figure 3.4).

The family of solutions for the system (3.10) is shown in Figure 3.4. In this thesis we introduce coordinates x, y such that $\xi = x + y$, $\eta = 2y$ (see Figure 3.4). Under these coordinates the system has a time-reversing symmetry that can be represented as a reflection. We write system (3.9) in the variables x, y:

$$\begin{aligned}\dot{x} &= 2g(x-y) + 2g(x+y) - g(-x-y) - (1/2)g(-2y)\\ &\quad -g(0) - g(y-x) - (1/2)g(2y),\\ \dot{y} &= g(y-x) + (1/2)g(2y) - g(-x-y) - (1/2)g(-2y).\end{aligned} \tag{3.11}$$

By using (3.2), we obtain

$$\begin{aligned}\dot{x} &= -2\sin(\alpha)\cos^2(y) + 24r\sin(x)\cos(x)\cos^2(y) - 6\sin(x)\cos(y)\cos(\alpha)\\ &+ 2\cos(x)\cos(y)\sin(\alpha) - 12r\sin(x)\cos(x),\\ \dot{y} &= -2\cos(x)\sin(y)\cos(\alpha) + 2\sin(x)\sin(y)\sin(\alpha) + 8r\cos^2(x)\sin(y)\cos(y)\\ &- 8r\sin(y)\cos(y) - 2\cos(\alpha)\sin(y)\cos(y) + 8r\sin(y)\cos^3(y).\end{aligned} \tag{3.12}$$

After substituting $\alpha = \pi/2, r = 0$ and simplifying of the above equations, we get

$$\begin{aligned} \dot{x} &= f(x,y) = 2\cos(y)\cos(x) - 2\cos^2(y), \\ \dot{y} &= g(x,y) = 2\sin(y)\sin(x), \end{aligned} \tag{3.13}$$

note that this system has a Hamiltonian structure which is investigated in Chapter four.

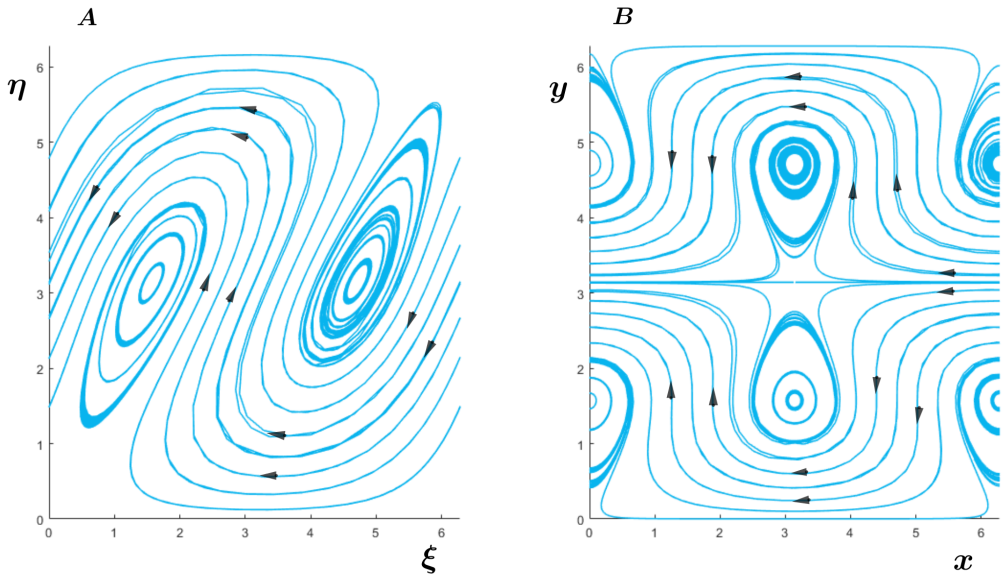

Figure 3.4: *Panel A shows the phase portrait for the system* (3.10) *[8]. Changes on coordinates for this system that are represented at phase portrait at panel B for the system* (3.13)*. Note the presence of a band of periodic solutions that wind around* ξ *and* x *coordinate, these solutions correspond to weak chimeras of the system.*

Numerical analysis of (3.9) is used in [8] to investigate the existence of birth and death of weak chimera states. Here, we use a similar numerical method to illustrate phase portraits for the system (3.11, 3.2) on varying α for $r = 0$ and $r = -0.01$(see Figures 3.5, 3.6 and 3.7). Moreover, we choose arbitrarily two initial points, one is near an equilibrium point and the other is far always, and simulate time series for these points to show where chimera states can be found. There are many observations one can get from these figures, but we will concentrate on the situation where the value of $\alpha = \pi/2$. Observe there is a set of neutrally stable weak chimera states that wind around x. There are also neutrally stable periodic orbits that are not chimera, winding around a centre equilibrium point.

3.3 Simulation and bifurcation of weak chimera in a six oscillator system

This section describes the changes in phase portraits and bifurcation diagrams for the system (3.12) within A_1 as a result of changing values of parameters α and r. Also, birth and death of weak chimera states are explained as α is varied. Bifurcation diagrams are computed using XPPAUT, and phase portraits are drawn using MATLAB. Note that the phase portraits of the new system (3.12) and of the old system (3.9) are different as illustrated in Figure 3.4, while the bifurcation diagrams are similar for both systems (see Figures 3.9, 3.8 and Figure 9 in [8]).

Phase portraits for the system (3.12) for increasing values of α and $r = 0, -0.01$ are shown in Figures 3.5, 3.6 and 3.7 with labels Ai to Ci (i=1,2,...,12). Figures 3.8, 3.9 show bifurcation diagrams with labels α_i, i = lower case letters and sketches A, B, C, D.

There is no a weak chimera at $\alpha = 0.5$ as shown in phase portrait C1, where a pitchfork bifurcation appears for an equilibrium point (see Figures 3.8). In addition, initial conditions pink/purple converge to a stable point at A1, B1. In C2 and C8, phase portraits present similar dynamics but different stability. That is illustrated at time series A2 and B2 where typical initial conditions converge to a non-chimera cycle while A8 and B8 show chimera states for pink and purple initial conditions. After the transition from C2 to C3 where $\alpha = 1.13016$, unstable spiral point and saddle point come together to create a saddle-connection for the weak chimera cycle at α_a and sketch D (Figure 3.8). The same scenario but with different stability happens at $C7$ and α_c in Figure 3.8D (i.e. stable spiral point and saddle point come together to create a saddle-connection).

The significant case is at $\alpha = 1.5,\ 1.64$. There are unstable and stable homoclinic bifurcations (non-chimera) as shown in transition from $C3$ to $C4$ and $C5$ to $C6$ which corresponds to branch (α_n, α_m) and sketches A, B respectively. Purple point converges to homoclinic orbits (non-chimera), while the pink point goes to a stable equilibrium point as shown in the time series A4, B4 respectively. At A6, time series have the similar structure for A4, whereas appearance of chimera state is clear at B6.

The case $\alpha = \alpha_b := \pi/2$ is interesting as there exist two families of neutral stable periodic orbits. One family consists of weak chimera state moves around x, and the other consists of periodic orbits that are not chimera in C5. There is a degenerate Andronov-Hopf bifurcation for the non-chimera cycle at branch α_b, α_o (see sketch C in Figure 3.8) that appears as many generic branches of periodic orbit for $r \neq 0$ in Figure 3.9. Purple initial condition converges to stable periodic orbit at A5, whereas existence of the weak chimera solution is evident for the limit of the pink initial condition B5.

In Figure 3.9, a slight change in the value of r from $r = 0$ to $r = -0.01$ leads to supercritical hopf bifurcation of three weak chimera cycle at α_b with the transition from $\alpha = 1.561$ (C9) to 1.558 (C10). Moreover, there is a saddle node bifurcation of two weak chimera-cycles at α_ℓ (C9). Also, there is a homoclinic bifurcation when transition from C10 to C11 that limits to heteroclinic at C12. Saddle connection bifurcations appear for the weak chimera cycle at $\alpha_a, \alpha_c, \alpha_k$ and α_e. Time series show convergence to an equilibrium point at A9, A10 and A11 and to an attracting chimera solution at B9, B10, B11, B12 and A12.

There is a saddle-node bifurcation for equilibrium point at C12 that corresponds to α_i and α_h. At Figure 3.9, the pink/purple initial conditions converge to a weak chimera cycle.

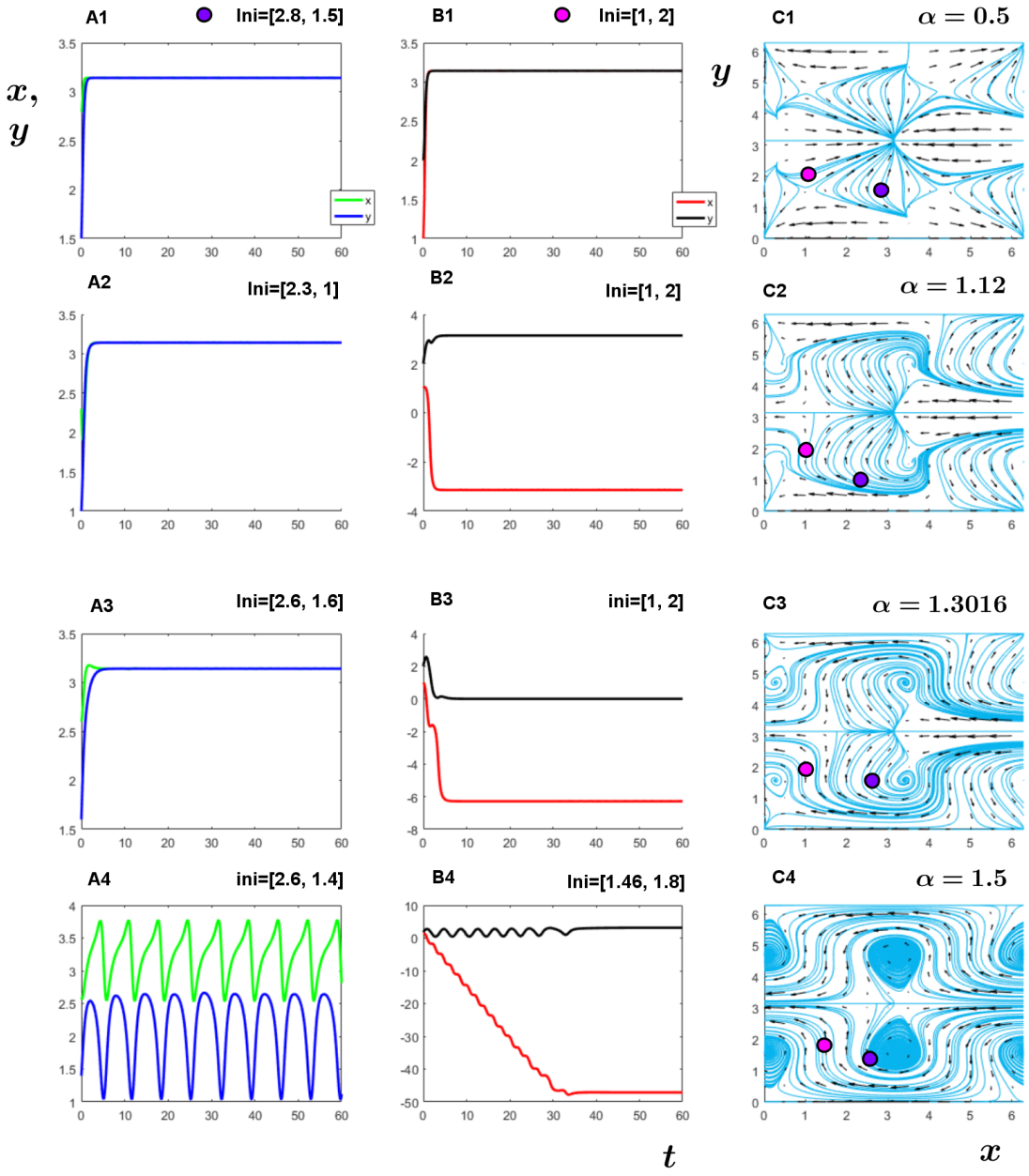

Figure 3.5: *This figure illustrates the dynamics of the system (3.2, 3.13) in the plane $x, y \in [0, 2\pi)$ with increasing values of parameters α and $r = 0$. The first two columns (Ai and Bi, i=1, 2, 3, 4) of panels show the time series $(x(t), y(t))$ for initial conditions shown as purple/pink dots in the third column (Ci, i=1, 2, 3, 4) which illustrate phase portraits. Arrows indicate the direction of flow in the phase plane. Noted in $\alpha = 0.5 - 1.3016$ the pink/ purple initial conditions have the similar dynamics and there are no chimera states. Nearly the same situation is at $\alpha = 1.5$ with slightly change that the purple point converges to a periodic orbit.*

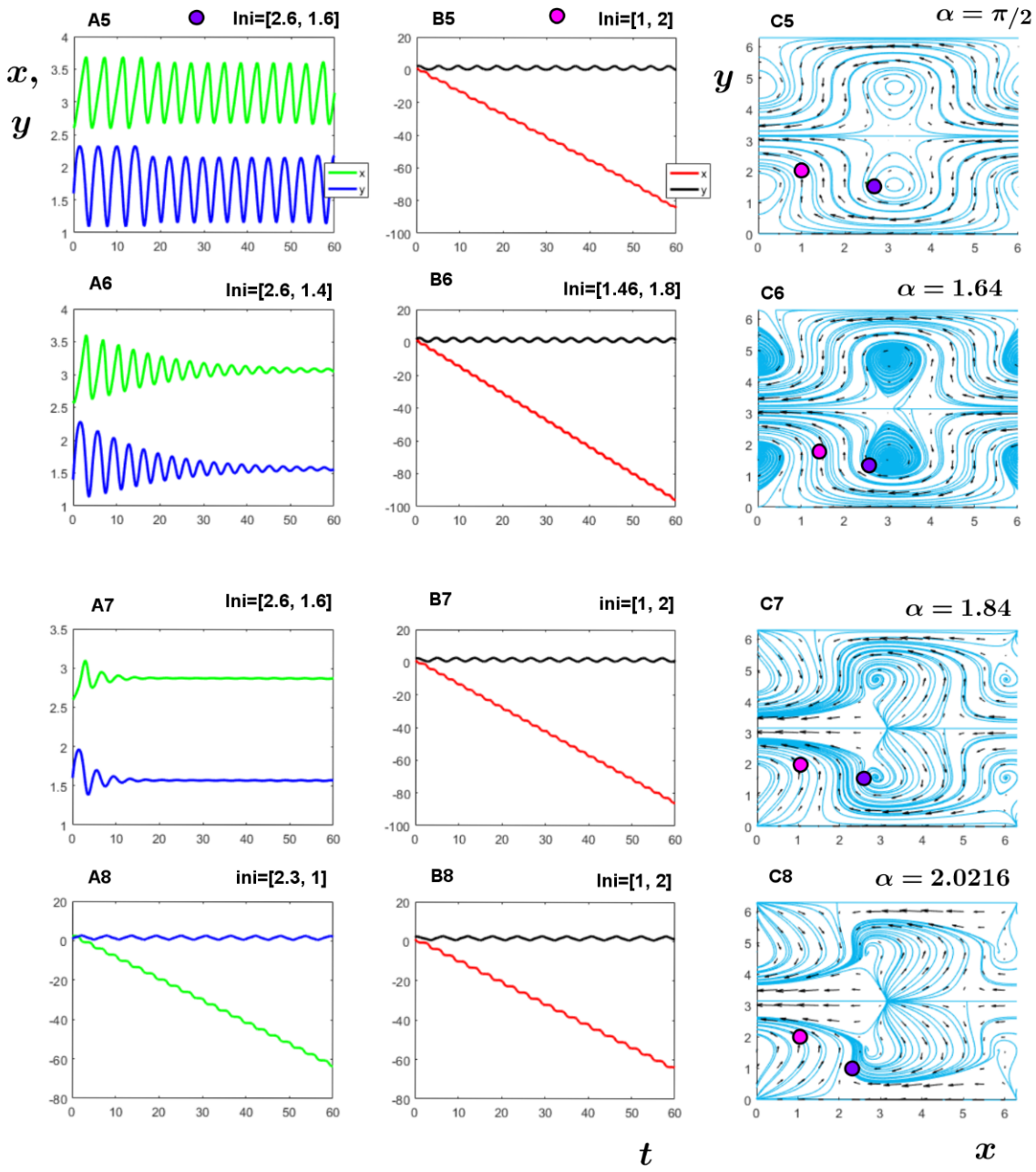

Figure 3.6: *(Description is as in Figure 3.5 except for further increasing values of α). For the conservative case α = π/2 at A5, B5, C5 shows the pink initial condition that evolves towards a weak chimera at B5, whereas purple initial condition is on a neutrally stable periodic orbit in C5. There is a homoclinic bifurcation at the transition from C6 to C7, and a saddle connection appears at C8. There is a weak chimera solution in the panels B5-B8 and A8 while the purple point converges to periodic orbit in (A5-A7).*

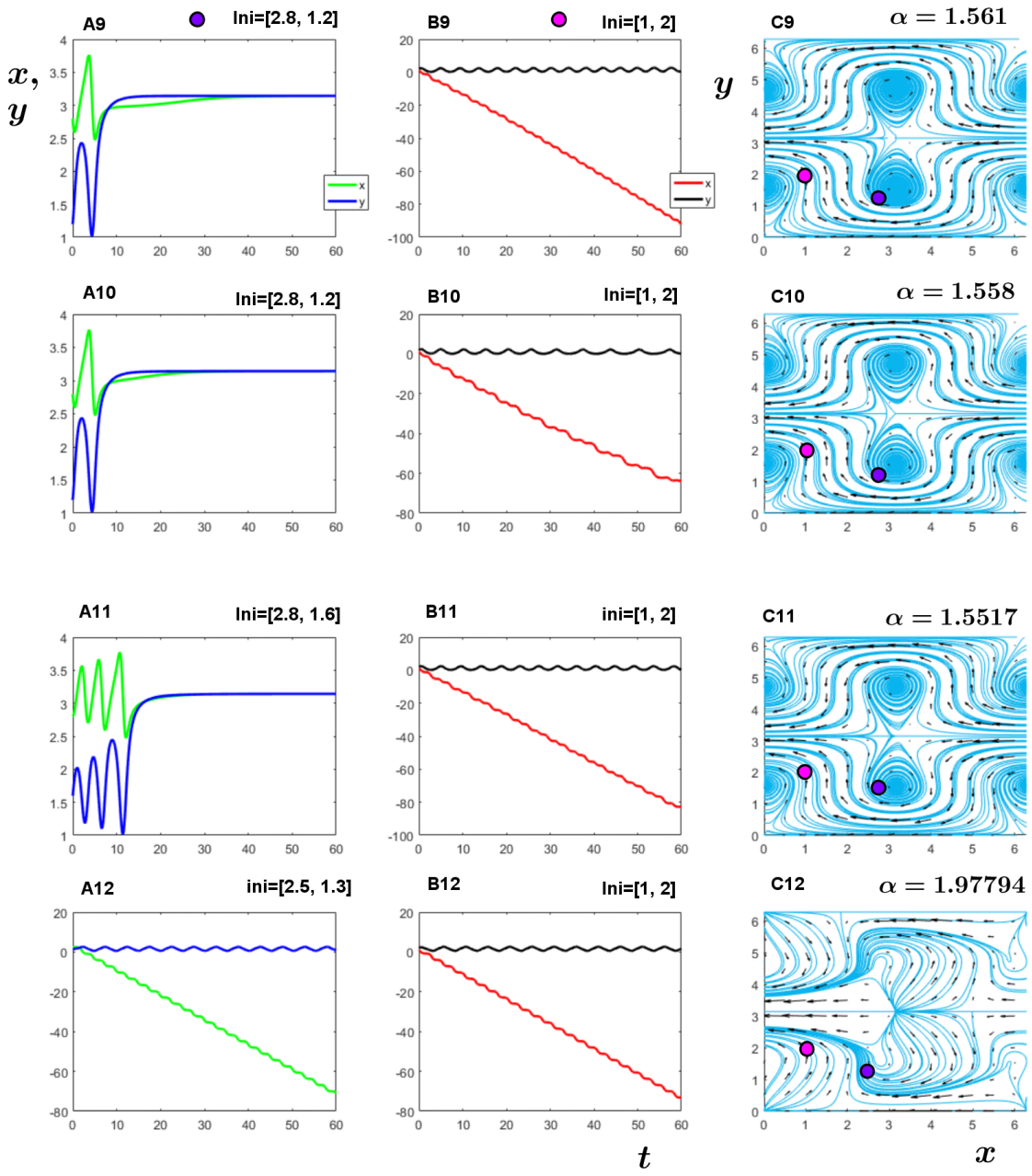

Figure 3.7: *(Description is as in Figure 3.5 except for further increasing values of α). Time series and phase portrait for the system (3.2, 3.12) depict what happens at r=-0.01 and α ∈* [1.561, 1.97794]. *At the left column, the initial condition (purple point) converges to a fixed point at A*9, *A*10, *A*11, *while a weak chimera still appears in A*12 *and the second column. Phase portraits (C9-C12) show different behaviours of trajectories as values of α vary.*

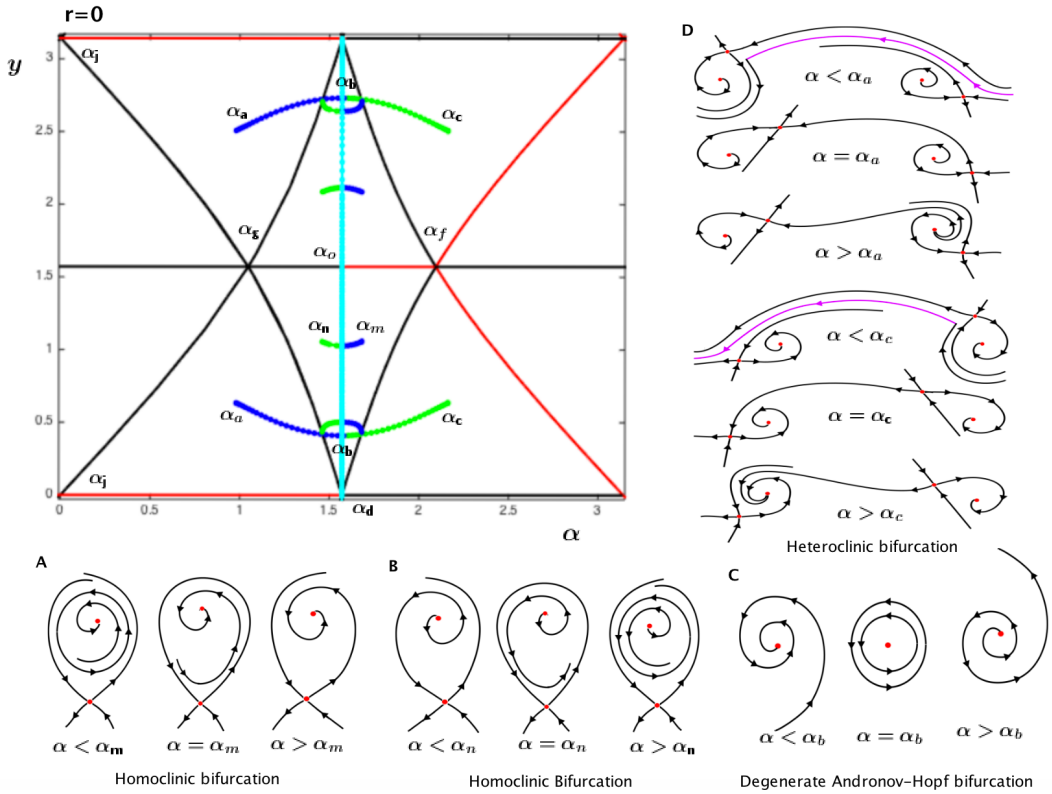

Figure 3.8: *Bifurcation diagram shows α against y for the system (3.2, 3.13) with Kuramoto-Sakaguchi coupling (r = 0) recomputed from [8]. Red/black lines refer to stable/unstable equilibria, green/blue lines indicate maxima/minima of y on stable/unstable periodic orbits and cyan line shows neutral periodic orbits. Red points in the sketches A, B, C, D refer to the saddle, spiral or center equilibria point. Purple lines for the sketch D refer to weak chimera cycles.*

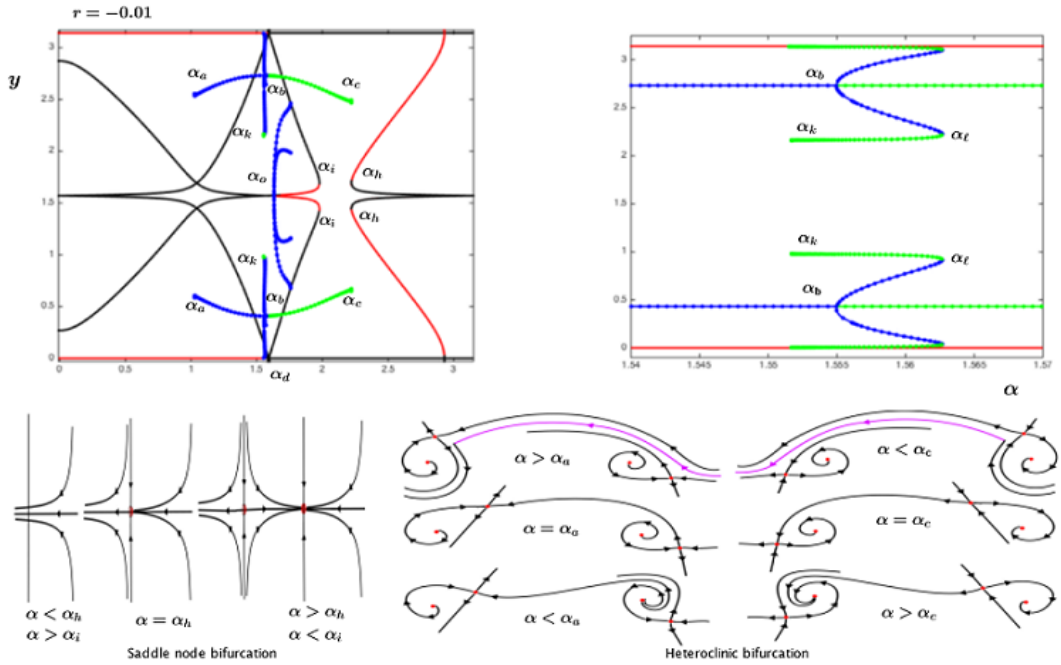

Figure 3.9: *(For details of the figure format, see Figure 3.8) Bifurcation diagram for the system (3.12) with r=-0.01 and varying α recomputed from [8]. The top right panel shows some details of the top left panel. The equilibria have saddle-node bifurcations at α_i, α_h shown in* C12.

3.4 Using parameter symmetries to relate $r > 0$ and $r < 0$

Ashwin and et al. [7] considered the dynamics of globally coupled phase oscillators depending on the coupling function (3.2) and the number of oscillators N. They showed that there are time-reversal symmetries for the behaviour of phase difference when the coupling function g is even. In addition, they concentrated on studying of parameter symmetries for two harmonic coupling

$$g(\phi) = q\sin(\phi - \alpha) + r\sin(2\phi - \beta)$$

where q, r, α and β are arbitrary constants. One can show [7] that there are symmetries that keep the coupling function $g(\phi) \to g(\phi)$ for all ϕ if

$$(q, r, \alpha, \beta) \to (-q, r, \alpha + \pi, \beta),$$

$$(q, r, \alpha, \beta) \to (q, -r, \alpha, \beta + \pi).$$

Moreover, there is a time-reversal parameter symmetry such that $g(\phi) \to -g(\phi)$ for all ϕ with $q = -1$ and $(r, \alpha, \beta) = (r, \alpha + \pi, \beta + \pi)$. They also find a phase-reversal parameter symmetry $(g(\phi) \to -g(-\phi))$ for all ϕ with assuming $q = -1$ and $(r, \alpha, \beta) = (r, -\alpha, -\beta)$.

Some parameter symmetry implications for (3.1) are studied in [7]. They can be used to reduce the number of parameters and to help understand the behaviour of the system on changing the sign of a parameter. We study effects of a particular parameter symmetry that has phase and time-reversal on the system (3.1). A parameter reversal occurs under reversing r and shifting α:

$$S_1(r, \alpha, \theta_i, t) \to (-r, \pi - \alpha, \theta_i, t).$$

Also, phase and time reversal happen at

$$S_2(r, \alpha, \theta_i, t) \to (r, \alpha, -\theta_i, -t)$$

such that $(g(\phi) \to g(-\phi))$. The system (3.1) has symmetry $S = S_1 \circ S_2$ so that $S(r, \alpha, \theta_i, t) = (-r, \pi - \alpha, -\theta_i, -t)$. One can check that the equation (3.2) is invariant under the symmetries of S. Using this symmetry, we can understand the behaviour of the system (3.1) just examining part of the entire parameter space.

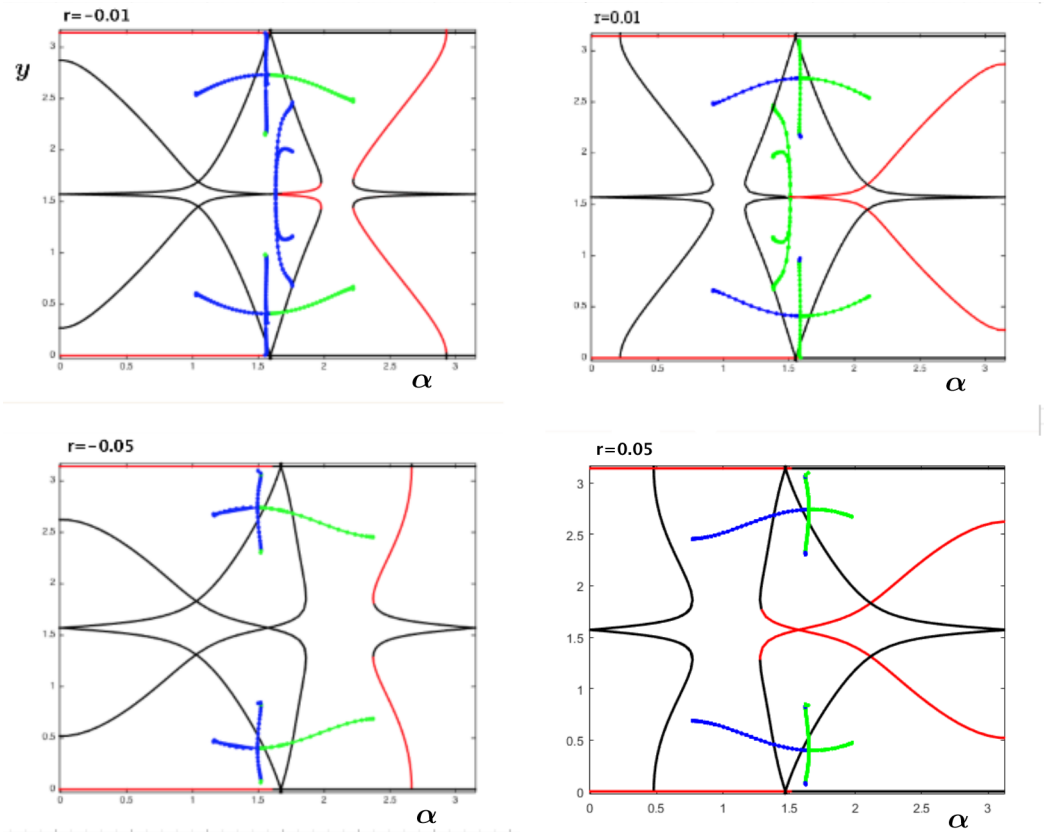

Figure 3.10: *Left column is bifurcation diagrams for the system (3.12) with parameters* $r = -0.01$ *and* -0.05. *Right column shows bifurcation diagrams for* $r = 0.01, 0.05$. *Note the presence of the parameter reversing symmetry given by* r, α *goes to* $-r, \pi - \alpha$ *represents parameter reversing symmetry of this system with* $\pi - \alpha$ *and* $r = 0.01,\ 0.05$. *Red/black lines refer to stable/unstable equilibria, green/blue lines indicate stable/unstable periodic orbits.*

A reflection of the diagram but with changes in the stability of the system (3.12) can be seen on changing the sign of r in the bifurcation diagram (Figure 3.10). These modifications of stability for equilibria points and periodic orbits are the implications of symmetry S. Suppose that $\varphi_{r,\alpha}(t, x(0), y(0))$ is time-t solution for (3.12) with parameters (r, α) and initial condition at $(x(0), y(0))$. Then this solution with S-symmetry means

$$\varphi_{r,\alpha}(t, x(0), y(0)) = (x(t), y(t)) \Leftrightarrow \varphi_{-r,\pi-\alpha}(-t, \pi - x(0), y(0)) = (\pi - x(t), y(t)),$$

for all $t, x(0), y(0), r, \alpha$. In particular, if (x^*, y^*) is an equilibrium point for (3.12) with (r, α) i.e. $\varphi_{r,\alpha}(t, (x(0), y(0)) = (x^*, y^*)$ for all t, then $\varphi_{-r,\pi-\alpha}(t, \pi - x(0), y(0)) = (\pi - x^*, y^*)$ for all t is an equilibrium point for $(-r, \pi - \alpha)$. Moreover, if $(x(0), y(0))$ is a saddle at α_h for (r, α)

with eigenvalues, $\lambda_0 < 0 < \mu_0$, then $(\pi - x(0), y(0))$ is still a saddle at α_{h^*} for $(-r, \pi - \alpha)$ with eigenvalues $-\mu_0 < 0 < -\lambda_0$. Also, if $(x(0), y(0))$ is a linearly stable equilibrium for (r, α) with eigenvalue $Rr(\lambda_0), Rr(\mu_0) < 0$, on the branches α_b, α_c, then $(\pi - x(0), y(0))$ is a linearly unstable equilibrium for $(-r, \pi - \alpha)$ with eigenvalue $-Rr(\lambda_0), -Rr(\mu_0) < 0$ at $\alpha_{b^*}, \alpha_{c^*}$.

In summary, this time-reversal parameter symmetry provides qualitative information about changes in behaviour and stability of equilibria or periodic orbits of the system (3.1) for suitably transformed parameters.

CHAPTER 4

WEAK CHIMERA SOLUTIONS AND INTEGRABILITY FOR A SYSTEM OF SIX OSCILLATORS

In [8], the authors have shown numerically that there are weak chimera states for a six oscillator networks (3.5, 3.2) with a range of parameters, and this is investigated in Chapter three 3. This chapter aims to give a rigorous analytical justification of this statement in the special case when $\beta = r = 0$. It consists of four sections. In Section 4.1 we prove the system of coupled phase oscillators has an integral of motion $E(x, y)$ when $\beta = r = 0$ working on a subset $M \subseteq \mathbb{T}^2$. Section 4.2 proves properties of the flow on subsets of M using a number of lemmas. Then, Section 4.3 illustrates the motion of trajectory in the whole M by reversing symmetry. Finally, Section 4.4 proves there is an infinite number of chimera states on the trajectories in A_1 for the special case.

4.1 Integrability and reversibility of the system in A_1 for $\beta = r = 0$

In this section we first demonstrate there is an integrable structure in the subspace A_1 for (3.5, 3.2) in the special case $r = \beta = 0$ and use this to prove existence of weak chimeras. More

precisely:

$$\begin{aligned} \dot{x} &= f(x,y) = 2\cos(y)\cos(x) - 2\cos^2(y), \\ \dot{y} &= g(x,y) = 2\sin(y)\sin(x). \end{aligned} \tag{4.1}$$

Lemma 4.1. *The system (3.5, 3.2) of six oscillators with $\beta = r = 0$ has an integral of motion within the subspace A_1 listed in Table 3.1.*

Proof. For the system on A_1 written as (4.1), we define

$$E(x,y) := y + \cos y \sin y - 2\sin y \cos x. \tag{4.2}$$

Taking partial derivatives of $E(x,y)$ with respect to both variables

$$\begin{aligned} \frac{\partial E}{\partial y} &= -2\sin y \sin x, \\ \frac{\partial E}{\partial y} &= 2\cos y \cos x + \sin^2 y - \cos^2 y - 1. \end{aligned} \tag{4.3}$$

Combining (4.1) and (4.3), the rate of change for E on trajectories of (4.1) is

$$\frac{d}{dt}\left[E(x(t),y(t))\right] = \frac{\partial E}{\partial x}\dot{x} + \frac{\partial E}{\partial y}\dot{y} = 0, \quad \forall x, y \in \mathbb{R}^2. \tag{4.4}$$

Hence $E(x,y)$ is constant on trajectories of (4.1) and does not depend explicitly on time (see Figure 4.1). Therefore, $E(x,y)$ is an integral of the motion. ■

Figure 4.1 illustrates the level curves of $E(x,y)$ in the (x,y) plane: each level curve is preserved by the dynamics of (4.1) and hence is a union of trajectories. We denote the level curve of $\tilde{E} \in \mathbb{R}$ by

$$C(\tilde{E}) = \left\{(x,y) \in \mathbb{T}^2 : E(x,y) = \tilde{E}\right\}.$$

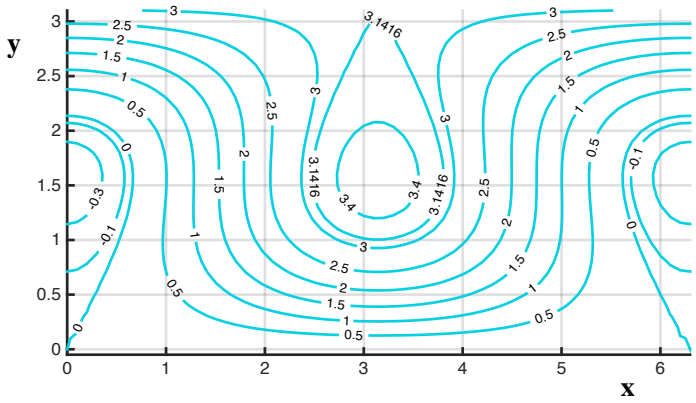

Figure 4.1: *Every level for $E(x,y)$ defined by (4.2) in the region $(x,y) \in [0,2\pi] \times [0,\pi]$ has a constant value on the domain M. Each connected component of a level curve is invariant for the flow (4.1).*

We consider the domain of (4.1) on the region $M = \{(x,y) : 0 < y < \pi \text{ and } 0 < x < 2\pi\} = H_r \cup H_\ell$, where $H_r := \{(x,y) : \pi < x < 2\pi \text{ and } 0 < y < \pi\}$ and $H_\ell := \{(x,y) : 0 < x < \pi \text{ and } 0 < y < \pi\}$. Note that the upper and lower boundaries of M are level curves for E and hence H_r and H_ℓ are invariant sets under the flow (see Figure 4.2). For almost all $\tilde{E} \in [0,\pi]$, the level curves in M consist of periodic trajectories though there are exceptional level curves that contain equilibria and connecting orbits.

In the reminder of this section, we prove there is periodic trajectories wind around the torus in the following sense,

Lemma 4.2. *For any $0 < \tilde{E} < \pi$ there is an initial condition $(x(0), y(0)) \in C(\tilde{E})$ and $T > 0$ such that if $(x(t), y(t))$ is a trajectory of the system (4.1) then $x(T) = x(0) - 2\pi$ and $y(T) = y(0)$.*

A prove of the above Lemma is in the section 4.3. The system (4.1) consists of coupled first-order differential equation and has an integral of motion. Also, this system has a reversing symmetry R_1 and a symmetry R_2 (see [56]) as follow,

$$R_1 \begin{pmatrix} x \\ y \end{pmatrix} := \begin{pmatrix} 2\pi - x \\ y \end{pmatrix}, \quad R_2 \begin{pmatrix} x \\ y \end{pmatrix} := \begin{pmatrix} x \\ 2\pi - y \end{pmatrix},$$

in the sense that if we write (4.1) as

$$\begin{pmatrix} \dot{x} \\ \dot{y} \end{pmatrix} = F \begin{pmatrix} x \\ y \end{pmatrix} = \begin{pmatrix} 2\cos y \cos x - 2\cos^2 y \\ 2\sin y \sin x \end{pmatrix},$$

then

$$F \circ R_1 \begin{pmatrix} x \\ y \end{pmatrix} = -R_1 \circ F \begin{pmatrix} x \\ y \end{pmatrix},$$

and

$$F \circ R_2 \begin{pmatrix} x \\ y \end{pmatrix} = R_2 \circ F \begin{pmatrix} x \\ y \end{pmatrix},$$

for all $(x, y) \in \mathbb{T}^2$ (see Appendix A.1 for details). A consequence of this is that the flow in H_r corresponds to the time reversed flow on $R_1(H_\ell)$.

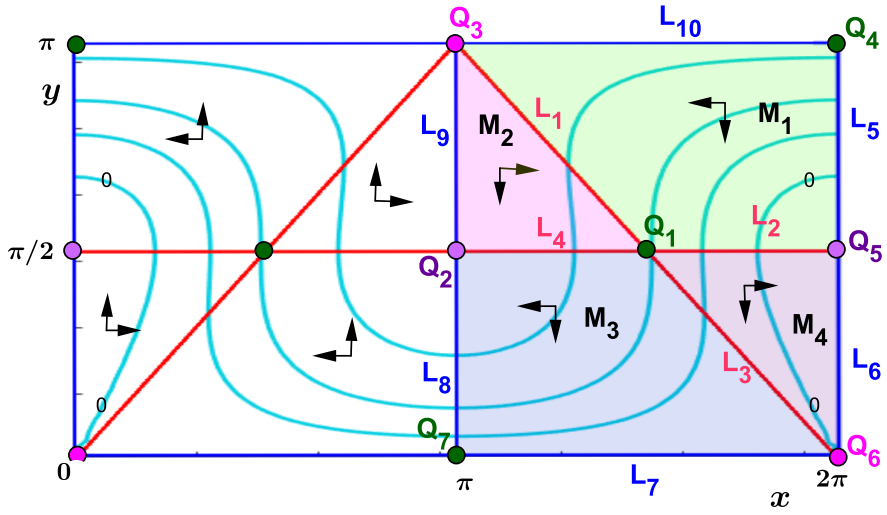

Figure 4.2: *The flow (4.1) on the invariant set* $\overline{M} \subset \mathbb{T}^2$*, where* $M = \{(x, y) : 0 < y < \pi, 0 < x < 2\pi\}$*. The regions* H_r *and* $H_\ell = R_1(H_r)$ *are shown as white and block of colored areas respectively. We define a partition of* H_r *into a union of four open regions: green* M_1*, pink* M_2*, blue* M_3*, and purple* M_4*, points* $Q_i, i = 1,2,3,4,5,6,7$ *and lines (without endpoints)* $L_i, i = 1,2,...,10$*. The pink points* Q_3*,* Q_6 *are degenerate saddles while the purple points* Q_2*,* Q_5 *are centre equilibria. Trajectories are cyan, and black arrows represent direction of* $\dot{x}$*,* $\dot{y}$*. Blue/red lines are nullclines where* $\dot{y} = 0$ *and* $\dot{x} = 0$ *respectively. The nullclines allow us to decompose* M *into a collection of open sets, in each of which the vector field points in one direction.*

4.1.1 Partition of the set M

In order to understand properties of trajectories inside the set M, we partition the set into bounded areas using nullclines for system (4.1). Then, some definitions will be introduced that describe the regions of $H_r \subset M$ (see Figure 4.2) as follow:

Definition 4.1. *The bounded areas of the set $H_r \subset M$ are:*

$M_1 = \{(x,y) : \pi/2 < y < \pi \text{ and } 2\pi - y < x < 2\pi\}$,

$M_2 = \{(x,y) : \pi/2 < y < \pi \text{ and } \pi < x < 2\pi - y\}$,

$M_3 = \{(x,y) : 0 < y < \pi/2 \text{ and } \pi < x < 2\pi - y\}$,

$M_4 = \{(x,y) : 0 < y < \pi/2 \text{ and } 2\pi - y < x < 2\pi\}$.

Definition 4.2. *The following nullclines segments L_i, $i = 1,2,...,10$. (see Figure 4.2) are:*

$L_1 = \{(x,y) : \pi/2 < y < \pi \text{ and } x = 2\pi - y\}$,

$L_2 = \{(x,y) : y = \pi/2 \text{ and } 3\pi/2 < x < 2\pi\}$,

$L_3 = \{(x,y) : 0 < y < \pi/2 \text{ and } x = 2\pi - y\}$,

$L_4 = \{(x,y) : y = \pi/2 \text{ and } \pi < x < 3\pi/2\}$,

$L_5 = \{(x,y) : \pi/2 < y < \pi \text{ and } x = 2\pi\}$,

$L_6 = \{(x,y) : 0 < y < \pi/2 \text{ and } x = 2\pi\}$,

$L_7 = \{(x,y) : y = 0 \text{ and } \pi < x < 2\pi\}$,

$L_8 = \{(x,y) : 0 < y < \pi/2 \text{ and } x = \pi\}$,

$L_9 = \{(x,y) : \pi/2 < y < \pi \text{ and } x = \pi\}$,

$L_{10} = \{(x,y) : y = \pi \text{ and } \pi < x < 2\pi\}$.

Note that the boundary of each M_i is a union of $\overline{L}_i$ as shown in Figure 4.2.

Definition 4.3. *Define the following points: $Q_1 = (3\pi/2, \pi/2)$, $Q_2 = (\pi, \pi/2)$, $Q_3 = (\pi, \pi)$, $Q_4 = (2\pi, \pi)$, $Q_5 = (2\pi, \pi/2)$, $Q_6 = (2\pi, 0)$, and $Q_7 = (\pi, 0)$, (see figure 4.2).*

Lemma 4.3. *Note that $\overline{H}_r = \cup_{i=1}^{4} \overline{M}_i$, where the closures of the regions M_i, $i = 1,2,3,4$ are as follows:* $\overline{M}_1 = L_1 \cup L_2 \cup L_5 \cup L_{10} \cup Q_1 \cup Q_3 \cup Q_4 \cup Q_5 \cup M_1$,

$\overline{M}_2 = L_1 \cup L_4 \cup L_9 \cup Q_1 \cup Q_3 \cup Q_2 \cup M_2$,

$\overline{M}_3 = L_4 \cup L_8 \cup L_3 \cup L_7 \cup Q_1 \cup Q_2 \cup Q_7 \cup Q_6 \cup M_3$,

$\overline{M}_4 = L_2 \cup L_3 \cup L_6 \cup Q_1 \cup Q_5 \cup Q_6 \cup M_4$.

Proof. This proof is a verification that the sets defined above in 4.2 have closures as stated.

■

Note 4.1. *There are only four equilibria points Q_i, $i = 3,2,5,6$ of the system (4.1) in $\overline{H}_r$.*

4.2 Dynamics for the integrable case

We present a sequence of lemmas that analyse and describe the motion of trajectories on $H_r \subset M$. These lemmas are divided into two groups. The first two Lemmas 4.4, 4.5 identify the direction of trajectory inside the bounded areas M_1, M_2, M_3 and M_4. The second shows what happen when the trajectory reaches the boundary of each area after some finite time (Lemmas 4.6, 4.7, 4.8, 4.9).

Lemma 4.4. *If $(x,y) \in M_1$ or M_3 then $f(x,y) < 0$ and $g(x,y) < 0$ for (4.1), (see Figure 4.2).*

Proof. After factorizing (4.1), we get

$$\begin{aligned} \dot{x} &= f(x,y) = 2\cos(y)(\cos(x) - \cos(y)), \\ \dot{y} &= g(x,y) = 2\sin(y)\sin(x). \end{aligned} \tag{4.5}$$

Suppose $(x,y) \in M_1$ then $\pi/2 < y < \pi$ and $2\pi - y < x < 2\pi$. Then, we get $\cos(y) < 0$ and $\cos(2\pi - y) < \cos(x) < \cos(2\pi)$, and simplifying, $\cos(y) < 0$ and $0 < \cos(x) - \cos(y) < 1 - \cos(y)$. Because $\cos(x)$ is monotonic increasing on $x \in (\pi, 2\pi)$, then $\cos(y) < 0$ and $\cos(x) - \cos(y) > 0$ and we get that $f(x,y) < 0$.

Also for the same point, we obtain $\sin(y) > 0$ and $-\sin(y) < \sin(x) < 0$ then $\sin(y) > 0$ and $\sin(x) < 0$ and we get that $g(x,y) < 0$.

The statement for M_3 has a similar proof. ■

Lemma 4.5. *If $(x,y) \in M_2$ or M_4 then $f(x,y) > 0$ and $g(x,y) < 0$ for (4.5).*

Proof. Suppose $(x,y) \in M_2$, this means $\pi/2 < y < \pi$ and $\pi < x < 2\pi - y$. Then, we get $\cos(y) < 0$ and $\cos(\pi) < \cos(x) < \cos(2\pi - y)$, This is the same $\cos(y) < 0$ and $-1 - \cos(y) < \cos(x) - \cos(y) < 0$ which implies that $f(x,y) > 0$.

Following that, at the same point $(x,y) \in M_2$, we get $\sin(y) > 0$ and $-\sin(y) < \sin(x) < 0$. Hence $\sin(y) > 0$ and $\sin(x) < 0$ which implies that $g(x,y) < 0$.

The statement for M_4 has a similar proof. ■

Note that the solution of (4.1) monotonically decreases or monotonically increases along the trajectory within a region such as M_i.

The following Lemmas are 4.7, 4.8 and 4.9 explain what happens for an initial condition after time T for (4.1).

Lemma 4.6. *If an initial condition* $(x(0), y(0)) \in M_1 \cup L_5$*, then there exist* $T > 0$ *such that* $(x(T), y(T)) \in L_1 \cup L_2 \cup Q_1$.

Proof. Suppose $(x(0), y(0)) \in M_1$, then $x(t)$ and $y(t)$ are monotonically decreasing as long as they remain in M_1. Either there exists $T > 0$ such that $(x(T), y(T)) \in \overline{M_1} \setminus M_1$ or $(x(t), y(t)) \in M_1$ for all $t > 0$. In the first case there are two possibilities to describe the path of trajectory. Firstly, if the initial point $(x(0), y(0)) \in M_1$ then the trajectory of this point will eventually hit the boundary of M_1 at $(L_1 \cup L_2 \cup Q_1)$. Secondly, if the initial point $(x(0), y(0)) \in L_5$ then we still have $f(x(0), y(0)) < 0$ so $x(t)$ is monotonically decreasing for initial condition on L_5. Here for arbitrary small $t > 0$, $(x(t), y(t)) \in M_1$ and we apply the argument above.

In the second case, let the greatest lower bound of $x(t)$ and $y(t)$ be x_∞ and y_∞ respectively, (according to theorem of limits of monotone functions [41]). We get that

$$\lim_{t\to\infty} (x(t), y(t)) = (x_\infty, y_\infty).$$

Then (x_∞, y_∞) is a limit point. Since a limit set is an invariant set which has a single point then it is an equilibrium point [74]. Note there are no equilibrium points in M_1 so $(x_\infty, y_\infty) \in \overline{M_1} \setminus M_1$. By monotonicity for $(x(t), y(t))$, it would be in $L_1 \cup L_2 \cup Q_1$ which is a contradiction because no equilibrium point belongs to $L_1 \cup L_2 \cup Q_1$. As a consequence, the second case can not happen. ■

Lemma 4.7. *If an initial condition* $(x(0), y(0)) \in M_2 \cup L_1$*, then there exist* $T > 0$ *such that* $(x(T), y(T)) \in L_4$.

Proof. Suppose $(x(0), y(0)) \in M_2$, then $x(t)$ is monotonically increasing and $y(t)$ is monotonically decreasing as long they remain in M_2. Either there exists $T > 0$ such that $(x(T), y(T)) \in \overline{M_2} \setminus M_2$ or $(x(t), y(t))$ stay in M_2 for all $t > 0$. In the first case there are two possibilities. Firstly, if the initial point $(x(0), y(0)) \in M_2$ then the trajectory of $(x(0), y(0))$ will eventually hit the boundary of M_2 at L_4. Secondly, if the initial point $(x(0), y(0)) \in L_1$ then we still

have $g(x,y)<0$ so $y(t)$ is still monotonically decreasing for initial condition on L_1. Here for arbitrary small $t>0$, $(x(t),y(t))\in M_2$ and we apply the argument above.

In the second case, let the least upper bound $x(t)$ and the greatest lower bound $y(t)$ be x_∞ and y_∞ respectively, (according to theorem of limits of monotone functions [41]). We get

$$\lim_{t\to\infty}(x(t),y(t))=(x_\infty,y_\infty).$$

Then (x_∞,y_∞) is an equilibrium point [74] and $(x_\infty,y_\infty)\in\overline{M_2}$. Note that there is no equilibrium point in M_2 so $(x_\infty,y_\infty)\in\overline{M_2}\setminus M_2$. By monotonicity for $(x(t),y(t))$, it would be in L_4 which is a contradiction because no equilibrium point belongs to L_4 . As a consequence, the second case can not happen. ■

Lemma 4.8. *If $(x(0),y(0))\in M_4\cup L_2$ then either there exists $T>0$ such that $(x(T),y(T))\in L_3\cup L_6$ or $\lim_{t\to\infty}(x(t),y(t))=Q_6$.*

Proof. Suppose $(x(0),y(0))\in M_2$ then $x(t)$ is monotonically increasing and $y(t)$ is monotonically decreasing as long they remain in M_4. Either there exists $T>0$ such that $(x(T),y(T))\in\overline{M_4}\setminus M_4$ or $(x(t),y(t))$ belongs to M_4 for all $t>0$. In the first case there are two possibilities. Firstly, if the initial point $(x(0),y(0))\in M_4$ then the trajectory of $(x(0),y(0))$ will eventually hit the boundary of M_4 at $L_3\cup Q_6\cup L_6$. As Q_6 is an equilibrium point, we can only hit the boundary at $L_3\cup L_6$. Secondly, if the initial point $(x(0),y(0))\in L_2$ then we still have $g(x,y)<0$ so $y(t)$ is still monotonically decreasing for initial condition on L_2. Here for arbitrary small $t>0$ $(x(t),y(t))\in M_4$ and we apply the argument above. In the second case, monotonicity [41] implies that

$$\lim_{t\to\infty}(x(t),y(t))=(x_\infty,y_\infty).$$

Thus, x_∞ is the least upper bound of $x(t)$ and y_∞ is the greatest lower bound of $y(t)$. This means that $(x(t),y(t))\to(x_\infty,y_\infty)$ is a limit point and then it is an equilibrium point as $t\to\infty$ [74]. Since Q_6 is the only equilibrium point in $\overline{M_4}$ we have that $(x_\infty,y_\infty)=Q_6$. ■

Lemma 4.9. *If $(x(0),y(0))\in M_3\cup L_4\cup L_3\cup Q_1$, then there exists $T>0$ such that $(x(T),y(T))\in L_8$.*

Proof. Suppose $(x(0), y(0)) \in M_2$, then $x(t)$ is monotonically increasing and $y(t)$ is monotonically decreasing as long they remain in M_3. Either there exists $T > 0$ such that $(x(T), y(T)) \in \overline{M_3} \setminus M_3$ or $(x(t), y(t))$ belongs to M_3 for all $t > 0$. In the first case there are two possibilities. Firstly, if the initial point $(x(0), y(0)) \in M_3$ then the trajectory of the of $(x(0), y(0))$ will eventually hit the boundary of M_3 at $L_8 \cup L_7 \cup Q_7$. However $(x(T), y(T)) \in L_7 \cup Q_7$ as $y = 0$ because it is invariant under the flow. Hence if it hits the boundary after finite time, it can only hit L_8. Secondly, if the initial point $(x(0), y(0)) \in L_4, L_3$ or Q_1 then we still have $g(x, y) < 0$ so $y(t)$ is still monotonically decreasing for initial condition on L_4, L_3 and Q_1. Here for arbitrary small $t > 0$ $(x(t), y(t)) \in M_3$ and we apply the argument above.

In the second case, let the greatest lower bound of $x(t)$ and $y(t)$ be x_∞ and y_∞ respectively, (according to theorem of limits of monotone functions [41]). We get that

$$\lim_{t\to\infty} (x(t), y(t)) = (x_\infty, y_\infty).$$

Then (x_∞, y_∞) is limit point. Since a limit set is an invariant set that is a single point then it is an equilibrium point [74]. Note there are no equilibrium points in M_3 so $(x_\infty, y_\infty) \in \overline{M_3} \setminus M_3$. By monotonicity for $(x(t), y(t))$, it would be in L_8 which is a contradiction because no equilibrium point belong to L_8. As a consequence, the second case can not happen. ■

4.3 Extending the trajectories on H_r to trajectories on M

In this section, we discuss the structure of trajectories on the set M. The first lemma gives a condition that implies existence of a periodic orbit that winds in the first component (x) of torus.

Proof. (Lemma 4.2) Let $0 < \tilde{E} < \pi$. We claim there is an $(x(0), y(0)) \in C(\tilde{E}) \cap L_5$. To see this, we consider $(x(0), y(0)) = (2\pi, z)$, $z \in (\pi/2, \pi)$ which parametrizes L_5. Note that

$$E(2\pi, z) = -2 + \pi/2 < 0 \text{ for } z = \pi/2,$$

and

$$E(2\pi, z) = \pi \text{ for } z = \pi.$$

Hence for any $\tilde{E} \in (0,\pi)$ there exists $z \in (\pi/2,\pi)$ such that $E(2\pi,z) = \tilde{E}$ by the Intermediate Value Theorem. In fact this is unique in the sense the derivative dE/dz does not change sign in $(0,\pi)$. Suppose $(x(t),y(t))$ is the trajectory of (4.1) that starts at $(x(0),y(0)) \in C(\tilde{E}) \cap L_5$. According to Lemma 4.6, there exists $T_1 > 0$ such that $(x(T_1),y(T_1)) \in L_1 \cup Q_1 \cup L_2$. We have the following

1. If $(x(T_1),y(T_1)) \in L_1$ then by Lemma 4.7 there exists $T_2 > T_1$ such that $(x(T_2),y(T_2)) \in L_4$, and then by Lemma 4.9, there exists $T_3 > T_2$ such that $(x(T_3),y(T_3)) \in L_8$.

2. If $(x(T_1),y(T_1)) \in Q_1$ then by Lemma 4.9, there exists $T_3 > T_1$ such that $(x(T_3),y(T_3)) \in L_8$.

3. If $(x(T_1),y(T_1)) \in L_2$ then by Lemma 4.8 and using the fact $\tilde{E} \geq 0$ on $L_6 \cup Q_6$ there exists $T_2 > T_1$ such that $(x(T_2),y(T_2)) \in L_3$. According to Lemma 4.9, there exists $T_3 > T_2$ such that $(x(T_3),y(T_3)) \in L_8$.

We now show that this trajectory reaches $x(T) = x(0) - 2\pi,\ y(T) = y(0)$ at $T := 2T_3$. Firstly, we have defined H_r and H_ℓ, such that $R_1(H_r) = H_\ell$. Let the trajectory $(x(t),y(t)) \in H_r$ for all $0 < t < T_3$ and we define $(\tilde{x}(t),\tilde{y}(t)) := R_1(x(t),y(t))$. Because R_1 is a reversing symmetry on the torus, note that $(\tilde{x}(-t),\tilde{y}(-t))$ is also a trajectory. Moreover, we note that $R_1(L_8) = L_8$ and define

$$\begin{aligned} \tilde{L}_5 &:= R_1(L_5) = \{(2\pi - x, y) : \pi/2 < y < \pi,\ x = 2\pi\} \\ &= \{(0,y) : \pi/2 < y < \pi\}. \end{aligned} \tag{4.6}$$

Note that $(x(0),y(0)) \in L_5 \cap C(\tilde{E})$ and $(x(T_3),y(T_3)) \in L_8$. Now $(\tilde{x}(-t),\tilde{y}(-t))$ is a trajectory on H_ℓ for $-T_3 < t < 0$. Also,

$$(\tilde{x}(0),\tilde{y}(0)) = R_1(x(0),y(0)) = (2\pi - x(0), y(0)) \in \tilde{L}_5,$$

and

$$(\tilde{x}(T_3),\tilde{y}(T_3)) = R_1(x(T_3),y(T_3)) = (x(T_3),y(T_3)) = L_8.$$

So if we define $(x(T_3+t), y(T_3+t)) = (\tilde{x}(T_3-t), \tilde{y}(T_3-t))$, $0 < t < T_3$ then $(x(t), y(t))$ is a trajectory for $0 < t < 2T_3$. In particular, we have shown there is a trajectory such that $x(T) = x(0) - 2\pi$ and $y(T) = y(0)$. ■

Recall that the ω-limit set $\Lambda^+(x,y)$, and the α-limit set $\Lambda^-(x,y)$ are defined:

$$\Lambda^+(x,y) := \bigcap_{T>0} \overline{\bigcup_{s>T} \varphi(x,y,s)},$$
$$\Lambda^-(x,y) := \bigcap_{T<0} \overline{\bigcup_{s<T} \varphi(x,y,s)},$$

where $\varphi(x,y,t)$ is the flow generated by (4.1).

Lemma 4.10. *Suppose $\tilde{E} = 0$, then there is a point $(x(0), y(0)) \in C(\tilde{E}) \cap L_5$ such that $(x(t), y(t))$ is a homoclinic orbit that limits to Q_6 (see Figure 4.2).*

Proof. For $\tilde{E} = 0$, we claim that there is an initial condition $(x(0), y(0)) \in C(\tilde{E}) \cap L_5$ such that $E(x(0), y(0)) = 0$. Consider $(x(0), y(0)) = (2\pi, z)$ where $z \in (\pi/2, \pi)$. By a similar argument to the proof of Lemma 4.2 there exists $z \in (\pi/2, \pi)$ such that $E(2\pi, z) = \tilde{E}$. If we write $(x(t), y(t))$ to be the solution of system (4.1) starting at the point $(x(0), y(0))$ then $E(x(t), y(t)) = 0$ for all $t > 0$. According to Lemma 4.6, there is $T_1 > 0$ such that the trajectory of $(x(t), y(t))$ will hit L_2. Depending on Lemma 4.8, either there is $T_2 > T_1$ such that $(x(T_2), y(T_2)) \in L_3 \cup L_6$ or $(x(t), y(t)) \in M_4$ stays at M_4 for all $t > 0$ and converges to Q_6 as $t \to \infty$. We will focus just on the second possibility. Because the system (4.1) is reversible then there is $T_2 < 0$ such that the trajectory of $(x(-t), y(-t))$ converges to Q_6 for all $0 > t > -T_2$. More precisely , we have

$$\lim_{t \to \pm\infty} E(x(t), y(t)) = Q_6,$$

so that $\Lambda^+(x,y) = \Lambda^-(x,y) = Q_6$ This trajectory is called a homoclinic orbit [59]. ■

4.4 Dynamics on A_1 and weak chimeras

This section relates the dynamics of (4.1) to synchrony and desynchrony of the phase oscillators. In particularly, we show existence of an infinite number of chimera states that are neutrally stable for integrable case (4.1).

Theorem 4.11. *Consider any $0 < \tilde{E} < \pi$, then the level curve $C(\tilde{E})$ for system (4.1) is a trajectory $(x, y) \in \mathbb{R}^2$ and there is $T = T(\tilde{E})$ such that $x(T) = x(0) - 2\pi$ and $y(T) = y(0)$. More precisely, if $(x, y) \in C(\tilde{E})$ then*

$$\lim_{t\to\infty} \frac{1}{t}\, y(t) = 0 \quad \textit{and} \quad \lim_{t\to\infty} \frac{1}{t}\, x(t) = \frac{2\pi}{T} \neq 0.$$

Proof. Define $Y_0 = \{(x,0) : 0 \le x \le 2\pi\}$, $Y_\pi = \{(x,\pi) : 0 \le x \le 2\pi\}$ as the lower and upper boundaries of M. Noted that Y_0 and $Y_\pi \subset \overline{M}$. These boundaries are invariant sets for the system (4.1) since $\dot{y} = 0$ for all Y_0 and Y_π, therefore

$$0 \le y(t) \le \pi, \qquad \forall\ t > 0,$$

and

$$0 \le \frac{y(t)}{t} \le \frac{\pi}{t}, \qquad \forall\ t > 0.$$

We now take the limit and obtain

$$0 \le \lim_{t\to\infty} \frac{1}{t}[y(t)] \le \lim_{t\to\infty} \frac{\pi}{t}.$$

In consequence, $\lim_{t\to\infty} \frac{1}{t}[y(t)] = 0$ for any $0 < \tilde{E} < \pi$ and $(2\pi, y) \in C(\tilde{E})$.

Now we will prove the second part of the result: Let $(x(0), y(0)) \in C(\tilde{E})$ such that $(x(0), y(0)) = (2\pi, y(0))$ by Lemma 4.2 there is a $0 < T < \infty$ such that $(x(T), y(T)) = (0, y(0))$. If we define $n = n(t) := \lfloor t/T \rfloor$ then

$$nT \le t < (n+1)T, \tag{4.7}$$

and hence

$$-2\pi(n+1) < x(t) \le -2\pi n. \tag{4.8}$$

Dividing (4.8) by (4.7), we get that

$$\frac{-2\pi n}{(n+1)T} > \frac{x(t)}{t} > \frac{-2\pi(n+1)}{nT}. \tag{4.9}$$

By taking the limit for (4.9), we get

$$\frac{-2\pi}{T} \ge \lim_{t\to\infty} \frac{x(t)}{t} \ge \frac{-2\pi}{T},$$

which can be simplified as follows

$$\lim_{t\to\infty}\frac{x(t)}{t}=\frac{-2\pi}{T}\neq 0.$$

■

Theorem 4.12. *The system (3.5, 3.2) of six oscillators with $\beta = r = 0$ has an infinite number of chimera states within A_1 that are neutrally stable.*

Proof. We know that $y=\frac{1}{2}(\phi_2-\phi_3)$ and $x=\phi_1-\phi_3-y$. Also, from Theorem 4.11 with given hypothesis, we have that for any $0<\tilde{E}<\pi$ there is t such that

$$\lim_{t\to\infty}\frac{1}{t}\,y(t)=0, \tag{4.10}$$

which is expanded to

$$\lim_{t\to\infty}\frac{1}{t}\,y(t)=\frac{1}{2}\lim_{t\to\infty}\frac{1}{t}[\phi_2(t)-\phi_3(t)]=\frac{1}{2}\Omega_{23}\quad\text{[Frquency differnce (3.4)]}. \tag{4.11}$$

Then from (4.10) and (4.11), we yield

$$\frac{1}{2}\Omega_{23}=\lim_{t\to\infty}\frac{1}{t}[y(t)]=0.$$

This means there is frequency synchronization between $\phi_2(T)$ and $\phi_3(T)$. To show that ϕ_1 and ϕ_3 are not frequency synchronized ($\Omega_{13}\neq 0$), we need to prove that a curve from $x=0$ to $x=2\pi$ is continuous and there is no an equilibrium point on the level curve. Let $(x(0),y(0))\in C(\tilde{E})$ and $0<\tilde{E}<\pi$ be an initial condition for the system (4.1). Then there is $T>0$ such that $(x(T),y(T))=(x(0)-2\pi,y(0))$ (Lemma 4.2), (i.e. the trajectory will return to its initial condition after time T). In addition, since the solution for this initial condition $\lim_{t\to\infty}\frac{1}{t}(x(t),y(t))=(-2\pi/T,0)\neq(0,0)$, (Theorem 4.11). That means this trajectory does not converge to a equilibrium point (Lemma 4.10) and continuous. According to our previous result we have

$$\lim_{t\to\infty}\frac{1}{t}\,x(t)=\frac{-2\pi}{T}<0.$$

which implies to

$$\lim_{t\to\infty}\frac{x(t)}{t}=\lim_{t\to\infty}\frac{\phi_1-\phi_3+y(t)}{t}=\lim_{t\to\infty}\frac{\phi_1-\phi_3}{t}+\lim_{t\to\infty}\frac{y(t)}{t}=\lim_{t\to\infty}\frac{\phi_1-\phi_3}{t}=\frac{-2\pi}{T}<0,$$

which implies that $\Omega_{13} \neq 0$. That refers to exist frequency dsynchronization between ϕ_1 and ϕ_3. From the above argument, we get a weak chimera solution (Definition 3.1). As a consequence, for each $\tilde{E}$ in the infinite set $(0,\pi)$ there is a distinct chimera state. As these are not isolated they are not hyperbolic. ■

CHAPTER 5

STABILITY OF WEAK CHIMERA CHIMERA SOLUTIONS FOR $\beta, r \neq 0$

In chapter 3, we found and studied chimera solutions for various values of α with $r = 0$ and -0.01 for system (3.12) by using XPPAUT (Numerical Continuation Methods). While in chapter 4, a weak chimera state was found analytically for $\beta = r = 0$. In this chapter, we analytically and numerically investigate chimera states for $\beta, r \neq 0$. In Section 5.1, the system (3.12) is translated from $(\alpha, r) = (\pi/2, 0)$ to the origin $\beta = \pi/2 - \alpha = 0$ and $r = 0$ in the parameters space. This enable us to study stability and bifurcation for chimera states when the parameters are sufficiently small. We also deduce an equation with one variable and two parameters from the planar system (3.12) and integral of motion (4.2). In addition, we compute an approximation for the period and other properties for chimera solutions. In Section 5.2, we use the first return map to approximate these weak chimera solutions in the near-integrable limit. Although these are not analytically solvable, we are able to approximate the integrals numerically and compare them to numerical continuation results (in section 3.3) in order to understand stability and bifurcation of these weak chimera states in the final section 5.3.

5.1 Calculating the period for the chimera solutions with $\beta, r = 0$

We simplify system (3.12) for $\alpha = \pi/2 - \beta$ to get the following system for $(x, y) \in \mathbb{T}^2$ depending on two parameters β and r,

$$\begin{aligned}
\dot{x} &= 24r\sin(x)\cos(x)\cos^2(y) - 6\sin(x)\cos(y)\sin(\beta) \\
&+ 2\cos(x)\cos(y)\cos(\beta) - 12r\sin(x)\cos(x) - 2\cos(\beta)\cos^2(y), \\
\dot{y} &= 2\sin(y)(4r\cos^2(x)\cos(y) + 4r\cos^3(y) + \sin(x)\cos(\beta) \\
&- \cos(x)\sin(\beta) - \cos(y)\sin(\beta) - 4r\cos(y)).
\end{aligned} \tag{5.1}$$

The above system has an integral motion for $\beta = 0$, $r = 0$ (according to Lemma 4.1) and the same function $E(x, y)$ as in (4.2), recall

$$E(x, y) := y + \cos y \sin y - 2\sin y \cos x. \tag{5.2}$$

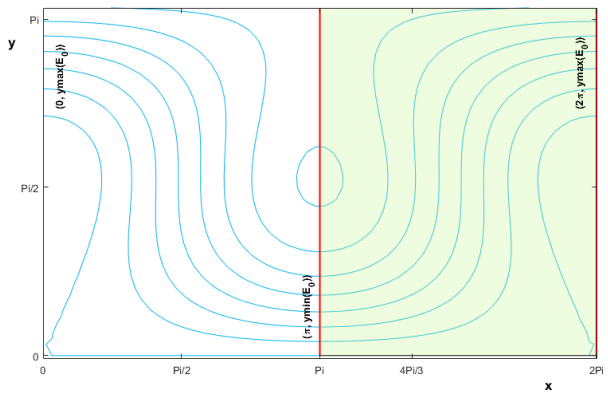

Figure 5.1: *This figure shows cyan level curves $C(\tilde{E})$ for (5.2) at some values of E on the set $M \in \mathbb{T}^2$ that is divided into two areas left H_ℓ and right H_r. Note that any value of $\tilde{E}$, $C(\tilde{E})$ is a graph over y within H_ℓ and H_r, but $C(\tilde{E})$ is not a graph over x or over y on M.*

In order to describe stability of chimera solutions for $\beta, r \neq 0$ and any level curves $0 < \tilde{E} < \pi$, we first need to understand properties of the level curves $C(\tilde{E})$ for $0 < \tilde{E} < \pi$. According

to Figure 5.1, the level curves are not graphs over x or y for the whole period $0 < t < T(\tilde{E})$, where $T(\tilde{E})$ is as in Theorem 4.11. Therefore, we highlight the region H_r from $x(0) = 2\pi k$ to $x(T/2) = 2\pi k - \pi$ (see the green right part H_r in Figure 5.1). The geometric properties of all the level curves on half period H_r is that each of these levels nullclines pass through maximum of y at $(2\pi k, y_{max}(\tilde{E}))$ to minimum of y at $(2\pi k - \pi, y_{min}(\tilde{E}))$, $k = 0, 1, ..., n \in \mathbb{N}$. In particular, in this range of $\tilde{E}$, the curve $(x, y) \in C(\tilde{E}) \cap H_r$ is a graph over

$$y_{min}(\tilde{E}) \leq y \leq y_{max}(\tilde{E}) \tag{5.3}$$

given by the unique solution of (5.2) $E(x, y) = \tilde{E}$ with $x \in [\pi, 2\pi]$, This can be written

$$x = \Delta_{\tilde{E}}(y) := 2\pi - \arccos\left[\frac{\cos y \sin y + y - \tilde{E}}{2 \sin y}\right], \tag{5.4}$$

where arccos is the usual inverse on $[0, \pi]$. In order to compute a numerical approximation for the period $T(\tilde{E})$, we firstly find the values of y_{max}, $y_{min} \in (0, \pi)$. Hence, substituting $x(0) = 2\pi$ and $x(T/2) = \pi$ in (5.2), we obtain

$$\begin{aligned} E(2\pi, y_{max}) &= y_{max} + \cos(y_{max}) \sin(y_{max}) - 2\sin(y_{max}) = \tilde{E}, \\ E(\pi, y_{min}) &= y_{min} + \cos(y_{min}) \sin(y_{min}) + 2\sin(y_{min}) = \tilde{E}. \end{aligned} \tag{5.5}$$

Then we solve above equations for y and note that the root is unique and smoothly depends on $\tilde{E}$ in this range. However the equations (5.5) are transcendental, we need to solve using Maple's `evalf` to get numerical approximation for values of y_{max} and y_{min} (see Figure 5.2 and Appendix A.2.1).

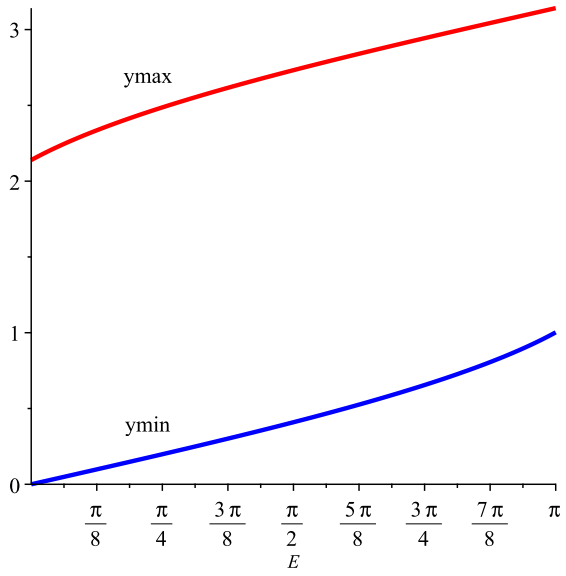

Figure 5.2: *The values of y_{max} and y_{min} against E for (5.5) are shown as curves.*

Now, we will compute the time of period $T(\tilde{E})$ of every level curve $0 < \tilde{E} < \pi$ for the system (5.1) with $\beta = r = 0$,

$$\dot{x} = f(x,y) = 2\cos(y)\cos(x) - 2\cos^2(y), \tag{5.6}$$

$$\dot{y} = g(x,y) = 2\sin(y)\sin(x). \tag{5.7}$$

From the equation (5.2), we have

$$\cos(x) = \frac{\cos(y)\sin(y) + y - \tilde{E}}{2\sin(y)}, \tag{5.8}$$

$$\sin(x) = \mp\frac{\sqrt{4\sin^2(y) - (\cos(y)\sin(y) + y - \tilde{E})^2}}{2\sin(y)}. \tag{5.9}$$

On the level curve $(x,y) \in C(\tilde{E})$, we can eliminate the variable x by substituting (5.9) in (5.7) to become

$$\dot{y} = g(\Delta_{\tilde{E}}(y), y) = -\sqrt{4\sin^2(y) - (\cos(y)\sin(y) + y - \tilde{E})^2}. \tag{5.10}$$

The core result for removing x is that all trajectories on the domain $M \in \mathbb{T}^2$ (see Figure 5.1) will be governed by the equation (5.10) with one variable y. If we integrate (5.10) over the

half period within H_r we obtain

$$\int_{t=0}^{T(\tilde{E})} dt \;=\; -2\int_{t=0}^{T(\tilde{E})/2} \frac{1}{\sqrt{4\sin(y)^2 - (\cos(y)\sin(y) + y - \tilde{E})^2}}\, dy.$$

Writing the integration limits in terms of y then gives

$$T(\tilde{E}) \;=\; 2\int_{y_{min}(\tilde{E})}^{y_{max}(\tilde{E})} \frac{1}{\sqrt{4\sin(y)^2 - (\cos(y)\sin(y) + y - \tilde{E})^2}}\, dy. \tag{5.11}$$

Figure 5.3 shows a numerical approximation of $T(\tilde{E})$ for $\tilde{E} \in (0,\pi)$ computed using Maple's `evalf`. Note that, $T(\tilde{E}) \to \infty$ as $\tilde{E} \to 0^+$ or $\tilde{E} \to \pi^-$ and T is finite between these limits. There is a symmetry $T(\tilde{E}) = T(-\tilde{E}+\pi)$ and $T(\tilde{E})$ has a unique minimum value at $\tilde{E} = \pi/2$.

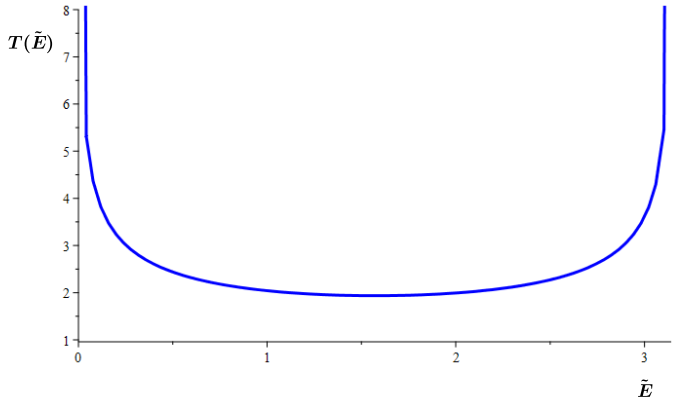

Figure 5.3: *Period $T(\tilde{E})$ of the weak chimera solution of (5.1) for $\tilde{E} \in (0,\pi)$ in the integrable case $\beta = r = 0$, computed using (5.11). Observe that the period tends to infinity as the level curve approaches the heteroclinic orbits at $\tilde{E} = 0$ and π.*.

5.2 Approximation of chimera solutions for $\beta, r \neq 0$

In the previous chapter, weak chimera states were analytically observed for the system (5.1) at specific parameter values $\beta, r = 0$. The aim of this section is to find an approximate Poincaré map for the more general case (5.1). Then, we use this map to prove existence of chimera states for $\beta, r \neq 0$. Let us choose a Poincaré section $\Sigma_p \subseteq \mathbb{T}^2$ where

$$\Sigma_p = \{(x,y) \in \mathbb{T}^2 : x = 2\pi \text{ and } y \in (0,\pi)\}.$$

The time of first return of $(x,y) \in \Sigma_p$ is defined by

$$\tau(x,y) = \inf\{t > 0 : \varphi(x,y,t) \in \Sigma_p \text{ and } (x,y) \in \Sigma_p\},$$

where $\varphi(x,y,t)$ is the flow of the system (5.1). The Poincaré first return map $P : \Sigma_p \to \Sigma_p$ is defined by $P(x,y) = \varphi(x,y,\tau(x,y))$. Let us write $P(2\pi, y) = P(2\pi, y_{max}(E))$ so that we parametrize the chimera using $E \in (0,\pi)$. Then

$$P(2\pi, y) = P(2\pi, y_{max}(E)) = (2\pi, y_{max}\tilde{P}(E))). \tag{5.12}$$

So the first return P can be understood as a map $\tilde{P} : (0,\pi) \to (0,\pi)$,

$$E_{n+1} = \tilde{P}(E_n). \tag{5.13}$$

We know in the integrable case, the chimera periodic orbits intersect Σ_p at fixed points of the Poincaré map, i.e $\tilde{P}(\tilde{E}) = \tilde{E}$ for all $\tilde{E}$ and $\beta = r = 0$. More generally, note from (5.2) that

$$\frac{d}{dt}\big[E(x(t), y(t))\big] = \frac{\partial E}{\partial x}\dot{x} + \frac{\partial E}{\partial y}\dot{y}, \tag{5.14}$$

for all $(x,y) \in \mathbb{R}^2$. Combining (5.1) and (5.14) we get

$$\frac{dE}{dt}(x,y) = G(x,y)\sin\beta + F(x,y)r \tag{5.15}$$

where

$$\begin{aligned} G(x,y) &:= 4\sin y\big[4\cos y\cos^2 x - \cos^3 y - 3\cos y\big], \\ F(x,y) &:= 4\sin y\big[4\cos^5 y - 4\cos^4 y\cos x \\ &\quad + 4\cos^3 y\cos^2 x - 16\cos^2 y\cos^3 x - 4\cos^3 y \\ &\quad + 16\cos^2 y\cos x + 6\cos^3 x - 6\cos x\big]. \end{aligned}$$

Substituting (5.4) in (5.15) and defining $G_{\tilde{E}}(y) := G(\Delta_{\tilde{E}}(y), y)$ and $F_{\tilde{E}}(y) := F(\Delta_{\tilde{E}}(y), y)$, such that $\Delta_{\tilde{E}}$ is the $x-$component of the level curve for $\tilde{E}$ at y (given in (5.4)), we get

$$\frac{dE}{dt}(\Delta_{\tilde{E}}(y), y) = G_{\tilde{E}}(y)\sin\beta + F_{\tilde{E}}(y)r, \tag{5.16}$$

where

$$\begin{aligned}
G_{\tilde{E}}(y) &= 4\sin(y)\big[\cos^3(y) - \cos(y)\,\frac{(\cos(y)\sin(y)+y-\tilde{E})^2}{\sin^2(y)} \\
&+ 3\cos(y)\big], \\
F_{\tilde{E}}(y) &= 4\sin(y)\big[-4\cos^5(y) + 2\cos^4(y)\,\frac{(\cos(y)\sin(y)+y-\tilde{E})}{\sin(y)} \\
&- \cos^3(y)\,\frac{(\cos(y)\sin(y)+y-\tilde{E})^2}{\sin^2(y)} \\
&+ 2\cos^2(y)\,\frac{(\cos(y)\sin(y)+y-\tilde{E})^3}{\sin^3(y)} \\
&+ 4\cos^3(y) - 8\cos^2(y)\,\frac{(\cos(y)\sin(y)+y-\tilde{E})}{\sin(y)} \\
&- 3/4\,\frac{(\cos(y)\sin(y)+y-\tilde{E})^3}{\sin^3(y)} \\
&+ 3\,\frac{(\cos(y)\sin(y)+y-\tilde{E})}{\sin(y)}\big].
\end{aligned} \tag{5.17}$$

Now assume that $(\beta, r) = (\epsilon\tilde{\beta}, \epsilon\tilde{r})$ and consider the behaviour of (5.1) in the limit $0 < \epsilon \ll 1$ for fixed $(\tilde{\beta}, \tilde{r}) \neq (0,0)$. Note that in this case the system is nearly Hamiltonian and we can use perturbations theory [95], [86] as follows,

$$\frac{dE}{dt}(\Delta_{\tilde{E}}(y), y) = \epsilon[G_{\tilde{E}}(y)\tilde{\beta} + F_{\tilde{E}}(y)\tilde{r}] + O(\epsilon^2), \tag{5.18}$$

and so on trajectories $(x(t), y(t))$, E varies slowly with t if ϵ is small.

Suppose now that $E_0 \in (0,\pi)$ and $(x(0), y(0)) \in \Sigma_p \cap C(E_0)$. For any $T > 0$ such that $(x(t), y(t)) \in H_r$ for all $0 < t < T$, we can approximate (5.4) to get

$$x(t) = \Delta_{\tilde{E}}(y(t)) = \Delta_{E_0}(y(t)) + O(\epsilon), \tag{5.19}$$

where the error term also depends linearly on T. Moreover, if $T(E_0) < \infty$ then (using the symmetry between H_r and H_ℓ there will be first return to Σ_p after time $T(E_0) + O(\epsilon)$ that is close to E_0.

We approximate this first return (5.13) in the case $\epsilon > 0$: for $(x(t), y(t)) \in H_r$, note that using (5.19) in (5.18) we have

$$\frac{dE}{dt}(\Delta_{\tilde{E}}(y), y) = \epsilon[G_{E_0}(y)\tilde{\beta} + F_{E_0}(y)\tilde{r}] + O(\epsilon^2). \tag{5.20}$$

If the trajectory next intersects Σ_p at $(0, y_{max}(E_1))$ after time $T = T(E_0) + O(\epsilon)$ then we can approximate

$$\begin{aligned} E_1 - E_0 &= \int_{t=0}^{T} \frac{dE}{dt}\, dt \\ &= 2\epsilon \int_{t=0}^{\frac{T(E_0)}{2}} [G_{E_0}(y)\tilde{\beta} + F_{E_0}(y)\tilde{r}]\, dt + O(\epsilon^2) \\ &= \epsilon \Lambda(E_0, \tilde{\beta}, \tilde{r}) + O(\epsilon^2). \end{aligned} \tag{5.21}$$

where (changing the limits of integration) and defining from (5.10) that $g_{E_0}(y) := g(\Delta_{E_0}(y), y)$ we can write

$$\begin{aligned} \Lambda(E_0, \tilde{\beta}, \tilde{r}) &:= -2 \int_{y_{min}(E_0)}^{y_m ax(E_0)} \frac{G_{E_0}(y)\tilde{\beta} + F_{E_0}(y)\tilde{r}}{g_{E_0}(y)}\, dy \\ &= -2(\Lambda_1(E_0)\tilde{\beta} + \Lambda_2(E_0)\tilde{r}), \end{aligned} \tag{5.22}$$

where

$$\begin{aligned} \Lambda_1(E_0) &:= \int_{y_{min}(E_0)}^{y_m ax(E_0)} \frac{G_{E_0}(y)}{g_{E_0}(y)}\, dy = \int_{y_{min}(E_0)}^{y_{max}(E_0)} \frac{\tilde{G}_{E_0}(y)}{\sqrt{4\sin^2(y) - (\cos(y)\sin(y) + y - E_0)^2}}\, dy, \\ \Lambda_2(E_0) &:= \int_{y_{min}(E_0)}^{y_m ax(E_0)} \frac{F_{E_0}(y)}{g_{E_0}(y)}\, dy = \int_{y_{min}(E_0)}^{y_{max}(E_0)} \frac{\tilde{F}_{E_0}(y)}{\sqrt{4\sin^2(y) - (\cos(y)\sin(y) + y - E_0)^2}}\, dy. \end{aligned}$$

Hence the Poincaré map $E_1 = \tilde{P}(E_0)$ satisfies

$$\begin{aligned} \tilde{P}(E_0) &= E_0 + \epsilon \Lambda(E_0, \tilde{\beta}, \tilde{r}) + O(\epsilon^2) \\ &= E_0 - 2\epsilon[\Lambda_1(E_0)\tilde{\beta} + \Lambda_2(E_0)\tilde{r}] + O(\epsilon^2). \end{aligned} \tag{5.23}$$

In the next theorem, we show the existence of a weak chimera state for $\Lambda(E_n, \tilde{\beta}, \tilde{r})$ at $E_0 = \pi/2$ and $(\beta, r) \neq (0, 0)$.

Theorem 5.1. *For the open set of $(\tilde{\beta}, \tilde{r})$ such that the first derivative of $\Lambda(E_0, \tilde{\beta}, \tilde{r})$ does not equal zero (i.e. $\Lambda_1'(\pi/2)\tilde{\beta} + \Lambda_2'(\pi/2)\tilde{r} \neq 0$), if ϵ is small enough then system (5.1) with $(\beta, r) = (\epsilon\tilde{\beta}, \epsilon\tilde{r})$ has a periodic orbit that is close to the level curve of (5.2) corresponding to $E_0 = \pi/2$. This periodic orbit corresponds to a weak chimera state of (5.22).*

Proof. Note that in the special case $E_0 = \pi/2$, (5.22) gives

$$\Lambda(\pi/2, \tilde{\beta}, \tilde{r}) = -2(\Lambda_1(\pi/2)\tilde{\beta} + \Lambda_2(\pi/2)\tilde{r}). \tag{5.24}$$

In this case, $y_{max} = \pi - y_{min}$ can be found from (5.5) and (5.2) using $E_0 = \pi/2$ to give

$$\begin{aligned} \pi/2 &= y_{max} + \cos y_{max} \sin y_{max} - 2 \sin y_{max}, \\ \pi/2 &= \pi - y_{max} - \cos y_{max} \sin y_{max} + 2 \sin y_{max}. \end{aligned}$$

Hence $y_{max} = \pi - y_{min}$ for $E = \pi/2$. We now compute

$$\begin{aligned} \Lambda_1(\pi/2) &= \int_{y_{min}}^{\pi/2} \hat{G}(y)\, dy + \int_{\pi/2}^{y_{max}} \hat{G}(y)\, dy, \\ \Lambda_2(\pi/2) &= \int_{y_{min}}^{\pi/2} \hat{F}(y)\, dy + \int_{\pi/2}^{y_{max}} \hat{F}(y)\, dy, \end{aligned}$$

where we define

$$\begin{aligned} \hat{G}(y) &= \frac{G_{\pi/2}(y)}{g_{\pi/2}(y)}, \\ \hat{F}(y) &= \frac{F_{\pi/2}(y)}{g_{\pi/2}(y)}. \end{aligned} \tag{5.25}$$

Because $\hat{G}(y) = -\hat{G}(\pi - y)$ and $\hat{F}(y) = -\hat{F}(\pi - y)$ we can compute

$$\Lambda_1(\pi/2) = \Lambda_2(\pi/2) = 0. \tag{5.26}$$

Hence, $\Lambda(\pi/2, \tilde{\beta}, \tilde{r}) = 0$ for all $\tilde{\beta}$, and $\tilde{r}$. On the other hand, one can check numerically that neither of $\Lambda_1'(\pi/2)$ or $\Lambda_2'(\pi/2)$ are zero (see Figure 5.4), which means that there is an open set of $\tilde{\beta}$ and $\tilde{r}$ such that

$$\Lambda_1'(\pi/2)\tilde{\beta} + \Lambda_2'(\pi/2)\tilde{r} \neq 0. \tag{5.27}$$

We approximate the derivative by using small h in

$$\Lambda_1'(\pi/2) \approx \frac{\Lambda_1(\pi/2 + h) - \Lambda_1(\pi/2)}{h},$$

and

$$\Lambda_2'(\pi/2) \approx \frac{\Lambda_2(\pi/2 + h) - \Lambda_2(\pi/2)}{h}.$$

Using $h = 0.0001$, we obtain $\Lambda_1'(\pi/2) = 10.1374$ and $\Lambda_2'(\pi/2) = 16.1335$. Hence the derivative $\frac{\partial \Lambda}{\partial E_0}(\pi/2, \tilde{\beta}, \tilde{r})$ is non-zero for almost all $\tilde{\beta}, \tilde{r}$. For these cases and small enough ϵ the Poincaré map $\tilde{P}$ will have a hyperbolic fixed point that limits to $E_0 = \pi/2$ as $\epsilon \to 0$. The flow trajectory corresponding to this fixed point is a periodic orbit will remain close to the contour $C(\pi/2)$: hence there is a chimera state for small enough $\epsilon > 0$. ■

Note that if (5.27) is not satisfied this implies that $\tilde{\beta} \approx -1.5914\tilde{r}$ which corresponds to a pitchfork bifurcation of chimera states: this is discussed in the next Section. Furthermore, the periodic orbit corresponding to the fixed point $E_0 = \pi/2$ has an extra symmetry of the form $(x(t+\frac{T}{2}), y(t+\frac{T}{2})) = (x(t)-\pi, \pi - y(t)), (mod 2\pi)$. This symmetry is broken at pitchfork bifurcation.

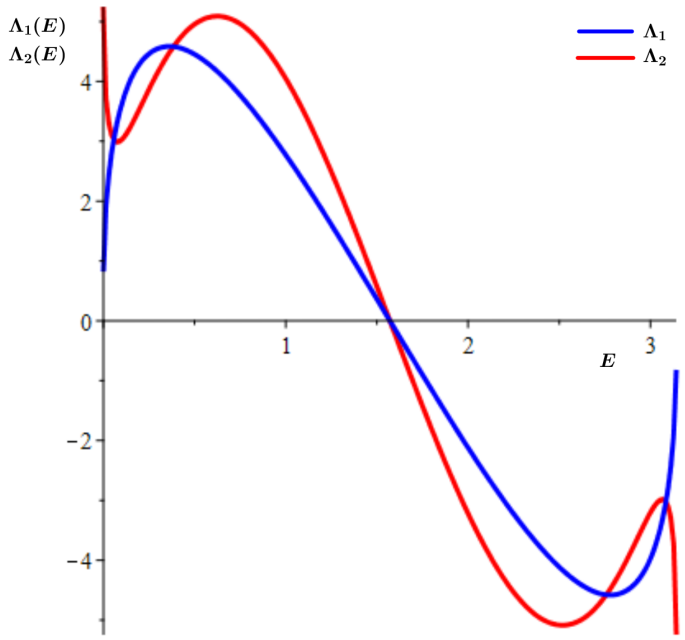

Figure 5.4: *The blue and red curves respectively show $\Lambda_1(E)$ and $\Lambda_2(E)$ from (5.22). Note that both functions have the symmetry $\Lambda_i(\pi - E) = -\Lambda_i(E)$ and both curves apparently have finite limit as $E \to 0$ or π.*

5.3 Bifurcation of the chimera solutions

It is well known [57, Theorem 9.3] that if the Poincaré map $\tilde{P}$ given in (5.23) has a fixed point E^* then the fixed point will be stable if $|\tilde{P}'(E^*)| < 1$ (resp. unstable if $|\tilde{P}'(E^*)| > 1$). Because

$$\tilde{P}'(E_0) = 1 + \epsilon\Lambda'(E_0, \tilde{\beta}, \tilde{r}) + O(\epsilon^2),$$

where

$$\Lambda'(E_0, \tilde{\beta}, \tilde{r}) = \Lambda_1'(E_0)\tilde{\beta} + \Lambda_2'(E_0)\tilde{r},$$

(and the error term is uniform in any closed subinterval of $E_0 \in (0,\pi)$) it follows that if there is an $E_0 \in (0,\pi)$ such that $\Lambda(E_0,\tilde{\beta},\tilde{r}) = 0$ and $\Lambda'(E_0,\tilde{\beta},\tilde{r}) < 0$ (resp. $\Lambda'(E_0,\tilde{\beta},\tilde{r}) > 0$) then there is a stable (resp. unstable) chimera periodic orbit near $C(E_0)$ for small enough $\epsilon > 0$. This means that bifurcations condition of chimera periodic orbits near $\epsilon = 0$ correspond to a nonhyperbolic fixed point E_0 such that $\Lambda(E_0,\tilde{\beta},\tilde{r}) = \Lambda'(E_0,\tilde{\beta},\tilde{r}) = 0$.

Figure 5.5 shows $\Lambda(E_0,\tilde{\beta},\tilde{r})$ on varying E_0 for a range of $\tilde{\beta} \in (-1,1)$ and fixed $\tilde{r} = -0.01$ computed using (5.22) and Maple's numerical integration `evalf/int`. The zeros of this clearly show the location of nontrivial zeros $\Lambda(E_0,\tilde{\beta},\tilde{r}) = 0$ that may be stable (negative slope) or unstable (positive slope) in the limit of small ϵ.

We also compute an asymptotic bifurcation diagram by numerically locating the zero contour

$$\Lambda(E_0,\tilde{\beta},\tilde{r}) = 0, \tag{5.28}$$

on varying $\tilde{\beta}$ and E_0 for fixed $\tilde{r}$, using Maple's `evalf`. This is shown in Figure 5.6: the lower case letters and index of $i = 1,\ldots,5$ refer to fixed points in Figure 5.5. Bifurcation points in Figure 5.6 can be identified as three types: there are saddle-node, pitchfork and homoclinic bifurcations that occur (for $\tilde{r} < 0$) at parameter values $\tilde{\beta}_{Sn} < \tilde{\beta}_{Pf} < \tilde{\beta}_{Hm}$ respectively in the limit $0 < \epsilon \to 0$.

The scenario for a saddle-node bifurcation has three stages: there is only one stable point b_1 for $\tilde{\beta} < \tilde{\beta}_{Sn}$. A saddle-node or tangent bifurcation of symetrically placed fixed points for the Poincaré map at $\tilde{\beta} = \tilde{\beta}_{Sn}$ creates degenerate fixed points a_2, c_2 (red curve for Figure 5.5) with $|P'(E_{a_2})| = |P'(E_{c_2})| = 1$. At these points (where the red curve is tangent to the E-axis) the qualitative behaviour of the system becomes structurally unstable, in that an arbitrarily small perturbation leads to a change of the qualitative dynamics of system. Finally, for $\tilde{\beta}_{Sn} < \tilde{\beta} < \tilde{\beta}_{Pf}$, two pairs of fixed points (unstable and stable) a_1, a_3 and c_1, c_3 appear as zeros of the green curve.

The pairs of fixed points a_1 and c_1 collide with b_1 on the cyan line at $\tilde{\beta} = \tilde{\beta}_{Pf}$ where the pitchfork bifurcation occurs. This is where the fixed point b_1 is marginally stable, $|P'(E_{b_1})| = 1$ and $\Lambda'(E_{b_1},\tilde{\beta},\tilde{r}) = 0$. For $\tilde{\beta}_{Pf} < \tilde{\beta}$ there are three fixed points (for example, a_5, c_5 and b_1 where the orange curve has zeros. The point b_1 is unstable while a_5 and c_5 are stable.

The two fixed points a_6 and c_6 hit the boundary of the domain $E \in [0,\pi]$ at the homoclinic bifurcation where $\tilde{\beta}_{H_m} = \tilde{\beta}$. At this point the period of the weak chimera solution becomes infinite in the limit: see Figure 5.3 and the magenta line for Figure 5.5. At the homoclinic bifurcation the points a_7 and c_7 move to the boundary and for $\tilde{\beta}_{H_m} < \tilde{\beta}$ the only remaining fixed point is at b_1. A similar scenario of bifurcations is found for $\tilde{r} > 0$ though with the stabilities reversed: there is a parameter-time reversing symmetry given by $(\beta, r, t) \mapsto (-\beta, -r, -t)$.

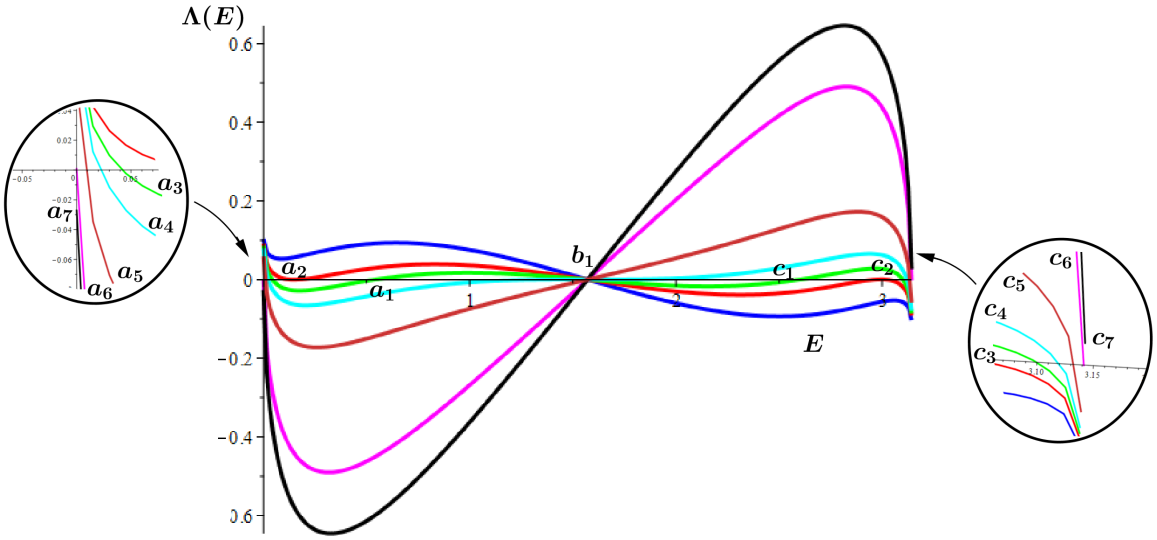

Figure 5.5: *Approximations of (5.22) for various values of* $\tilde{\beta}$ *and* $\tilde{r} = -0.01$*, where zeros of* $\Lambda(E) = -2[\Lambda_1(E)\tilde{\beta} + \Lambda_2(E)\tilde{r}]$ *correspond to fixed points of the approximate Poincaré map. The points* b_1 *and* a_i, c_i, $i = 1,..,6$ *represent various fixed points on varying* $\tilde{\beta}$*. The red curve is at the saddle-node bifurcation at* $\tilde{\beta} = 0.0081$ *while the cyan curves is at the pitchfork bifurcation where* $\tilde{\beta} = 0.0159$*. The homoclinic bifurcation can be seen for the magenta curve,* $\tilde{\beta} = 0.063$*.*

Asymptotic approximations of the bifurcations from (5.22) are compared to continuation results for the original system (5.1) on varying β, for $r = -0.01$ using `XPPAUT` as in [8]: see Figure 5.6 and Table 5.1. We find good agreement for saddle-node and pitchfork bifurcations of weak chimeras from the asymptotic theory and from numerical continuation respectively, while the homoclinic bifurcation seems to have errors that grow faster with ϵ. This is not too surprising, as we expect the approximation errors to be larger in the high period limit. Figure 5.7 summarises and compares the bifurcations of chimeras for (5.22) and (5.1) in the

parameter space (β, r).

Type of Bif.	β using (5.22)	β using (5.1)
Sn of LC	0.0081	0.0081
Pf of LC	0.0159	0.0158
Hom of LC	0.063	0.0192

Table 5.1: *Comparison of the approximations of β at saddle node of limit cycle, pitchform and homoclinic bifurcations of weak chimeras for $r = -0.01$. The first column gives the asymptotic approximate system (5.22) for the limit $\epsilon \to 0$. The second column gives values from continuation of (5.1) using XPPAUT. Observe there is very good agreement for the first two bifurcations while the third only gives better agreement closer to the integrable limit: see Figure 5.7.*

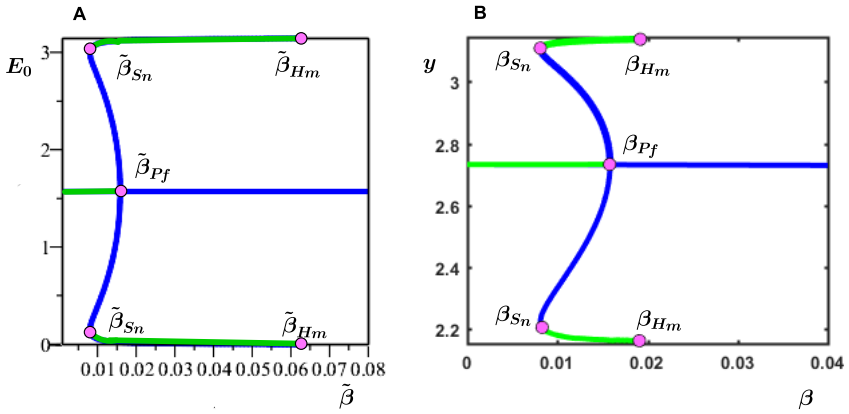

Figure 5.6: *Left panel (A) shows bifurcation digram ($\tilde{\beta}$ against E) for system (5.22) when $\tilde{r} = -0.01$ (numerically approximated by Maple for the limit $\epsilon \to 0$), while right panel (B) shows bifurcation diagram (β against y) for system (5.1) and $r = -0.01$ (numerically approximated by XPPAUT). Blue and green lines denote unstable/stable periodic orbit. In both Panels A and B, there is saddle-node bifurcation for limit cycle at points $\tilde{\beta}_{Sn}$ and β_{Sn} and pitchfork at points $\tilde{\beta}_{Pf}$ and β_{Pf}. The points $\tilde{\beta}_{Hm}$ and β_{Hm} indicate homoclinic bifurcation.*

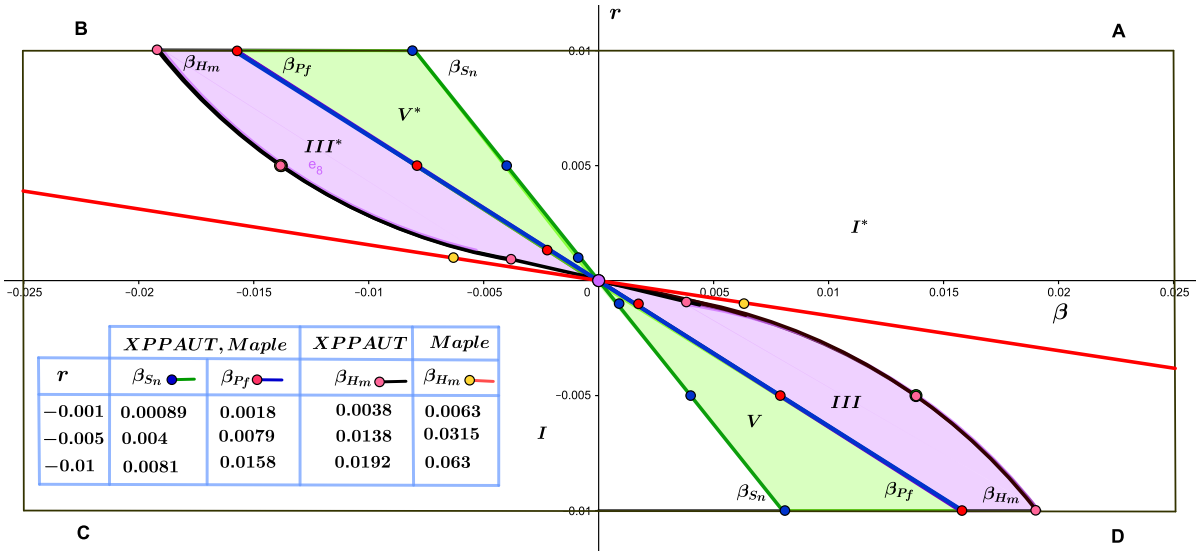

	XPPAUT, Maple		XPPAUT	Maple
r	β_{Sn}	β_{Pf}	β_{Hm}	β_{Hm}
−0.001	0.00089	0.0018	0.0038	0.0063
−0.005	0.004	0.0079	0.0138	0.0315
−0.01	0.0081	0.0158	0.0192	0.063

Figure 5.7: *Bifurcation diagrams for the asymptotic approximation (5.22) computed with Maple and the continuation (5.1) computed with XPPAUT in the parameter space* (β, r) *close to the integral case* $(0,0)$. *Bifurcations for (5.1) are computed varying* β *for* $r = \pm 0.001, \pm 0.005$ *and* ± 0.01*: these are shown as coloured points. Bifurcation lines for (5.22) are computed using Maple and represented by the blue and green lines showing* $(\beta, r) = \epsilon(\tilde{\beta}, \tilde{r})$ *for* $\epsilon \in \mathbb{R}$. *Note that quadrants A (resp. B) and C (resp. D) have the same qualitative dynamics on reversing time because of the time-reversing parameter symmetry* $(\beta, r, t) \mapsto (-\beta, -r, -t)$. *There are four coloured regions (green and purple) where multiple chimera states coexist in the asymptotic limit. There is only one chimera within the white regions: this is stable in* I *and unstable in* I^*. *Five branches of chimera (three stable and two unstable) are in the green area* V, *(also, two stable and three unstable at* V^**), bounded by a saddle node of limit cycles (green line) and a pitchfork of limit cycles (blue line). There are two stable chimera and one unstable in purple area* III, *(also, one stable and two unstable at* III^**), bounded by the pitchfork and the homoclinic bifurcation (black curve) that are only present in the XPPAUT calculations, (homoclinic bifurcation: the red line is computed using Maple).*

CHAPTER 6

WEAK CHIMERAS AND BIFURCATIONS WITHIN A_6

In chapter three, we listed in Table 3.1 a number of invariant subspaces for the six-oscillator network (3.6) shown in Figure 3.2(a). This includes the exotic invariant subspaces A_i, $i = 1,...,7$. In addition, we have rewritten the full system (3.6) in the subspace A_1 to explore chimera states and study their stability and bifurcation. As pointed by Yuri Maistrenko (pers. comm.) there are other weak chimeras in this system, in particular within A_6. In section 6.1, we consider the network of six coupled phase oscillators (3.6) with coupling (3.2) within the invariant subspace A_6 and determine regions where a chimera state exists in the parameter space. We find this is bounded by lines of saddle-node bifurcation. Section 6.2 explains the reduction for the full system (3.6) in term of phase difference and computes eigenvalues for the nonhyperbolic equilibrium on the bifurcation lines. Section 6.3 presents numerical simulations that help us to prove that chimera states are not only stable within the invariant set A_6 but also can be found to be stable in the full system.

6.1 Bifurcation of chimera solution within A_6

We consider the dynamics of the system (3.6) within the following invariant subspace

$$A_6 = (\theta_1, \theta_2, \theta_3, \theta_4, \theta_5, \theta_6) = (\phi_1, \phi_1 + \pi, \phi_2, \phi_1, \phi_1 + \pi, \phi_2 + \pi),$$

such that $\phi_1,\ \phi_2 \in \mathbb{T}^2$. Note that the system (3.6) can be written in these coordinates as

$$\begin{aligned}\dot{\phi_1} &= w + 2g(-\pi) + g(\phi_1 - \phi_2) + g(\phi_1 - \phi_2 - \pi),\\ \dot{\phi_2} &= w + 2g(\phi_2 - \phi_1) + 2g(\phi_2 - \phi_1 - \pi).\end{aligned} \tag{6.1}$$

Using the coupling function (3.2), we obtain

$$\begin{aligned}\dot{\phi_1} &= w - 2\sin(\alpha) + 2r\sin(2\phi_1 - 2\phi_2),\\ \dot{\phi_2} &= w - 4r\sin(2\phi_1 - 2\phi_2),\end{aligned} \tag{6.2}$$

which can be formulated in term of phase difference $\psi := \phi_1 - \phi_2$, so that

$$\dot{\psi} = -2\sin(\alpha) + 6\ r\sin(2\psi), \tag{6.3}$$

a first order differential equation in $\psi \in \mathbb{T}$.

Now, we demonstrate the system (6.3) has chimera states for some parameter values of α and r, which are born at a saddle-node bifurcation. The equilibria for the one-dimensional system (6.3) satisfy

$$f(\psi) = -2\sin(\alpha) + 6\ r\sin(2\psi) = 0.$$

Hence, equilibria are

$$\sin(2\psi) = \sin(\alpha)/3r, \qquad \cos(2\psi) = \pm\sqrt{1 - (\sin(\alpha)/3r)^2},$$

which depend on two parameters α and r and these points can classified using linear stability analysis by computing

$$f'(\psi) = 12r\cos(2\psi) = \pm 12r\sqrt{1 - (\sin(\alpha)/3r)^2}.$$

Recall that equilibrium ψ is linearly stable when $f'(\psi) < 0$. The dynamical behaviour for the system (6.3) is visualized in Figure 6.1. Panel (a) presents $\dot{\psi}$ as a function of ψ which shows three curves corresponding to three values for α and $r = -0.01$. There are two equilibria points red/black are stable/unstable on the black curve when $\alpha = -0.015$, $r = -0.01$ ($\sin(\alpha) < 3r$), hence $|\sin(\alpha)/3r| < 1$. That means the coupling between the two

oscillators is strong which implies these oscillators move together with the same frequency and are synchronized

All trajectories in Figure 6.1(a) are attracted to the red stable point as t goes to infinity. As the parameter α is varied to the point where

$$r = \pm\frac{\sin(\alpha)}{3}, \tag{6.4}$$

the red/black points move toward each other then collide to appear as a pink bifurcation point on the blue line. This point is a non-hyperbolic and $f'(\psi) = 0$ for $\psi = \pi/4$ or $\psi = 3\pi/4$. In this case the orbit is homoclinic because it starts and ends at the same equilibrium. Finally, if $|\sin(\alpha)/3r| > 1$, (e.g. $\alpha = -0.045$, $r = -0.01$), then the nonhyperbolic point vanishes (magenta curve) and a limit cycle appears. This attracting periodic orbit corresponds to the chimera state because in this case ψ, the phase difference between ϕ_1 and ϕ_2, grows linearly with time. Note that all the points within A_6 are in this chimera state and therefore it is the typical behaviour for initial conditions.

The saddle node bifurcation at (6.4) is illustrated in Figure 6.1(b). Red/black lines indicate stable/unstable equilibria in the bifurcation diagram shown in space (r, ψ). In the other words, the red/black points on the black curve at (a) correspond to stable/unstable points on red/black curves in (b), while the pink point is a bifurcation point at $\psi = \pi/4$ in both (a) and (b).

We can examine the dynamics of phase oscillators on the circle by time series. Figure 6.1 also shows time series of ϕ_1 and ϕ_2 for the system (6.2) for several initial conditions near two points (red/black) on the black curve (a). Note that all the initial conditions converge to the same trajectory since they have frequency synchrony (c), (e). Also, time lines in (d) for initial conditions around the pink point on the blue curve (a) have dynamics which is similar to (e). Finally, the time series for initial conditions near the magenta curve (a) reveal chimera states, because the time series for ϕ_1 and ϕ_2 separate at an approximately linear rate (f).

The relation between strength coupled parameters α and r has remarkable effects on the appearance of chimera states. The bifurcation diagram at Figure 6.1(g) for the parameters space (α, r) provides us important information about this relation. This figure is divided

into three regions according to values of the coupled parameters and every region has a different dynamical behaviour. Two yellow regions refer to $-3r < \sin(\alpha) < 3r$ which implies to exist stable and unstable equilibria, (i.e no chimera states). The blue area indicates to exist chimera states because this region satisfies $\sin(\alpha) > 3r$ or $\sin(\alpha) < -3r$. The boundary of the blue area represents the pink bifurcation lines L_1 and L_2 for a saddle-node bifurcation where $\sin(\alpha) = \pm 3r$ in (6.4).

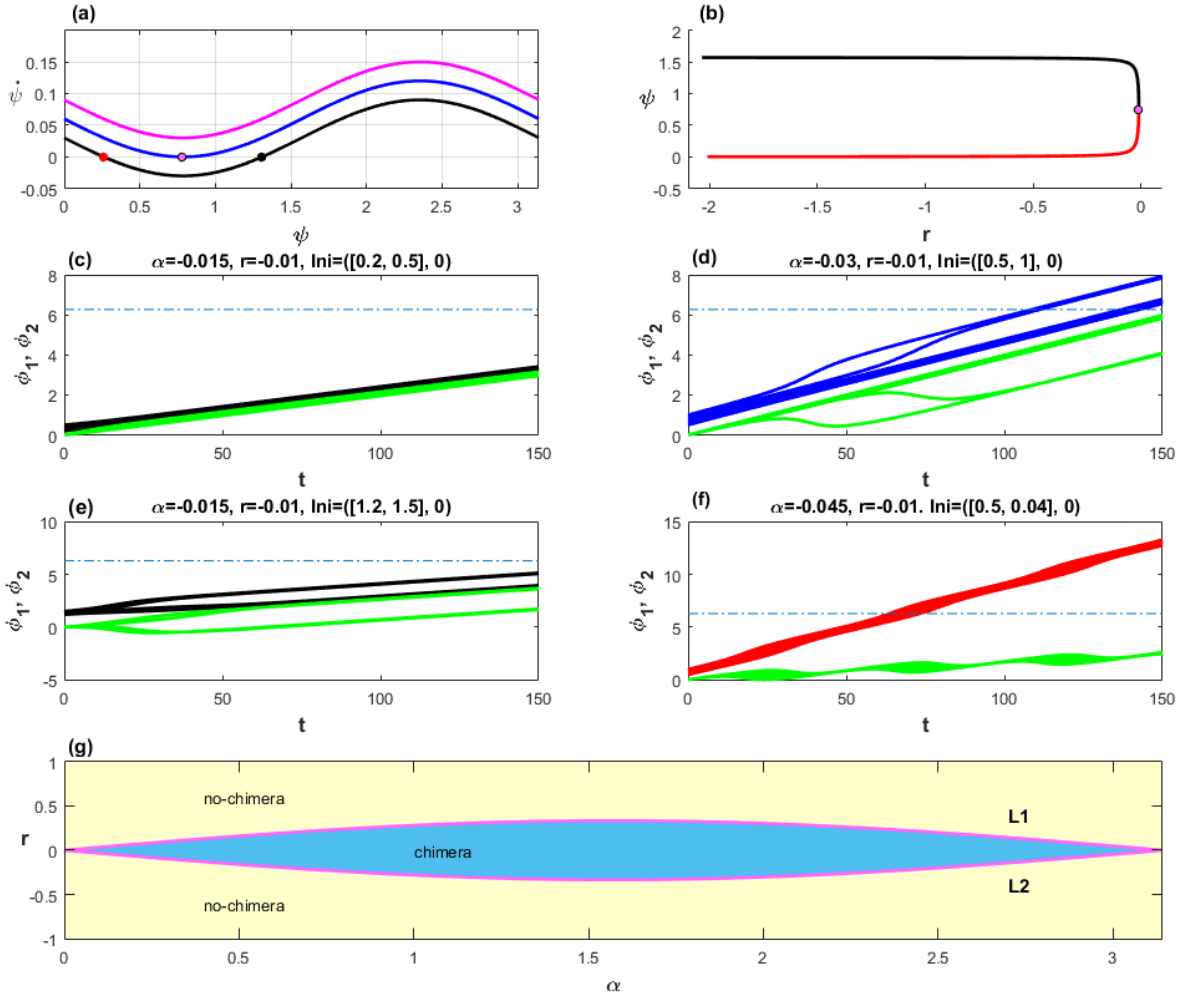

Figure 6.1: Panel (a) shows three curves for (6.3) magenta, blue and black that refer to $r = -0.01$ with different values of $\alpha = -0.045, -0.03$ and -0.015. The black curve has red/black equilibria points that are stable/unstable, the blue curve has one saddle point which is pink while there is a chimera state on at the magenta carve. Panel (b) shows saddle-node bifurcation for (6.3) where r against ψ and $\alpha = -0.03$. Red/black curves represent stable/unstable branches for equilibrium point. The pink point is a saddle-node bifurcation at $(r, \psi) = (-0.01, 0.747)$. The time series $(c)/(e)$ show frequency synchrony of the different initial conditions (ϕ_1, ϕ_2) for the system (6.2) around the red/black point. Time series (d) is for starting points near the pink point At (f), the dynamics of the phases ϕ_1, ϕ_2 exposes a chimera state by every phase go to the different path. Panel (g) is a parameter diagram for r against α that illustrates the regions of existence of chimera states in the invariant subspaces A_6, bounded by the pink bifurcation lines L_1, L_2.

6.2 Stability of chimera states near the saddle-node bifurcation

In the previous section, the system of six coupled phase oscillators (3.6) is written within invariant subspaces on A_6 as ODE (6.3) in one dimension (as flow on the circle). In addition, we identified the bifurcation lines and the regions where attracting chimera states exist. We recall, this system (3.6) is described as ODEs on the torus $(\theta_1, ...\theta_6) \in \mathbb{T}^6$.

Defining $\xi_k = \theta_k - \theta_6$, $k = 1,2,3,4,5$. The system (3.6) can be written in term of phase differences,

$$\begin{aligned}
\dot{\xi_1} &= g(\xi_1-\xi_2)+g(\xi_1-\xi_3)+g(\xi_1-\xi_5)-g(-\xi_1)\\
&- g(-\xi_2)-g(-\xi_3)-g(-\xi_4)-g(-\xi_5),\\
\dot{\xi_2} &= g(\xi_2-\xi_1)+g(\xi_2-\xi_3)+g(\xi_2-\xi_4)-g(-\xi_1)\\
&- g(-\xi_2)-g(-\xi_3)-g(-\xi_4)-g(-\xi_5),\\
\dot{\xi_3} &= g(\xi_3-\xi_1)+g(\xi_3-\xi_2)+g(\xi_3-\xi_4)+g(\xi_3-\xi_5)\\
&- g(-\xi_1)-g(-\xi_2)-g(-\xi_4)-g(-\xi_5),\\
\dot{\xi_4} &= g(\xi_4-\xi_2)+g(\xi_4-\xi_3)+g(\xi_4-\xi_5)-g(-\xi_1)\\
&- g(-\xi_2)-g(-\xi_3)-g(-\xi_4)-g(-\xi_5),\\
\dot{\xi_5} &= g(\xi_5-\xi_1)+g(\xi_5-\xi_3)+g(\xi_5-\xi_4)-g(-\xi_1)\\
&- g(-\xi_2)-g(-\xi_3)-g(-\xi_4)-g(-\xi_5).
\end{aligned} \tag{6.5}$$

We use the equation (6.3) to demonstrate numerically the existence of stable chimera states in the full system (6.5) for the coupling (3.2). Finding explicit solutions is often impossible for such systems (6.5), so we use quantitative analysis and numerical simulations. The first condition to analyse a stability near an equilibrium state is to specify a direction of a slope at equilibria points using linearization. The nonhyperbolic points for the one dimensional system (6.3) are $\psi = \pi/4, 3\pi/4$ at (6.4). We know that $\psi = \phi_1 - \phi_2$, if $\psi = \pi/4$ is chosen, then we can say $\phi_1 = \pi/4$ and $\phi_2 = 0$. In terms of phase differences, the equilibrium

point for (6.5) invariant set A_6 becomes

$$\begin{aligned} \xi^* = (\xi_1,\xi_2,\xi_3,\xi_4,\xi_5) &= (\phi_1-\phi_2-\pi,\phi_1-\phi_2,-\pi,\phi_1-\phi_2-\pi,\phi_1-\phi_2) \\ &= (-\pi/4,3\pi/4,-\pi,-\pi/4,3\pi/4)\in\mathbb{T}^5. \end{aligned} \tag{6.6}$$

This point corresponds to a periodic orbit of the system (3.6) which is

$$\Theta^* = \{(\phi_1+\varphi,\phi_1+\pi+\varphi,\phi_2+\varphi,\phi_1+\varphi,\phi_1+\pi+\varphi,\phi_2+\pi+\varphi) \ : \ \text{for all } \varphi\in\mathbb{T}\}.$$

If $\varphi = 0$, then we can choose an initial condition $\theta^*\in\Theta$ such that $\theta^* = (\phi_1,\phi_1+\pi,\phi_2,\phi_1,\phi_1+\pi,\phi_2+\pi) = (\pi/4,5\pi/4,0,\pi/4,5\pi/4,\pi)\in\mathbb{T}^6$.

We can understand the local behaviour of nonlinear system (6.5) through linear approximation around the equilibrium. The stability of this point is determined by sign of eigenvalues of the Jacobian. Here, we want to examine stability of ξ^* over a range of values of parameter $\alpha\in(0,\pi)$ and (6.4), along the pink bifurcation lines L_1, L_2 of nonhyperbolic points $\psi = \pi/4$ in Figure 6.2(b).

Numerically we find (using Maple) the eigenvalues of the Jacobian at the equilibrium point ξ^*. This gives a set of five eigenvalues at every point on the bifurcation lines L_1, L_2 (see Table 6.1). The real parts of eigenvalues along these lines is plotted as a function of α in Figure (6.2, (a), (c)). Red/black lines represent negative/positive eigenvalues that are real. Green/blues lines indicate negative/positive real parts of eigenvalues that are complex. The equilibrium ξ^* is nonhyperbolic, because it has a zero eigenvalue at the bifurcation point.

Figures 6.2((a), (c)) are divided into five regions (a, b, c, d, e) and (a^*, b^*, c^*, d^*,e^*) respectively, according to signs of eigenvalues that refer to appear or disappear stable and unstable manifold. The invariant subspaces of the linearized system spanned by eigenvalues E^s, E^u and E^c are tangent to the stable, unstable and center manifold respectively at a, e, a^* and e^* for linearization of the system (6.5). Cases of two dimensional E^u and E^c can be seen at b, c and b^*. There are only stable and center manifolds for d, c^* and d^*.

As conclusion for these two sections above, we have analysed the system (6.3) over a range values of $\alpha\in(0,\pi)$ and r. Before the saddle node bifurcation, almost every initial condition $\psi\in\mathbb{T}$ converges to stable node, and the only initial that does not converge to

this point is the unstable node (see yellow regions Figure 6.2 (b)). On the bifurcation curves (see L_1 and L_2 in Figure 6.2(b)) all initial conditions in A_6 go to bifurcating points. After the saddle node, the initial conditions converge to a periodic orbit that is an attracting chimera state. As a result, the bifurcation curves L_1 and L_2 indicate transition from a stable node to a stable chimera in A_6. Dividing curves of eigenvalues to five areas make the road easier to detect a stable and unstable manifold.

L_1, $r=\sin(\alpha)/3$	Eigenvalues λ	L_2, $r=-\sin(\alpha)/3$	Eigenvalues λ
$\alpha \in (0, 0.78)$	$Re(\lambda_1)=Re(\lambda_2)>0$, $Re(\lambda_3)>0, Re(\lambda_4)<0$, $\lambda_5=0$.	$\alpha \in (0, 0.8)$	$Re(\lambda_1)=Re(\lambda_2)>0$, $Re(\lambda_3)<0, Re(\lambda_4)>0$,. $\lambda_5=0$.
$\alpha \in (0.8, 1.28)$	$Re(\lambda_1)=Re(\lambda_2)>0$, $Re(\lambda_3)>0, Re(\lambda_4)>0$, $\lambda_5=0$.	$\alpha \in (0.82, 0.98)$	$Re(\lambda_1)=Re(\lambda_2)>0, C.No.$ $Re(\lambda_3)=Re(\lambda_4)>0$, $\lambda_5=0$.
$\alpha \in (1.30, 2.14)$	$Re(\lambda_1)=Re(\lambda_2)>0$, C.No. $Re(\lambda_3)=Re(\lambda_4)>0$, $\lambda_5=0$.	$\alpha \in (1, 1.84)$	$Re(\lambda_1)=Re(\lambda_2)<0$, C.No $Re(\lambda_3)=Re(\lambda_4)<0$, $\lambda_5=0$.
$\alpha \in (2.16, 2.32)$	$Re(\lambda_1)=Re(\lambda_2)<0$, C.No. $Re(\lambda_3)=Re(\lambda_4)<0$, $\lambda_5=0$.	$\alpha \in (1.86, 2.34)$	$Re(\lambda_1)=Re(\lambda_2)<0$, $Re(\lambda_3)<0, Re(\lambda_4)<0$, $\lambda_5=0$.
$\alpha \in (2.36, 3.14)$	$Re(\lambda_1)=Re(\lambda_2)<0$, $Re(\lambda_3)>0, Re(\lambda_4)<0$, $\lambda_5=0$.	$\alpha \in (2.36, 3.14)$	$Re(\lambda_1)=Re(\lambda_2)<0$, $Re(\lambda_3)<0, Re(\lambda_4)>0$, $\lambda_5=0$.

Table 6.1: *Table of eigenvalues λ_i of the Jacobian at equilibrium point ξ^* for system (6.5). These are numerically computed using Maple in the range values of parameter $\alpha \in (0, \pi)$ and $r = \pm\sin(\alpha)/3$ which correspond to L_1 and L_2.*

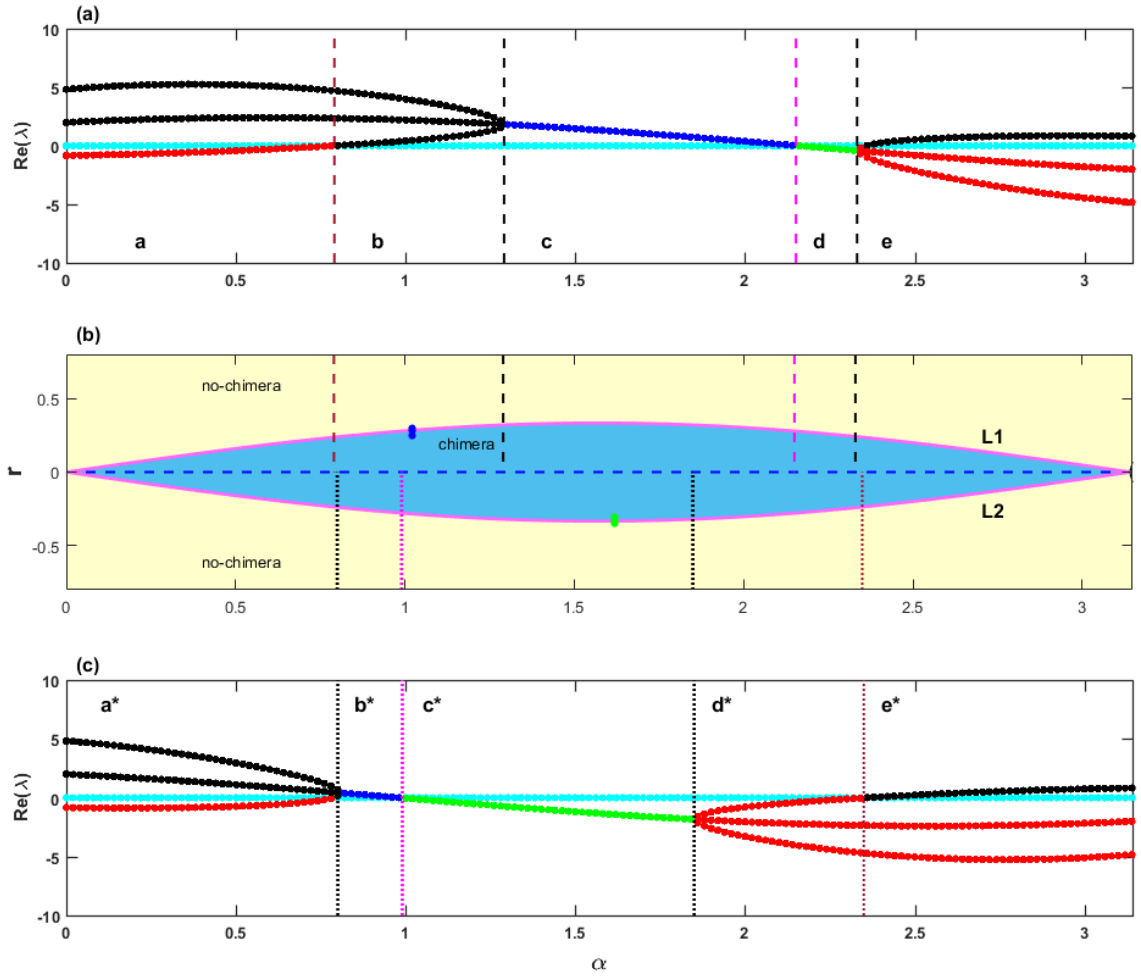

Figure 6.2: *Panel (b) shows the bifurcation diagram described in Figure 6.1(b). The pink curves L_1/L_2 refer to bifurcation points at (6.4). The real part of eigenvalues λ at bifurcation point ξ^* and parameters values on L_1, L_2 against $\alpha \in (0,\pi)$ for the system (6.5) are plotted in panels (a) and (c) respectively. Red/black lines are negative/positive real part of real number eigenvalues at regions a, b, e, a^*, d^* and e^*. Green/blue lines refer negative/positive real part of complex number eigenvalues at c, d, b^* and c^* and the cyan line is zero real part of eigenvalues for all value of α.*

6.3 Stability of chimera states in the full system

We find the stability regions for the bifurcation point ξ^* in the previous section. There are two interesting regions we examine. The first one, where eigenvalues of the saddle node for the system (6.5), are not negative in parts b and c at Figure 6.2(a). The second is where

there are eigenvalues that are not positive in the two parts c^* and d^* (Figure 6.2(c)). We aim to understand this result in the full system (6.5). In particular, we examine if there are attracting chimera states in some ranges of α and r.

Numerical simulation is used to examine this, by choosing an initial condition $\theta^* \in A_6$ and comparing between dynamical behaviour for this point and a randomly chosen perturbation that is within 0.1 of each component of θ^*. MATLAB simulations of this behaviour are plotted in Figures 6.3, 6.4 and 6.5.

In the next steps, we concentrate on these two regions $(b-c)$ and (c^*-d^*) at Figure 6.2(a), (c). If we choose an initial condition $\theta^* \in A_6$ at point v^* corresponding to $(\alpha, r) = (1.62, -0.35)$ on L_2 and two points $u^* = (1.62, -0.3329)$ and $w^* = (1.62, -031)$ on both sides of L_2. These points of parameters are where no unstable manifold, which correspond to the part c^* in Figure 6.2(c). The dynamical behaviour for θ^* is depicted for parameter values v^*, u^* and w^* by time series ((a), (d), (g)) , phase snapshots at the end of the simulation ((b), (e), (h)) and approximate frequency is

$$\Omega_i(T) = \frac{\theta_i(T)}{T}, \tag{6.7}$$

versus time $((c), (f), (i))$ respectively at Figure 6.3.

We note that the time series (a) for all components of the initial condition at parameter point u^* go to $-\infty$ at the same rate. We also note there is phase locking because the phase differences are bounded along time t and then, there is frequency synchrony Ω_i has the same value for all θ_i. The similar state can be seen at v^*, (see Figure 6.3(d)). Snapshots of the final stationary state confirm that this point still belongs to A_6, (see Panels (b), (e)).

For the parameter value w^*, a chimera state is apparent in the time series Figure 6.3(g) and frequency time (i), such that θ_i, $i = 1,2,4,5$ have the same frequency $\Omega_1 = \Omega_2 = \Omega_4 = \Omega_5$, while θ_3 and θ_6 have a different frequency $\Omega_3 = \Omega_6$. Note also that the final state of the time series in Figure 6.3 ((b),(e),(h)) shows that the trajectory has in all cases remained within A_6: observe that $\theta_1 = \theta_4$, $\theta_2 = \theta_5 = \theta_1 + \pi$ and $\theta_3 = \theta_6 + \pi$. This is expected as we start with an initial condition in the invariant subspace A_6.

We then examine stability of these solutions to a perturbation that is transverse to the invariant subspace A_6. In particular, we consider an initial condition that corresponds to

θ^* except that all components θ_i are perturbed by a random number multiplied by $\zeta = 0.1$ away from θ^*. We plot simulations in Figure 6.4 in a similar way to Figure 6.3 at the same parameters u^*, v^* and w^*. Note by comparing between panels of time series at ((a), (d) and (g)) in Figures 6.3 and 6.4, that in our perturbed case the trajectory converges to the same behaviour as unperturbed case suggesting that the attracting dynamics within A_6 is also stable within the full system. In particular, the dynamics of this perturbed initial condition suggests that the chimera state in A_6 shown in Figure 6.4 is an attractor for the full system (3.6). Phase snapshots (b), (e) and (h) and frequency time (c),(f) and (i) assert these consequences by the perpetuated point ends up within A_6 and shows frequency states for their components.

Whether the weak chimera within A_6 is an attractor for the full system or not, depends on whether there are only transversely stable directions to A_6 or some transversely unstable directions. For example, we consider the same initial condition that is perturbed close to A_6 for three parameter points $(\alpha, r) = u := (1.02, 0.3)$, $v := (1.02, 0.284)$ or $w := (1.02, 0.25)$ in Figure 6.2(b) where there is no stable manifold. For the saddle-node bifurcation in this case, there are additional unstable directions as shown in Figure 6.2(a). In this case we show in Figure 6.5 that the initial condition evolves according to (3.6) away from A_6 to a frequency synchronized attractor that is far from A_6. As a result, θ_i, $i = 1, 2, .., 6$ have the similar time series $((a), (d), (g))$ and their approximate frequencies Ω_i, $i = 1, 2, ..., 6$ at $((b), (e), (h))$ are equal. Both of these observations lead to deduce that chimera states in A_6 are not attractors in the full system where there is unstable manifold at the bifurcation point.

In a summary, we present numerical evidence of attracting chimera states in the full system for specific parameters. These results are based on a linear approximation at a critical solution ξ^* and simulations at particular an initial condition θ^* for the system (3.6). Firstly, we analysed the full system within invariant subspace A_6 and exposed a region in the parameter space where the system has chimera states.

Linearization of the nonhyperbolic points ξ^* at bifurcation allows us to determine the stability of chimera states in the full system. In particular if the saddle node is transversally stable, we find chimera states are also stable. In the case where there are center and unstable

directions (see Figure 6.5) we find chimeras are not stable. In the case where there are only stable directions, we find the chimeras are stable (see Figure 6.4).

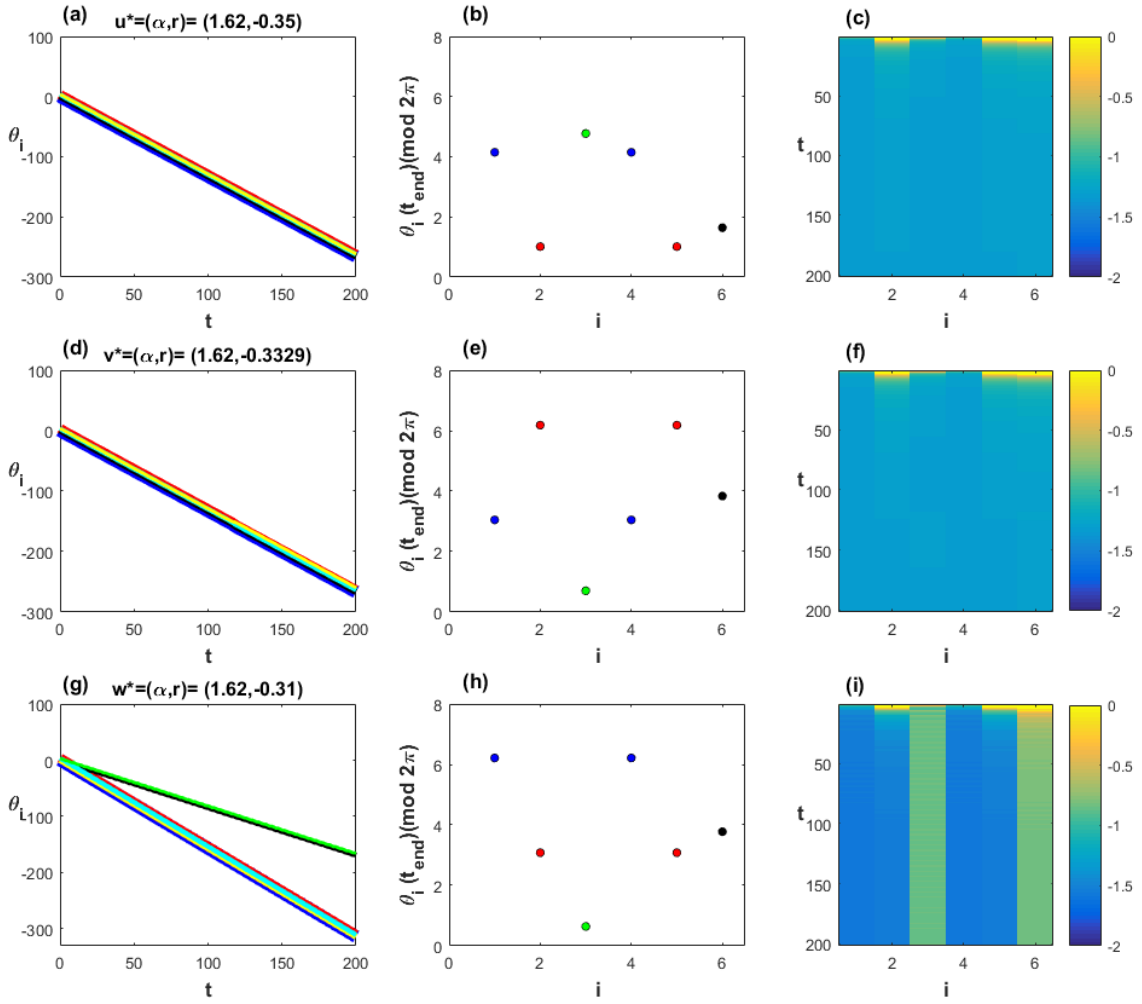

Figure 6.3: *The first, second and third rows illustrate the dynamics of the system (3.6) starting within A_6 for a parameter at points u^*, v^*, w^* respectively in Figure in Figure 6.2(b). The left column shows time series for $\theta_i(t)$: different colours correspond to different i. The middle column shows the final phases modulo 2π: observe that they remain in A_6 in all case. Approximate frequencies for the (6.7) of oscillator i over the time interval $[0,t]$ are illustrated at the right column. Note that in the bottom right panel there is partial frequency synchrony corresponding to attraction to a weak chimera in A_6.*

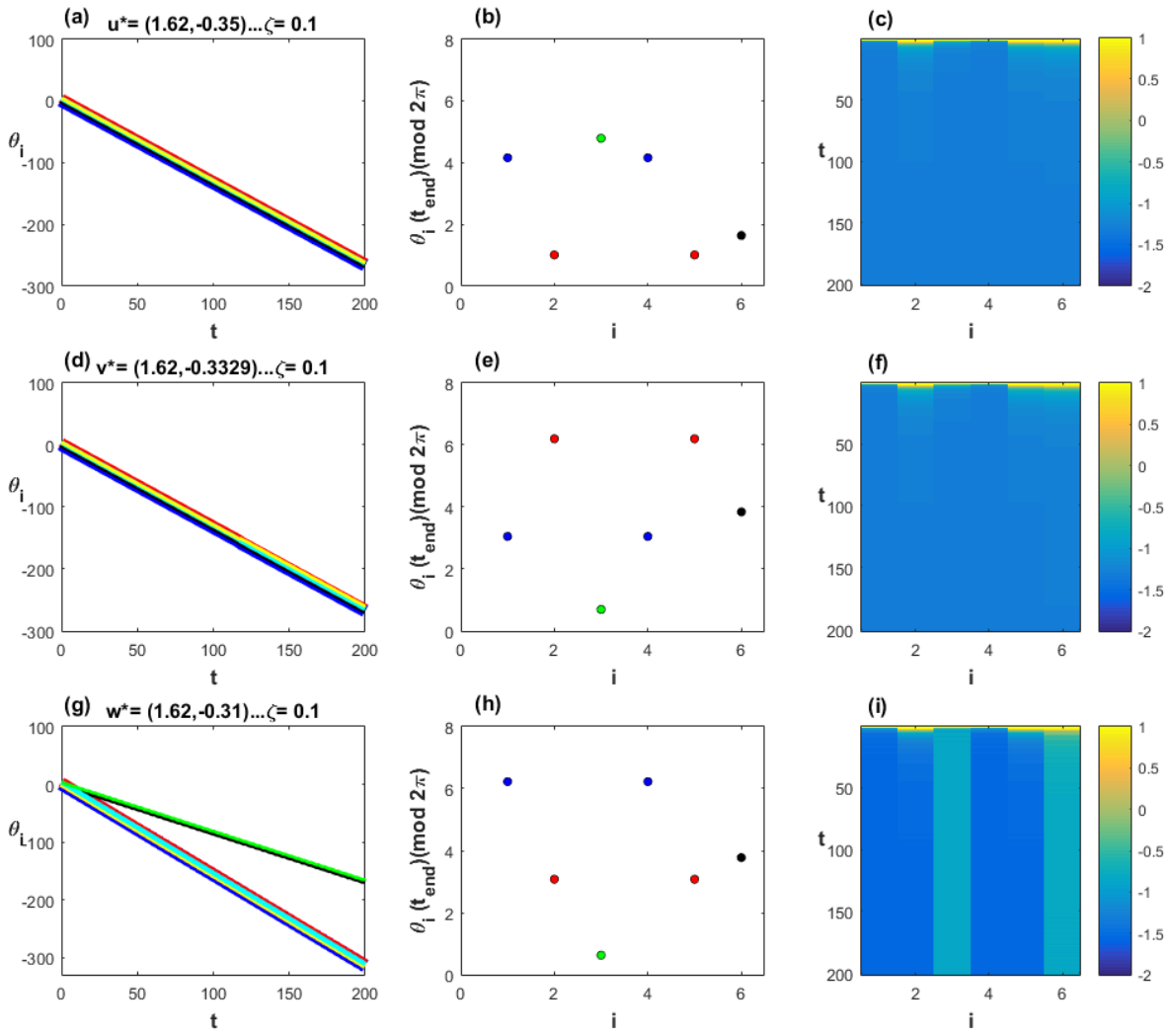

Figure 6.4: *As Figure 6.3 except starting at a randomly chosen point that is within* 0.1 *of a point in* A_6 *in all coordinates. Observe the same long-term dynamics, indicating in particular that the weak chimera in the lower right is stable to perturbations in the full system.*

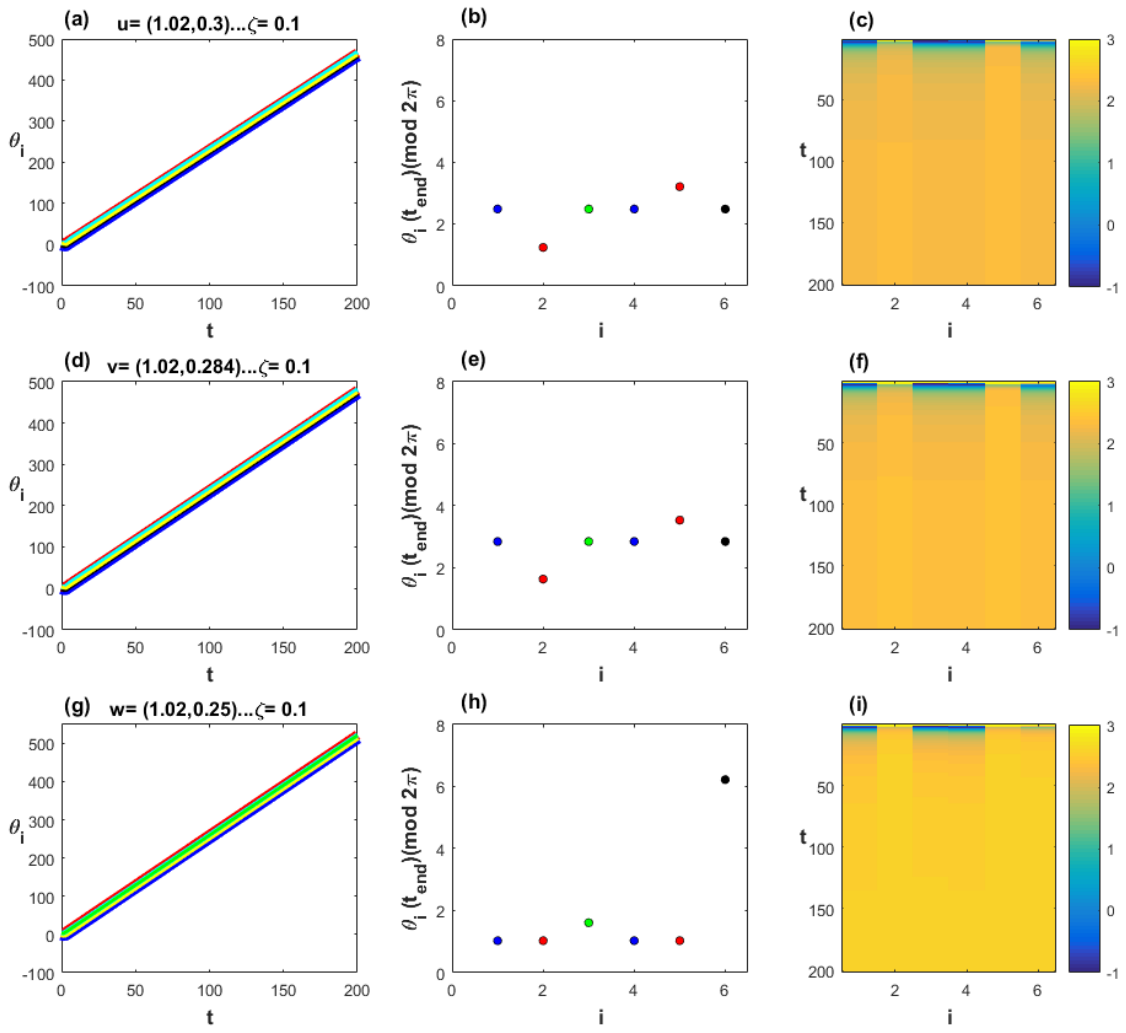

Figure 6.5: *Description as in Figure 6.4 for an initial condition started close to A_6, except that the top/middle/bottom panels correspond to points u, v, w in parameter space 6.2(b). In all of these cases the solutions converge towards a frequency synchronized state that is not in A_6. This suggests that the weak chimera in A_6 expected for w is not stable to perturbations transverse to A_6.*

CHAPTER 7

CONCLUSION

In this final chapter, we summarise and discuss the results obtained in this thesis, and conclude an outline of further directions of research. Chimera states have attracted researchers' attentions because they appear in a wide range of coupled oscillator systems. At chimeras, the oscillators separate into two clusters, one and synchronized and the other desynchronized. Chimera states correspond to broken spatiotemporal symmetry and are helpful to understand many real-world phenomena. This thesis is an investigation of chimera states in a network of six identical and indistinguishable phase oscillators with neighbour and next-neighbour coupling. Our analysis and numerical calculation of chimeras uses a generalization of the Kuramoto model with two harmonic coupling.

7.1 Summary and main results

In chapter two, we present introductory material on invariant subspaces as discussed in [8] and summarised in Table 3.1. We focus on two exotic invariant subspaces that contain chimeras: A_1 was studied in [8] and in chapters three, four and five, while A_6 is studied in chapter six. A symmetry of a dynamical system is that a system unchanged under the group action, (i.e. elements of group commutes with the vector field). Two methods are

mentioned to explore flow invariant subspaces: the first one depends on finding an isotropy subgroup of spatiotemporal symmetries of $S_n \times \mathbb{T}^1$ of networks of identical oscillators [11], while the second considers balanced polydiagonal from an equivalence relation between cells of networks (Exotic balanced colouring).

Chapter three investigates weak chimera states within invariant subspace A_1 and follows the analysis in Ashwin and Burylco [8] of phase space. We have written the system (3.6, 3.2) within specific invariant subspace A_1 to get a planar system of coupled phase oscillators. The coordinates of the phase portrait for the system (3.10) from [8] have a time-reversing symmetry that is not a reflection, rotation or translation at particular values of parameters α and r. We change these coordinates so that our system (3.13) has a time-reversing symmetry that is a reflection. Numerical simulations are used to plot phase portraits and time series for various values of the parameters α and r.

We use numerical continuation software (XPPAUT) to plot the bifurcation diagram within A_1 for various values of interaction parameters. We investigated numerically a number of weak chimeras state in the coupled phase system (3.12). In the bifurcation diagram, we illustrate the effects of parameter symmetry and phase and time-reversal on stability and bifurcation.

Chapter four focuses on proving analytically the existence of chimera states in the system (3.5, 3.2) for the particular value of coupled parameters β, r within A_1. We demonstrate that there is an integrable structure $E(x, y)$ for the system (3.5, 3.2) in the special case $r = 0$, $\alpha = \pi/2$ which corresponding to $\beta = \pi/2 - \alpha$ working on the region $M \subset \mathbb{T}^2$ split into two halves H_ℓ and H_r. Also, at these values of parameters, this system has a reversing symmetry R_1 and a symmetry R_2.

Nullclines for the system (3.13) are used to partition the set M into bounded areas and prove a sequence of lemmas. These lemmas help us to understand the structure of phase space within $H_r \subset M$. A reversing symmetry is employed to prove Lemma 4.2 that extends the trajectories from H_r to H_ℓ, (i.e. describe the motion of the trajectories on the whole M). This lemma is used to prove the appearance of a periodic orbit that winds around the first component (x) on the torus. The main results of this chapter are stated in two essential

theorems: Theorem 4.11 shows each level curve is a weak chimera according to Definition 3.1. Theorem 4.12 proves the existence of an infinite number of chimera states that are neutrally stable for the integrable case.

In chapter five, we prove (or investigate) there are chimera states using the Poincare return map near the integrable case $E(x,y)$ when $\beta, r \neq 0$. We give an integral form for the time of period for every level curves when $0 < \tilde{E} < \pi$ and other properties for chimera solutions with $\beta, r = 0$. Then, we approximate the first return map. Theorem (5.1) states there is a periodic orbit for $\Lambda(E_n, \tilde{\beta}, \tilde{r})$ at $E_0 = -\pi/2$ and almost all $(\beta, r) \neq (0,0)$, which corresponds to chimera solutions. This procedure allows us to continue certain weak chimera states for such nearby parameters.

We use these perturbation techniques and the fact that $E(x,y)$ (5.2) is slowly varying to describe existence, stability and bifurcation of weak chimera solutions for this regime. Although these are not analytically solvable, we can approximate the integrals numerically and compare them to numerical continuation results in chapter three in order to understand stability and bifurcation of these weak chimera states. We note that depending on the ratio of β/r, the number of chimeras and their type changes as we approach the integrable limit (see Figure 5.7). These computations still require approximation of integrals: it would clearly be of interest to find a completely analytical explanation of these bifurcations. XPPAUT and Maple are used for drawing bifurcation diagram to investigate stability and bifurcations for chimera states.

Chapter six highlights the existence of a stable chimera state within A_6 that can be found in the full system. We write the system (3.6, 3.2) within A_6 and use phase differences to get the ordinary differential equitation (6.3) for one variable $\psi \in \mathbb{T}$. This reveals there is a weak chimera state in A_6 at a particular region in parameter space (α, r). We rewrite the system (3.6) in term of phase differences to obtain the system (6.5). Linear approximation at nonhyperbolic equilibrium point ξ is used to detect eigenvalues along bifurcation lines L_1 and L_2. These eigenvalues gives us information about stable regions in the system (6.5). This chapter reveals there can be attracting weak chimeras in the full system by using a perturbed initial condition. We use MATLAB to plot time series as well as phase snapshots

and approximate frequencies for the system (3.6)

7.2 Future work

There are a number of possible future research questions suggested by this work. These include the following:

- Investigation of weak chimera states in this thesis and [8] is limited to the invariant subspace A_1 and A_6. We have not checked if there are chimera states in other invariant subspaces.
- The proof of existence of weak chimera states is restricted to one example of the network of six oscillators. Future work could generalize this result other networks of phase oscillators.
- It would be interesting to study other models, for example, Van der Pol with the same network to see if similar behaviour can be obtained for an appropriate coupling function.
- We find a number of bifurcations in A_1 and A_6 that give rise to weak chimeras but have not fully analysed these. It would be good to do this, in particular for the saddle node bifurcations in chapter 6 that have centre manifold of dimension more than one.
- In chapter four and five, we find multiple chimera solutions within A_1. It would be interesting to investigate their stability in the full system.
- We have investigated weak chimera solutions for a specific system and particular definition. Another extension of the work worth considering would be found other possible definition for chimera states.
- We have focussed on theory rather than applications in this thesis, but in would be interesting to see how relevant this results found are in applications..

APPENDIX A

APPENDICES

A.1 Reversing symmetries of the six oscillator system for $r = 0,\ \alpha = \pi/2$

In order to prove the system (4.1) has a reversing symmetry with variables $(x, y) \in \mathbb{T}^2$. We define maps R_1 and R_2 as follows

$$R_1\begin{pmatrix} x \\ y \end{pmatrix} = \begin{pmatrix} -x \\ y \end{pmatrix} = \begin{pmatrix} 2\pi - x \\ y \end{pmatrix}, \quad R_2\begin{pmatrix} x \\ y \end{pmatrix} = \begin{pmatrix} x \\ -y \end{pmatrix} = \begin{pmatrix} x \\ 2\pi - y \end{pmatrix}$$

are reversing symmetry and a symmetry respectively. We write system (4.1) in the form

$$\begin{pmatrix} \dot{x} \\ \dot{y} \end{pmatrix} = F\begin{pmatrix} x \\ y \end{pmatrix} = \begin{pmatrix} 2\cos(y)\cos(x) - 2\cos^2(y) \\ 2\sin(y)\sin(x) \end{pmatrix}.$$

We begin to prove reversing symmetry R_1,

$$F\left(R_1\begin{pmatrix} x \\ y \end{pmatrix}\right) = F\begin{pmatrix} -x \\ y \end{pmatrix} = \begin{pmatrix} 2\cos(y)\cos(x) - 2\cos^2(y) \\ -2\sin(y)\sin(x) \end{pmatrix},$$

and

$$R_1\left(F\begin{pmatrix} x \\ y \end{pmatrix}\right) = R_1\begin{pmatrix} 2\cos(y)\cos(x) - 2\cos^2(y) \\ 2\sin(y)\sin(x) \end{pmatrix} = \begin{pmatrix} -(2\cos(y)\cos(x) - 2\cos^2(y)) \\ 2\sin(y)\sin(x) \end{pmatrix}.$$

So

$$F \circ R_1 \begin{pmatrix} x \\ y \end{pmatrix} = -R_1 \circ F \begin{pmatrix} x \\ y \end{pmatrix} \quad \forall (x, y) \in \mathbb{T}^2.$$

Similar wary, we prove that R_2 is symmetry,

$$F\left(R_2 \begin{pmatrix} x \\ y \end{pmatrix}\right) = F \begin{pmatrix} x \\ -y \end{pmatrix} = \begin{pmatrix} 2\cos(y)\cos(x) - 2\cos^2(y) \\ -2\sin(y)\sin(x) \end{pmatrix}.$$

and

$$R_2\left(F \begin{pmatrix} x \\ y \end{pmatrix}\right) = R_2 \begin{pmatrix} 2\cos(y)\cos(x) - 2\cos^2(y) \\ 2\sin(y)\sin(x) \end{pmatrix} = \begin{pmatrix} (2\cos(y)\cos(x) - 2\cos^2(y)) \\ -2\sin(y)\sin(x) \end{pmatrix}.$$

So

$$F \circ R_2 \begin{pmatrix} x \\ y \end{pmatrix} = R_2 \circ F \begin{pmatrix} x \\ y \end{pmatrix} \quad \forall x, y \in \mathbb{T}^2.$$

Then R_1 is a reversing symmetry and R_2 is a symmetry for system (4.1).

A.2 Maple code for the chapter 5

A.2.1 Code for Figures 5.2, 5.3 and 5.5

```
restart;
with(plots):
# increase infolevel to get more info on  integration problems
# infolevel[‘evalf/int‘]:=0:
# integral for beta=r=0
EE:=(x,y)->y+cos(y)*sin(y)-2*cos(x)*sin(y);
# integrable limit
intlimit:={beta=0,r=0};
# equation 5
g:=phi->cos(phi+beta)+r*sin(2*phi);
# equation 8
dxdt:=(x,y)->2*(g(x-y)+g(x+y))-g(-x-y)-g(0)-g(y-x)-(g(-2*y)+g(2*y))/2;
dydt:=(x,y)->g(y-x)-g(-x-y)+(g(2*y)-g(-2*y))/2;
dEdt:=expand(simplify(diff(EE(x,y),x)*dxdt(x,y)+diff(EE(x,y),y)*dydt(x,y)));
# check: should be zero!
simplify(subs(intlimit,dEdt));
G0:=simplify(subs(beta=0,diff(dEdt,beta)));
F0:=simplify(subs(r=0,diff(dEdt,r)));
Emax:=EE(2*Pi,y);
Emin:=EE(Pi,y);
p1:=plot([Emin,Emax],y=0..Pi,color= ["blue","red"],thickness=3);
# Return solution in appropriate range
ymaxroot:=RootOf(Emax=E,y,2.0-0.00001*I..3.2+0.00001*I);
ymax:=E0->evalf(Re(subs(E=E0,ymaxroot)));
```

```
# Return solution in appropriate range
yminroot:=RootOf(Emin=E,y,-0.001-0.0001*I..1.6+0.0001*I);
ymin:=E0->evalf(Re(subs(E=E0,yminroot)));
p2:=display([plot(['ymin(E)','ymax(E)'],E=0..Pi,color= ["blue","red"],thickness=3),
textplot([[0.7,2.7,"ymax",'font'=["times","roman",12]],
[0.7,0.4,"ymin",'font'=["times","roman",12]]])]);
# Integrand for period T(E) vs E
YY:=E->1.0/(4*sin(y)^2-(cos(y)*sin(y)+y-E)^2)^(1/2);
# Integral for period T(E) vs E
T:=E->int(YY(E),y=ymin(E)..ymax(E));
#infinite at endpoints so stop short of them
eta:=1e-4;
p3:=plot('T(E)', E=eta..Pi-eta, 1..8, labels=["E","T(E)"],
 thickness=3,color=blue,numpoints=80,adaptive=false);
Dx:=(E,y)->evalf(2*Pi)-arccos((y+cos(y)*sin(y)-E)/(2.0*sin(y)));
#Dx:=(E,y)->arccos((y+cos(y)*sin(y)-E)/(2.0*sin(y)));
G0;
F0;
# These should be the same as G0 and F0
G1:=4.0*sin(y)*(4.0*cos(y)*cos(x)^2-cos(y)^3-3.0*cos(y));
F1:=4.0*sin(y)*(4.0*cos(y)^5-4.0*cos(y)^4*cos(x)+4.0*cos(y)^3*cos(x)^2-16.0*
  cos(y)^2*cos(x)^3-4.0*cos(y)^3+16.0*cos(y)^2*cos(x)+6.0*cos(x)^3-6.0*cos(x);
gg:=2.0*sin(y)*sin(x);
Delta1:=(E,yy)->simplify(subs({x=Dx(E,yy),y=yy},G1/gg));
Delta2:=(E,yy)->simplify(subs({x=Dx(E,yy),y=yy},F1/gg));
eta:=1e-4;
# Computes the integral only to fixed digits accuracy
Lambda1:=xx->Int(Delta1(xx,y),y=subs(E=xx,ymin(xx))+eta..subs(E=xx,ymax(E))
  -eta,digits=6); #,method =_NCrule);#,method=_d01ajc));#,method=_Gquad));
```

```
Lambda2:=xx->Int(Delta2(xx,y),y=subs(E=xx,ymin(xx))+eta..subs(E=xx,ymax(E))
  -eta,digits=6);#,method = _NCrule);#,method = _d01ajc));#,method=_Gquad));
N:=105;
Es:=Array([evalf((k-1)*Pi/(2*(N-1))) $ k=1..2*N-1]);
L1s:=Array([0 $ k=1..2*N-1]);
L2s:=Array([0 $ k=1..2*N-1]);
# compute the values of Lambda1 and Lambda2 at points Es
for kk from 1 to N do
L1s[kk] := evalf[25](Lambda1(Es[kk]));
L2s[kk] := evalf[25](Lambda2(Es[kk]));
if (kk<N) then
L1s[2*N-kk] := evalf(-L1s[kk]);
L2s[2*N-kk] := evalf(-L2s[kk]);
end if;
end do:
# Plot Lambda1 and Lambda2
p4:=plot(Es,L1s,color= "blue",thickness=3):
p5:=plot(Es,L2s,color= "red",thickness=3):
display({p4,p5})
p6:=plot(Es,-2*(0.0062*L1s-0.01*L2s),color= "blue",thickness=3,
  labels=['E','Lambda(E)']):
p7:=plot(Es,-2*(0.0081*L1s-0.01*L2s),color= "red",thickness=3):
p8:=plot(Es,-2*(0.0125*L1s-0.01*L2s),color= "green",thickness=3):
p9:=plot(Es,-2*(0.0159*L1s-0.01*L2s),color= "cyan",thickness=3):
p12:=plot(Es,-2*(0.028*L1s-0.01*L2s),color= "orange",thickness=3):
p10:=plot(Es,-2*(0.063*L1s-0.01*L2s),color= "magenta",thickness=3):
p11:=plot(Es,-2*(0.08*L1s-0.01*L2s),color= "black",thickness=3):
display([p6,p7,p8,p9,p10,p11, p12]);
```

A.2.2 Code for Figures 5.6

```
restart;
with(plots):
# increase infolevel to get more info on integration problems
# infolevel[‘evalf/int‘]:=0:
# integral for beta=r=0
EE:=(x,y)->y+cos(y)*sin(y)-2*cos(x)*sin(y);
# integrable limit
intlimit:={beta=0,r=0};
# equation 5
g:=phi->cos(phi+beta)+r*sin(2*phi);
# equation 8
dxdt:=(x,y)->2*(g(x-y)+g(x+y))-g(-x-y)-g(0)-g(y-x)-(g(-2*y)+g(2*y))/2;
dydt:=(x,y)->g(y-x)-g(-x-y)+(g(2*y)-g(-2*y))/2;
dEdt:=expand(simplify(diff(EE(x,y),x)*dxdt(x,y)+diff(EE(x,y),y)*dydt(x,y)));
# check: should be zero!
simplify(subs(intlimit,dEdt));
G0:=simplify(subs(beta=0,diff(dEdt,beta)));
F0:=simplify(subs(r=0,diff(dEdt,r)));
Emax:=EE(2*Pi,y);
Emin:=EE(Pi,y);
p1:=plot([Emin,Emax],y=0..Pi,color= ["blue","red"],thickness=3);
# Return solution in appropriate range
ymaxroot:=RootOf(Emax=E,y,2.0-0.00001*I..3.2+0.00001*I);
ymax:=E0->evalf(Re(subs(E=E0,ymaxroot)));
# Return solution in appropriate range
yminroot:=RootOf(Emin=E,y,-0.001-0.0001*I..1.6+0.0001*I);
```

```
ymin:=E0->evalf(Re(subs(E=E0,yminroot)));
p2:=display([plot(['ymin(E)','ymax(E)'],E=0..Pi,color= ["blue","red"],
  thickness=3),textplot([[0.7,2.7,"ymax",'font'=["times","roman",12]],
[0.7,0.4,"ymin",'font'=["times","roman",12]]])]);
# Integrand for period T(E) vs E
YY:=E->1.0/(4*sin(y)^2-(cos(y)*sin(y)+y-E)^2)^(1/2);
# Integral for period T(E) vs E
T:=E->int(YY(E),y=ymin(E)..ymax(E));
#infinite at endpoints so stop short of them
eta:=1e-4;
eta := 0.0001
p3:=plot('T(E)',E=eta..Pi-eta,1..8,labels=["E","T(E)"],
  thickness=3,color=blue,numpoints=80,adaptive=false)
Dx:=(E,y)->evalf(2*Pi)-arccos((y+cos(y)*sin(y)-E)/(2.0*sin(y)));
#Dx:=(E,y)->arccos((y+cos(y)*sin(y)-E)/(2.0*sin(y)));
G0;
F0;
# These should be the same as G0 and F0
G1:=4.0*sin(y)*(4.0*cos(y)*cos(x)^2-cos(y)^3-3.0*cos(y));
F1:=4.0*sin(y)*(4.0*cos(y)^5-4.0*cos(y)^4*cos(x)+4.0*cos(y)^3*cos(x)^2
-16.0*cos(y)^2*cos(x)^3-4.0*cos(y)^3+16.0*cos(y)^2*cos(x)+6.0*cos(x)^3-6.0*cos(x));
gg:=2.0*sin(y)*sin(x);
Delta1:=(E,yy)->simplify(subs({x=Dx(E,yy),y=yy},G1/gg));
Delta2:=(E,yy)->simplify(subs({x=Dx(E,yy),y=yy},F1/gg));
#Delta2(2,y);
eta:=1e-4;
# Computes the integral only to fixed digits accuracy
Lambda1:=xx->Int(Delta1(xx,y),y=subs(E=xx,ymin(xx))+eta..subs(E=xx,ymax(E))-eta,
  digits=6); #,method = _NCrule);#,method = _d01ajc));#,method=_Gquad));
```

```
Lambda2:=xx->Int(Delta2(xx,y),y=subs(E=xx,ymin(xx))+eta..subs(E=xx,ymax(E))-eta,
  digits=6);#,method = _NCrule);#,method = _d01ajc));#,method=_Gquad));
N:=101;
Es:=Array([evalf(k*Pi/(2*N)) $ k=0..N]);
L1s:=Array([0 $ k=0..N]);
L2s:=Array([0 $ k=0..N]);
# compute the values of Lambda1 and Lambda2 at points Es
for kk to N+1 do
L1s[kk] := evalf[25](Lambda1(Es[kk]));
L2s[kk] := evalf[25](Lambda2(Es[kk]))
end do:
L2s;
E2:=eta+(1-1)*(Pi-2*eta)/(nsteps-1);
E2:=eta+(101-1)*(Pi-2*eta)/(nsteps-1);
nbeta:=80;
b1:=Vector(nbeta);
nsteps:=102;
EE:=Vector(nsteps):
C1:=Vector(nsteps):
C2:=Vector(nsteps):
for i from 1 to nsteps do:
C1[i]:= L1s[i] ;
C2[i]:= L2s[i];
end:
C1;
C2;
F:=Matrix(nbeta,nsteps*2);
EEE:=Vector(nsteps*2);
forget(ii);
```

```
for ii from 1 to nbeta do;
for jj from 1 to nsteps do;
b1[ii]:=0.001*ii;
F[ii,jj]:=2*(-(C1[jj]*sin(b1[ii])-0.01*C2[jj]));
F[ii,nsteps+jj]:=-2*(-(C1[nsteps+1-jj]*sin(b1[ii])-0.01*C2[nsteps+1-jj]));
EEE[jj]:=Es[jj];
EEE[nsteps+jj]:=Es[jj]+evalf(Pi/2);
od;
od;
print(F);
print(b1);
print(EEE);
# plots only zero contour
d1:=dataplot(b1,EEE,F,contours=[0],orientation=[-90,0,0],labels=["beta","E"," "],
  'color' = "blue",thickness=4,filled="false",style="contour");
```

A.2.3 Code for Figures 6.2(a),(b)

```
# Find eigenvalues for chapter six
restart;
with(LinearAlgebra):
with(plots):
f1:=(theta1, theta2,theta3,theta4,theta5,theta6)->g(theta1-theta2)
  +g(theta1-theta3)+g(theta1-theta5)+g(theta1-theta6);
f2:=(theta1,theta2,theta3,theta4,theta5,theta6)->g(theta2-theta1)+
  g(theta2-theta3)+g(theta2-theta4)+g(theta2-theta6);
f3:=(theta1,theta2,theta3,theta4,theta5,theta6)->g(theta3-theta1)
  +g(theta3-theta2)+g(theta3-theta4)+g(theta3-theta5);
f4:=(theta1,theta2,theta3,theta4,theta5,theta6)->g(theta4-theta2)
  +g(theta4-theta3)+g(theta4-theta5)+g(theta4-theta6);
```

```
f5:=(theta1,theta2,theta3,theta4,theta5,theta6)->g(theta5-theta1)
  +g(theta5-theta3)+g(theta5-theta4)+g(theta5-theta6);
f6:=(theta1,theta2,theta3,theta4,theta5,theta6)->g(theta6-theta1)
  +g(theta6-theta2)+g(theta6-theta4)+g(theta6-theta5);
xi1d:=f1(xi1, xi2, xi3, xi4, xi5, 0)-f6(xi1, xi2, xi3, xi4, xi5, 0);
xi2d:=f2(xi1, xi2, xi3, xi4, xi5, 0)-f6(xi1, xi2, xi3, xi4, xi5, 0);
xi3d:=f3(xi1, xi2, xi3, xi4, xi5, 0)-f6(xi1, xi2, xi3, xi4, xi5, 0);
xi4d:=f4(xi1, xi2, xi3, xi4, xi5, 0)-f6(xi1, xi2, xi3, xi4, xi5, 0);
xi5d:=f5(xi1, xi2, xi3, xi4, xi5, 0)-f6(xi1, xi2, xi3, xi4, xi5, 0);
g:=phi->-sin(phi-alpha)+r*sin(2*phi);
with(VectorCalculus):
D1:=Jacobian([xi1d, xi2d, xi3d, xi4d, xi5d],[xi1, xi2, xi3, xi4, xi5]=
  [-3*Pi/4, Pi/4, -Pi, -3*Pi/4, Pi/4]);
with(plots):
upcurve:=sin(alpha1)/3;
downcurve:=-sin(alpha1)/3;
F:=plot(upcurve, alpha1 = 0 .. Pi,'color' = "blue"):
G:=plot(downcurve, alpha1= 0 .. Pi):
display([F,G]);
nvalues:=158:
alpha2:=Vector(nvalues):
rabove:=Vector(nvalues):
rdown:=Vector(nvalues):
for i from 1 to nvalues do:
aa:=evalf(Pi*(i-1)/(nvalues-1)):
alpha2(i):=aa;
rabove(i):=subs(alpha1=aa,upcurve);
rdown(i):=subs(alpha1=aa,downcurve);;
end do:
```

```
eigabove:=Vector(nvalues):
eigdown:=Vector(nvalues):
for i from 1 to nvalues do;
eigabove(i):=Eigenvalues(map(evalf,subs(r=rabove(i),alpha=alpha2(i), D1)));
eigdown(i):=Eigenvalues(map(evalf,subs(r=rdown(i),alpha=alpha2(i), D1)));
end do:
nvalues2:=nvalues*5:
aa:=Vector(nvalues2):
ear:=Vector(nvalues2):
edr:=Vector(nvalues2):
eai:=Vector(nvalues2):
edi:=Vector(nvalues2):
printlevel := 2:
k:=0:
for i from 1 to nvalues do:
alpha=alpha2(i);
for j from 1 to 5 do:
k:=k+1;
aa(k):=alpha2(i);
ear(k):=Re(eigabove(i)(j));
edr(k):=Re(eigdown(i)(j));
eai(k):=Im(eigabove(i)(j));
edi(k):=Im(eigdown(i)(j));
end  do:
end  do:
# Real parts of eigenvalues on upper branch
plot(aa,ear,style=‘point‘);
```

BIBLIOGRAPHY

[1] D. M. ABRAMS, R. MIROLLO, S. H. STROGATZ, AND D. A. WILEY, *Solvable model for chimera states of coupled oscillators*, Physical Review Letters, 101 (2008), p. 084103.

[2] D. M. ABRAMS AND S. H. STROGATZ, *Chimera states for coupled oscillators*, Physical Review Letters, 93 (2004), p. 174102.

[3] ——, *Chimera states in a ring of nonlocally coupled oscillators*, International Journal of Bifurcation and Chaos, 16 (2006), pp. 21–37.

[4] J. M. ALONGI AND G. S. NELSON, *Recurrence and topology*, vol. 85, American Mathematical Soc., 2007.

[5] F. ANTONELI AND I. STEWART, *Symmetry and synchrony in coupled cell networks 1: Fixed-point spaces*, International Journal of Bifurcation and Chaos, 16 (2006), pp. 559–577.

[6] ——, *Symmetry and synchrony in coupled cell networks 2: Group networks*, International Journal of Bifurcation and Chaos, 17 (2007), pp. 935–951.

[7] P. ASHWIN, C. BICK, AND O. BURYLKO, *Identical phase oscillator networks: Bifurcations, symmetry and reversibility for generalized coupling*, Frontiers in Applied Mathematics and Statistics, 2 (2016), p. 7.

[8] P. ASHWIN AND O. BURYLKO, *Weak chimeras in minimal networks of coupled phase oscillators*, Chaos: An Interdisciplinary Journal of Nonlinear Science, 25 (2015), p. 013106.

[9] P. ASHWIN, O. BURYLKO, AND Y. MAISTRENKO, *Bifurcation to heteroclinic cycles and sensitivity in three and four coupled phase oscillators*, Physica D: Nonlinear Phenomena, 237 (2008), pp. 454–466.

[10] P. ASHWIN AND M. FIELD, *Heteroclinic networks in coupled cell systems*, Archive for Rational Mechanics and Analysis, 148 (1999), pp. 107–143.

[11] P. ASHWIN AND J. W. SWIFT, *The dynamics ofn weakly coupled identical oscillators*, Journal of Nonlinear Science, 2 (1992), pp. 69–108.

[12] S. ASSENZA, R. GUTIÉRREZ, J. GÓMEZ-GARDENES, V. LATORA, AND S. BOCCALETTI, *Emergence of structural patterns out of synchronization in networks with competitive interactions*, Scientific reports, 1 (2011), p. 99.

[13] T. BANERJEE AND D. GHOSH, *Transition from amplitude to oscillation death under mean-field diffusive coupling*, Physical Review E, 89 (2014), p. 052912.

[14] B. K. BERA, D. GHOSH, AND M. LAKSHMANAN, *Chimera states in bursting neurons*, Physical Review E, 93 (2016), p. 012205.

[15] C. BICK AND P. ASHWIN, *Chaotic weak chimeras and their persistence in coupled populations of phase oscillators*, Nonlinearity, 29 (2016), p. 1468.

[16] S. L. BRESSLER, *Cortical coordination dynamics and the disorganization syndrome in schizophrenia*, Neuropsychopharmacology, 28 (2003), p. S35.

[17] L. M. CHILDS AND S. H. STROGATZ, *Stability diagram for the forced kuramoto model*, Chaos: An Interdisciplinary Journal of Nonlinear Science, 18 (2008), p. 043128.

[18] O. COMPLETES DE CHRISTIAAN HUYGENS, *publiées par la société hollandaise des sciences*, La Haye, 1944 (1888).

[19] Q. DAI, M. ZHANG, H. CHENG, H. LI, F. XIE, AND J. YANG, *From collective oscillation to chimera state in a nonlocally coupled excitable system*, Nonlinear Dynamics, (2018), pp. 1–9.

[20] E. J. DOEDEL, A. R. CHAMPNEYS, T. F. FAIRGRIEVE, Y. A. KUZNETSOV, B. SANDSTEDE, X. WANG, ET AL., *Continuation and bifurcation software for ordinary differential equations (with homcont)*, AUTO97, Concordia University, Canada, (1997).

[21] B. ERMENTROUT, *Simulating, analyzing, and animating dynamical systems: a guide to XPPAUT for researchers and students*, vol. 14, Siam, 2002.

[22] G. ERMENTROUT AND N. KOPELL, *Oscillator death in systems of coupled neural oscillators*, SIAM Journal on Applied Mathematics, 50 (1990), pp. 125–146.

[23] G. B. ERMENTROUT AND N. KOPELL, *Frequency plateaus in a chain of weakly coupled oscillators, i.*, SIAM journal on Mathematical Analysis, 15 (1984), pp. 215–237.

[24] J. FELL AND N. AXMACHER, *The role of phase synchronization in memory processes*, Nature Reviews Neuroscience, 12 (2011), pp. 105–118.

[25] W. FULTON AND J. HARRIS, *Representation theory: a first course*, vol. 129, Springer Science & Business Media, 1991.

[26] L. V. GAMBUZZA, A. BUSCARINO, S. CHESSARI, L. FORTUNA, R. MEUCCI, AND M. FRASCA, *Experimental investigation of chimera states with quiescent and synchronous domains in coupled electronic oscillators*, Physical Review E, 90 (2014), p. 032905.

[27] W. J. GILBERT AND W. K. NICHOLSON, *Modern algebra with applications*, vol. 66, John Wiley & Sons, 2004.

[28] P. GLENDINNING, *Stability, instability and chaos: an introduction to the theory of nonlinear differential equations*, vol. 11, Cambridge university press, 1994.

[29] M. GOLUBITSKY AND I. STEWART, *The symmetry perspective: from equilibrium to chaos in phase space and physical space*, vol. 200, Springer Science & Business Media, 2003.

[30] M. GOLUBITSKY, I. STEWART, ET AL., *Singularities and groups in bifurcation theory*, vol. 2, Springer Science & Business Media, 1988.

[31] M. GOLUBITSKY, I. STEWART, AND A. TÖRÖK, *Patterns of synchrony in coupled cell networks with multiple arrows*, SIAM Journal on Applied Dynamical Systems, 4 (2005), pp. 78–100.

[32] R. GOPAL, V. CHANDRASEKAR, A. VENKATESAN, AND M. LAKSHMANAN, *Observation and characterization of chimera states in coupled dynamical systems with nonlocal coupling*, Physical Review E, 89 (2014), p. 052914.

[33] J. GUCKENHEIMER AND P. J. HOLMES, *Nonlinear oscillations, dynamical systems, and bifurcations of vector fields*, vol. 42, Springer Science & Business Media, 2013.

[34] S.-Y. HA, E. JEONG, AND M.-J. KANG, *Emergent behaviour of a generalized viscek-type flocking model*, Nonlinearity, 23 (2010), p. 3139.

[35] A. M. HAGERSTROM, T. E. MURPHY, R. ROY, P. HÖVEL, I. OMELCHENKO, AND E. SCHÖLL, *Experimental observation of chimeras in coupled-map lattices*, Nature Physics, 8 (2012), p. 658.

[36] H. HAKEN, *Synergetics*, Physics Bulletin, 28 (1977), p. 412.

[37] D. HANSEL, G. MATO, AND C. MEUNIER, *Clustering and slow switching in globally coupled phase oscillators*, Physical Review E, 48 (1993), p. 3470.

[38] I. N. HERSTEIN, *Abstract algebra*, Macmillan New York, 1996.

[39] M. W. HIRSCH, M. SHUB, AND C. C. PUGH, *Invariant manifolds*, Springer, 1977.

[40] F. C. HOPPENSTEADT AND E. M. IZHIKEVICH, *Weakly connected neural networks*, vol. 126, Springer Science & Business Media, 1997.

[41] J. K. HUNTER, *An introduction to real analysis*.

[42] E. M. IZHIKEVICH AND Y. KURAMOTO, *Weakly coupled oscillators*, Encyclopedia of mathematical physics, 5 (2006), p. 448.

[43] G. D. JAMES, *The representation theory of the symmetric groups*, in Proc. Symposia in Pure Math, vol. 47, 1987, pp. 111–126.

[44] P. JAROS, S. BREZETSKY, R. LEVCHENKO, D. DUDKOWSKI, T. KAPITANIAK, AND Y. MAISTRENKO, *Solitary states for coupled oscillators with inertia*, Chaos: An Interdisciplinary Journal of Nonlinear Science, 28 (2018), p. 011103.

[45] Ö. KARABACAK AND P. ASHWIN, *Heteroclinic ratchets in networks of coupled oscillators*, Journal of nonlinear science, 20 (2010), pp. 105–129.

[46] N. KOPELL AND G. ERMENTROUT, *Symmetry and phaselocking in chains of weakly coupled oscillators*, Communications on Pure and Applied Mathematics, 39 (1986), pp. 623–660.

[47] Y. KURAMOTO, *Self-entrainment of a population of coupled non-linear oscillators*, in International symposium on mathematical problems in theoretical physics, Springer, 1975, pp. 420–422.

[48] ——, *Chemical oscillations, waves, and turbulence*, Courier Corporation, 2003.

[49] Y. KURAMOTO AND H. ARAKAI, *Chemical oscillations,waves and turbulence.*, 1984.

[50] Y. KURAMOTO AND D. BATTOGTOKH, *Coexistence of coherence and incoherence in nonlocally coupled phase oscillators*, arXiv preprint cond-mat/0210694, (2002).

[51] Y. A. KUZNETSOV, *Elements of applied bifurcation theory*, vol. 112, Springer Science & Business Media, 2013.

[52] C. R. LAING, *Chimera states in heterogeneous networks*, Chaos: An Interdisciplinary Journal of Nonlinear Science, 19 (2009), p. 013113.

[53] ——, *Chimeras in networks of planar oscillators*, Physical Review E, 81 (2010), p. 066221.

[54] ——, *Chimeras in networks with purely local coupling*, Physical Review E, 92 (2015), p. 050904.

[55] C. R. LAING AND C. C. CHOW, *Stationary bumps in networks of spiking neurons*, Neural Computation, 13 (2001), pp. 1473–1494.

[56] J. LAMB, J. A. ROBERTS, AND H. CAPEL, *Conditions for local (reversing) symmetries in dynamical systems*, Physica A: Statistical Mechanics and its Applications, 197 (1993), pp. 379–422.

[57] G. LAYEK, *"An Introduction to Dynamical Systems and Chaos"*, Springer, 2015.

[58] D. A. LINKENS, *Nonlinear circuit mode analysis*, IEE Proceedings A-Physical Science, Measurement and Instrumentation, Management and Education-Reviews, 130 (1983), pp. 69–87.

[59] S. LYNCH, *Dynamical systems with applications using Mathematica®*, Springer Science & Business Media, 2007.

[60] E. A. MARTENS, S. THUTUPALLI, A. FOURRIÈRE, AND O. HALLATSCHEK, *Chimera states in mechanical oscillator networks*, Proceedings of the National Academy of Sciences, 110 (2013), pp. 10563–10567.

[61] J. MILTON AND P. JUNG, *Epilepsy as a dynamic disease*, Springer Science & Business Media, 2013.

[62] J. MURDOCK, A. SANDERS, AND F. VERHULST, *Averaging methods in nonlinear dynamical systems*, Appl. Math. Sci, 59 (2007).

[63] J. MURRAY, *Mathematical biology. 1989*, C271.

[64] M. E. NEWMAN, *The structure and function of complex networks*, SIAM Review, 45 (2003), pp. 167–256.

[65] E. OMEL'CHENKO, Y. L. MAISTRENKO, AND P. A. TASS, *Chimera states: The natural link between coherence and incoherence*, Physical Review Letters, 100 (2008), p. 044105.

[66] ——, *Chimera states induced by spatially modulated delayed feedback*, Physical Review E, 82 (2010), p. 066201.

[67] I. OMELCHENKO, A. ZAKHAROVA, P. HÖVEL, J. SIEBERT, AND E. SCHÖLL, *Nonlinearity of local dynamics promotes multi-chimeras*, Chaos: An Interdisciplinary Journal of Nonlinear Science, 25 (2015), p. 083104.

[68] H. OSINGA AND J. G.-V. B. KRAUSKOPF, *Numerical continuation methods for dynamical systems*, 2007.

[69] E. OTT AND T. M. ANTONSEN, *Low dimensional behavior of large systems of globally coupled oscillators*, Chaos: An Interdisciplinary Journal of Nonlinear Science, 18 (2008), p. 037113.

[70] D. A. PALEY, N. E. LEONARD, R. SEPULCHRE, D. GRUNBAUM, AND J. K. PARRISH, *Oscillator models and collective motion*, IEEE control systems, 27 (2007), pp. 89–105.

[71] M. J. PANAGGIO AND D. M. ABRAMS, *Chimera states on a flat torus*, Physical Review Letters, 110 (2013), p. 094102.

[72] ——, *Chimera states on the surface of a sphere*, Physical Review E, 91 (2015), p. 022909.

[73] M. J. PANAGGIO, D. M. ABRAMS, P. ASHWIN, AND C. R. LAING, *Chimera states in networks of phase oscillators: the case of two small populations*, Physical Review E, 93 (2016), p. 012218.

[74] L. PERKO, *Differential equations and dynamical systems*, vol. 7, Springer Science & Business Media, 2013.

[75] C. C. PINTER, *A book of abstract algebra*, Courier Corporation, 2012.

[76] K. PREMALATHA, V. CHANDRASEKAR, M. SENTHILVELAN, AND M. LAKSHMANAN, *Impact of symmetry breaking in networks of globally coupled oscillators*, Physical Review E, 91 (2015), p. 052915.

[77] R. P. RAO, *Brain-computer interfacing: an introduction*, Cambridge University Press, 2013.

[78] H. SAKAGUCHI AND Y. KURAMOTO, *A soluble active rotater model showing phase transitions via mutual entertainment*, Progress of Theoretical Physics, 76 (1986), pp. 576–581.

[79] L. SCHMIDT, K. SCHÖNLEBER, K. KRISCHER, AND V. GARCÍA-MORALES, *Coexistence of synchrony and incoherence in oscillatory media under nonlinear global coupling*, Chaos: An Interdisciplinary Journal of Nonlinear Science, 24 (2014), p. 013102.

[80] G. C. SETHIA AND A. SEN, *Chimera states: the existence criteria revisited*, Physical Review Letters, 112 (2014), p. 144101.

[81] G. C. SETHIA, A. SEN, AND F. M. ATAY, *Clustered chimera states in delay-coupled oscillator systems*, Physical Review Letters, 100 ((2008)), p. 144102.

[82] J. SIEBER, E. OMEL'CHENKO, AND M. WOLFRUM, *Controlling unstable chaos: stabilizing chimera states by feedback*, Physical Review Letters, 112 (2014), p. 054102.

[83] W. SINGER, *Synchronization of cortical activity and its putative role in information processing and learning*, Annual Review of Physiology, 55 (1993), pp. 349–374.

[84] P. S. STEIN, *Neurons, networks, and motor behavior*, MIT press, 1999.

[85] I. STEWART, M. GOLUBITSKY, AND M. PIVATO, *Symmetry groupoids and patterns of synchrony in coupled cell networks*, SIAM Journal on Applied Dynamical Systems, 2 (2003), pp. 609–646.

[86] S. H. STROGATZ, *Nonlinear dynamics and chaos with applications to physics, biology, chemistry, and engineering; 1994*, Reading: Perseus Books Publishing.

[87] ——, *From kuramoto to crawford: exploring the onset of synchronization in populations of coupled oscillators*, Physica D: Nonlinear Phenomena, 143 (2000), pp. 1–20.

[88] M. R. TINSLEY, S. NKOMO, AND K. SHOWALTER, *Chimera and phase-cluster states in populations of coupled chemical oscillators*, Nature Physics, 8 (2012), p. 662.

[89] M. S. TITCOMBE, R. EDWARDS, AND A. BEUTER, *Mathematical modelling of parkinsonian tremor.*, Nonlinear Studies, 11 (2004).

[90] P. UHLHAAS, G. PIPA, B. LIMA, L. MELLONI, S. NEUENSCHWANDER, D. NIKOLIĆ, AND W. SINGER, *Neural synchrony in cortical networks: history, concept and current status*, Frontiers in integrative neuroscience, 3 (2009), p. 17.

[91] B. VAN DER POL, *Lxxxviii. on "relaxation-oscillations"*, The London, Edinburgh, and Dublin Philosophical Magazine and Journal of Science, 2 (1926), pp. 978–992.

[92] B. VAN DER POL, *Vii. forced oscillations in a circuit with non-linear resistance.(reception with reactive triode)*, The London, Edinburgh, and Dublin Philosophical Magazine and Journal of Science, 3 (1927), pp. 65–80.

[93] B. VAN DER POL AND J. VAN DER MARK, *Lxxii. the heartbeat considered as a relaxation oscillation, and an electrical model of the heart*, The London, Edinburgh, and Dublin Philosophical Magazine and Journal of Science, 6 (1928), pp. 763–775.

[94] J. L. P. VELAZQUEZ, *Brain research: a perspective from the coupled oscillators field*, NeuroQuantology, 4 (2006).

[95] S. WIGGINS, *Introduction to applied nonlinear dynamical systems and chaos*, vol. 2, Springer Science & Business Media, 2003.

[96] ——, *Global bifurcations and chaos: analytical methods*, vol. 73, Springer Science & Business Media, 2013.

[97] D. A. WILEY, S. H. STROGATZ, AND M. GIRVAN, *The size of the sync basin*, Chaos: An Interdisciplinary Journal of Nonlinear Science, 16 (2006), p. 015103.

[98] R. J. WILSON, *Introduction to Graph Theory*, John Wiley & Sons, Inc., New York, NY, USA, 1985.

[99] A. T. WINFREE, *Biological rhythms and the behavior of populations of coupled oscillators*, Journal of theoretical biology, 16 (1967), pp. 15–42.

[100] ——, *The geometry of biological time*, vol. 12, Springer Science & Business Media, 2001.

[101] M. WOLFRUM AND E. OMEL'CHENKO, *Chimera states are chaotic transients*, Physical Review E, 84 (2011), p. 015201.

[102] M. WOLFRUM, O. E. OMEL'CHENKO, AND J. SIEBER, *Regular and irregular patterns of self-localized excitation in arrays of coupled phase oscillators*, Chaos: An Interdisciplinary Journal of Nonlinear Science, 25 (2015), p. 053113.